

END-OF-STUDIES INTERNSHIP
DEGREE IN AEROSPACE ENGINEERING
TFG

DESIGN OF A HELICAL COIL HEAT EXCHANGER AND EXPERIMENTAL STUDY OF FLOW-INDUCED VIBRATIONS

Ferran Santonja Soto

INTERNSHIP SUPERVISOR: Dr Njuki Mureithi
COORDINATOR IN FRANCE: Dr Didier Saury

2019/04/04 - 2019/09/09
POLYTECHNIQUE MONTRÉAL



Table of Contents

| | |
|-------------------------------------------------------|----|
| Acknowledgements | 1 |
| Summary | 2 |
| List of figures | 3 |
| List of Tables | 4 |
| 1. Introduction..... | 5 |
| 1.1 Polytechnique Montréal..... | 5 |
| 1.2 Explanation of the HCHE | 6 |
| 1.3 Objectives of the project | 8 |
| 2. Background – Study of the phenomenon..... | 9 |
| 3. Project methodology..... | 14 |
| 3.1 Applied hypothesis | 14 |
| 3.2 Theoretical knowledge and first calculations..... | 14 |
| 3.2.1 Parametric Study of Beta..... | 17 |
| 3.2.2 Natural Frequency of the Helicoid | 20 |
| 3.3 The water tunnel | 23 |
| 3.4 Experimental analysis devices | 24 |
| 3.4.1 High-speed camera..... | 24 |
| 3.4.2 The MATLAB code to analyse the images | 25 |
| 3.4.3 The displacement photoelectric sensor | 30 |
| 4. Design and manufacturing of the Prototypes | 31 |
| 4.1 The elements to prevent leaks | 32 |
| 4.2 The support structure for the helical coil..... | 34 |
| 4.3 The helical model of the heat exchanger | 36 |
| 5. Experimental results..... | 39 |
| 5.1 Natural frequency in air..... | 39 |
| 5.2 Water induced vibration | 42 |
| 5.2.1 Prototype 1..... | 42 |
| 5.2.2 Prototype 2..... | 43 |
| 5.2.3 Prototype 3..... | 46 |
| 6. Analysis of the experimental results | 54 |
| 7. Conclusions and recommendations | 57 |
| Bibliography..... | 59 |
| Appendices | 60 |
| Appendix 1: MATLAB codes..... | 60 |
| Appendix 2: Additional graphics..... | 68 |
| Appendix 3: SolidWorks simulated frequencies..... | 69 |
| Appendix 4: Parts drawings..... | 71 |

Acknowledgements

Throughout this project I have worked with different methods and completely new tools for me. It is therefore, I have received the help and support of several people from the Polytechnique. That is why I would like to make the following thanks:

First of all, to my advisor, the professor Njuki Mureithi. He gave me this great opportunity to do research in this respected centre of applied sciences. Furthermore, he has helped me at each stage of the project with weekly meetings where we discussed the results and the progress made during the week. He has meant a true guide for me in order to overcome the different problems and challenges that have arisen throughout the project.

Secondly, to Abdallah Hadji, the research assistant. He has helped me with the design of the prototypes as well as with other experimental parts of the project. His experience in the field of research in this laboratory is really wide, with answers for almost any experimental challenge.

To the laboratory technicians Jean François and Peter, who have helped me with the laboratory devices, especially with 3D printers and with my adaptation to the imperial system of measures and other methodologies.

Also, to my colleagues in the office and PHD students: Loay, Sameh, and Ibrahim with whom I have made a good friendship. Their profound knowledge in this field has made possible to answer some of my questions throughout the project.

I would like to thank my parents, sister and friends for the support they have sent me all the way from Europe and to my new friends here in Montréal.

Finally, I would like to thank the Erasmus mobility program and the Polytechnique Montréal for the respective economic studentships.

This internship in research has been a really enriching opportunity to finish my engineering studies with which I have gained knowledge from the vast field of fluid-structural interactions. Furthermore, due to the diversity of laboratory tools that I have had at my disposal I have been able to do a practical engineering activity.

Summary

The helical coil heat exchangers are a common type of heat exchangers used nowadays. The performance of this devices is based on the movement of the fluids around a helical tube to produce the heat exchange. Fluid-structure interactions are produced in the helical coil because of the flow, which produces flow-induced vibrations that can damage the structure with fatigue. The main objectives of the project are to design and manufacture a helical coil heat exchanger model and to perform experimental tests of flow-induced vibrations with the designed model.

With the realisation of a bibliographical review and the application of the hypothesis in this topic, it has been designed 3 different prototypes of helical coil heat exchanger in order to study how they react to the flow. The prototypes have been designed with SolidWorks, and they have been manufactured with 3D printing. The prototypes design has been modified several times till obtaining the final design due to the restrictions of the test chamber among other factors. Then, the three of them have been tested in a flow-channel and it has been used a photoelectric sensor and a high-speed camera to analyse the flow-induced vibrations in the structure.

The 3 prototypes have been useful in order to study the flow-induced vibrations, with the third as the most valid one due to the small diameter of the helical tube. The experimental results obtained with the sensors show clearly the flow-induced vibrations in the different prototypes produced by the vortex shedding phenomenon. Future research could be done using other experimental methods as particle image velocimetry (PIV) to analyse the vortex shedding phenomenon as well as computational fluid dynamics (CFD) simulations to study it deeply.

Key words:

Vortex Shedding – Fluid-structure interaction – Flow-Induced Vibrations – Helical coil heat exchanger
Water tunnel – Experimental investigation

List of figures

| | |
|----------------------------------------------------------------------------------------------------------------------------------------------------------------------------------------------------------------------------------------------------------------------------------------------------|----|
| FIGURE 1: BUILDINGS OF THE POLYTECHNIQUE MONTRÉAL | 5 |
| FIGURE 2: SEAL OF POLYTECHNIQUE MONTRÉAL..... | 6 |
| FIGURE 3: EXAMPLE OF HELICAL COIL HEAT EXCHANGER (HCHE)..... | 7 |
| FIGURE 4: EXPERIMENTAL CASE OF VORTEX SHEDDING IN A CYLINDRICAL TUBE | 10 |
| FIGURE 5: DETACHMENT OF THE BOUNDARY LAYER IN A CYLINDER..... | 10 |
| FIGURE 6: TWO VARIATIONS OF VORTEX SHEDDING: SYMMETRIC (ON THE LEFT) AND KÁRMÁN (ON THE RIGHT) | 11 |
| FIGURE 7: STROUHAL NUMBER (SR) AS A FUNCTION OF THE REYNOLDS NUMBER (R) FOR A CYLINDER..... | 12 |
| FIGURE 8: VIBRATION AMPLITUDE OF A TUBE IN A BUNDLE AS A FUNCTION OF FLOW-RATE (PAÏDOUSSIS ET AL., 2011) | 13 |
| FIGURE 9: BETA AS A FUNCTION OF THE EXTERNAL DIAMETER IN AIR FLOW WITH CONSTANT WALL THICKNESS..... | 17 |
| FIGURE 10: BETA AS A FUNCTION OF THE WALL THICKNESS IN AIR FLOW..... | 18 |
| FIGURE 11: BETA AS A FUNCTION OF THE EXTERNAL DIAMETER IN WATER FLOW WITH CONSTANT WALL THICKNESS | 19 |
| FIGURE 12: BETA AS A FUNCTION OF THE WALL THICKNESS IN WATER FLOW..... | 19 |
| FIGURE 13: RELATION BETWEEN THE NORMALIZED AMPLITUDE OF THE VIBRATION AND THE REDUCED VELOCITY (KANEKO ET AL., 2013) | 20 |
| FIGURE 14: : EXAMPLE OF NATURAL FREQUENCY SIMULATION WITH SOLIDWORKS | 21 |
| FIGURE 15: SOLIDWORKS DESIGN OF THE TEST CHAMBER AND REAL TEST CHAMBER..... | 23 |
| FIGURE 16: PUMP WATER OF THE WATER TUNNEL..... | 24 |
| FIGURE 17: SETTING UP OF THE HIGH-SPEED CAMERA USED IN THE EXPERIMENT..... | 25 |
| FIGURE 18: ORIGINAL IMAGE (ON THE TOP) AND FILTERED IMAGE OBTAINED FROM THE HIGH-SPEED CAMERA..... | 26 |
| FIGURE 19: EXAMPLE OF V-SHAPE DETECTED BY THE MATLAB CODE ALONG THE HELICOID | 26 |
| FIGURE 20: EXAMPLE OF THREE PIXELS OF AN HELICOID IMAGE WITH DIFFERENT GREY INDEX | 27 |
| FIGURE 21: EXAMPLE OF A BAD SELECTION OF THE INITIAL CENTRAL POINT IN THE MATLAB CODE | 29 |
| FIGURE 22: SETTING UP OF THE PHOTOELECTRIC SENSOR WITH THE PROTOTYPE 3..... | 30 |
| FIGURE 23: EXAMPLE OF A HELICOID MODEL WITH 6 TUBES PERFORMED WITH AUTOCAD | 31 |
| FIGURE 24: PROTOTYPE 3 INSIDE THE TEST SECTION (BLUE ROWS REPRESENT THE DIRECTION OF THE FLOW) | 32 |
| FIGURE 25: PLUG MODEL FROM THE TOP PART OF THE TEST CHAMBER | 33 |
| FIGURE 26: 3D IMPRESSION OF A PLUG..... | 33 |
| FIGURE 27: SOLIDWORKS FINAL DESIGN OF THE SUPPORT PLATE | 34 |
| FIGURE 28: BOLT TYPE USED TO ATTACH THE PLATE TO THE CHAMBER TEST | 35 |
| FIGURE 29: SUPPORT CYLINDERS TESTS FOR THE SCREWS (ON THE LEFT) AND HEXAGONAL HOLES TESTS FOR THE NUTS (ON THE RIGHT) | 36 |
| FIGURE 30: SUPPORT PLATE AND HELICOID FROM PROTOTYPE 3..... | 37 |
| FIGURE 31: HELICOID WITH THE TREE-SHAPED SUPPORT STRUCTURE OF THE 3D PRINTING AND AFTER REMOVING THE SUPPORT STRUCTURE | 37 |
| FIGURE 32: VERTICAL AND HORIZONTAL DISPLACEMENT OF THE PROTO 3 FROM THE PHOTOELECTRIC SENSOR | 39 |
| FIGURE 33: LASER FREQUENCY SPECTRUMS FOR THE 3 PROTOTYPES: VERTICAL FOR PROTO 1 (TOP LEFT), HORIZONTAL FOR PROTO 1 (TOP RIGHT), VERTICAL FOR PROTO 2 (CENTRE LEFT), HORIZONTAL FOR PROTO 2 (CENTRE RIGHT), VERTICAL FOR PROTO 1 (DOWN LEFT), HORIZONTAL FOR PROTO 1 (DOWN RIGHT) | 40 |
| FIGURE 34: HIGH-SPEED CAMERA FREQUENCY SPECTRUMS FOR THE 3 PROTOTYPES: VERTICAL FOR PROTO 1 (TOP LEFT), HORIZONTAL FOR PROTO 1 (TOP RIGHT), VERTICAL FOR PROTO 2 (CENTRE LEFT), HORIZONTAL FOR PROTO 2 (CENTRE RIGHT), VERTICAL FOR PROTO 1 (DOWN LEFT), HORIZONTAL FOR PROTO 1 (DOWN RIGHT) | 41 |
| FIGURE 35: VERTICAL DISPLACEMENT AT A VELOCITY 0.497M/S FOR PROTO 2..... | 43 |
| FIGURE 36: PSD 3D GRAPHIC OF THE VERTICAL MOVEMENT FOR PROTO 2..... | 44 |
| FIGURE 37: FFT 3D GRAPHIC OF THE VERTICAL MOVEMENT FOR PROTO 2 | 44 |
| FIGURE 38: PSD VERTICAL FREQUENCY SPECTRUM AT A VELOCITY OF 0.497 FOR PROTO 2 | 45 |
| FIGURE 39: FFT VERTICAL FREQUENCY SPECTRUM AT A VELOCITY OF 0.477 M/S FOR PROTO 2..... | 45 |
| FIGURE 40: FLOW-INDUCED VIBRATIONS USING RMS FOR PROTO 27.2.2 PROTOTYPE 3 | 46 |
| FIGURE 41: VERTICAL AND HORIZONTAL DISPLACEMENT AT A VELOCITY 0.304 M/S FOR PROTO 3..... | 46 |
| FIGURE 42: VERTICAL AND HORIZONTAL DISPLACEMENT AT A VELOCITY 0.412 M/S FOR PROTO 3..... | 47 |
| FIGURE 43: VERTICAL AND HORIZONTAL DISPLACEMENT AT A VELOCITY 0.477 M/S FOR PROTO 3..... | 47 |

FIGURE 44: PSD 3D GRAPHIC OF THE VERTICAL MOVEMENT FOR PROTO 3..... 48

FIGURE 45: PSD 3D GRAPHIC OF THE HORIZONTAL MOVEMENT FOR PROTO 3 48

FIGURE 46: PSD VERTICAL AND HORIZONTAL FREQUENCY SPECTRUM AT A VELOCITY OF 0.282 M/S FOR PROTO 3 49

FIGURE 47: PSD VERTICAL AND HORIZONTAL FREQUENCY SPECTRUM AT A VELOCITY OF 0.497 M/S FOR PROTO 3 49

FIGURE 48: FFT 3D GRAPHIC OF THE VERTICAL MOVEMENT FOR PROTO 3 50

FIGURE 49: FFT 3D GRAPHIC OF THE HORIZONTAL MOVEMENT FOR PROTO 3..... 50

FIGURE 50: VERTICAL AND HORIZONTAL FREQUENCY SPECTRUM AT A VELOCITY OF 0.282 M/S FOR PROTO 3 51

FIGURE 51: VERTICAL AND HORIZONTAL FREQUENCY SPECTRUM AT A VELOCITY OF 0.434 M/S FOR PROTO 3..... 51

FIGURE 52: EVOLUTION OF THE FIRST VORTEX SHEDDING FREQUENCY FOR PROTO 3 52

FIGURE 53: VORTEX SHEDDING PHENOMENON USING RMS OF THE DISPLACEMENT FOR PROTO 3..... 52

List of Tables

TABLE 1: DIFFERENT SOLIDWORKS HELICOID DESIGNS FREQUENCIES AND FLOW VELOCITIES..... 22

TABLE 2: COMPARISON OF NATURAL FREQUENCIES BETWEEN SENSORS..... 42

1. Introduction

1.1 Polytechnique Montréal

The Polytechnique Montréal is one of the most important engineering schools in Canada. It was founded in 1873. At that moment, it was a small engineering school where subjects like Technical Drawing and others applied arts were taught. Nowadays, it is a public centre of applied scientific studies where there are 12 different graduate programs divided in 7 departments with more than 4500 students per academic year. Some of the offered programs are: biomedical, civil, industrial, computer science, mechanic or aeronautic. There is a big diversity of scientific studies what allows to perform projects in different domains at the same time.



Figure 1: Buildings of the Polytechnique Montréal

The geographic location of the Polytechnique has not always been the same. Although at the beginning it was located in an old building in the city of Montréal, after a few years it moved to the emblematic street of Saint-Denis. In 1958 they decided to move the school to the current location on the campus of the Université de Montréal. After this last relocation, the Polytechnique has grown considerably year after year, with different buildings each of them destined for a specific field of studies.

Although it started as a simple engineering school, little by little, it turned more and more to research. This one was a path that started in the late 50's. Now, it is a leading research institution of applied sciences in Canada and the biggest engineering school in the francophone province of Quebec. The emblematic symbol of the school it is composed of a bee that evokes the planned and organized work of the engineer and the beam that represents civil engineering, the first discipline taught at school. Also, the gear wheel symbolizes the industrial boom in the century of its foundation and the laurel wreaths represent excellence. To complete the symbol, it has at the bottom the motto '*Ut tensio sic vis*' what means: the extension is proportional to the force, from the famous Hooke's law for a spring.



Figure 2: Seal of Polytechnique Montréal

Located on the north face of the Mount Royal, the school has different pavilions such as the Lassonde Pavilions or the J.- Armand-Bombardier Pavilion, or the ANDRE-AISENSTADT Pavilion. During this internship, the work has been performed in some of these buildings, and most of the time in the Main Pavilion, which is the oldest and largest. Specifically, the experimental part has been performed in the lab called 'Fluid-Structure Interaction Laboratory'. Professors and researchers study in this laboratory different vibratory phenomena induced by the influence of the fluid on the structure. Consequently, it contains a series of devices where the fluid flows at a certain speed in liquid, gaseous or both states, giving way to a biphasic fluid. Most of these devices operate in high-pressure conditions what makes necessary to work with some clear and specific security measures.

In this type of laboratory, one of the main problems is fluid leaks, such as water leaks. When a new experiment is being set in the lab, it is necessary to pay close attention to the design of the experimental model that is going to be tested to avoid any problem related to leaks. The lab is divided in 4 parts. Inside the 1st part there is a water pump connected to a channel with biphasic flux (water and air) flowing through the section to study the interaction of this type of flow in cylindrical structures. Also, there are two high precision 3D printers that have been used to build the experimental model for this internship. In the 2nd part of the lab, there is a wide variety of general laboratory tools such as screwdrivers, wrenches, files, drills, clamps etc. In this section there are also two water channels, one of them will be used in this experiment. Inside the 3rd section of the lab there is a wind tunnel with a cross section of 60 x 60 cm² and finally in the last 4th part of the lab there are different machines to test fatigue applying high temperatures.

1.2 Explanation of the HCHE

The main object of study of this project is the helical coil heat exchanger (HCHE) which is a common type of heat exchanger used nowadays for different cooling systems in several industrial sectors. Some examples of its utility are seen in the automotive sector, in food production plants or in renewable energy systems. There are several reasons why HCHE are widely used. The first reason of its widespread use in the industry is the highly efficient use of space. This is due to its coil shape. These heat exchangers can have a bigger heat exchange

surface in a reduced space, which allows its use in many areas where space is limited. Another important point is that these heat exchangers are useful if any of the fluids that produce the thermal exchange inside has multiphase states (gas, liquid), since its helical shape avoids in long term the pipe plugging.

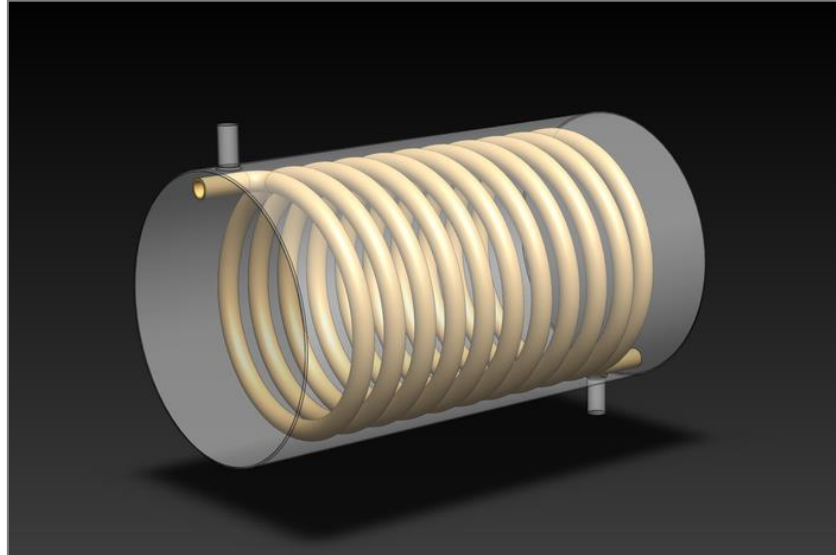


Figure 3: Example of Helical Coil Heat Exchanger (HCHE)

The performance of the HCHE is based on the thermal exchange between two fluids. One of the fluids, the coolant, flows through the interior of the helical tube. It enters the tube at low temperature and it comes out the heat exchanger at high temperature. In fact, in the last part of the helical tube, the fluid may be in a gaseous state performing a diphasic process. The second fluid that takes part in the process, it passes through the exterior part of the coil at a certain speed in order to cool down. Thereby, the heat exchange is produced through the surface of the helical tube. During this process the exterior fluid is transferring the thermal energy to the coolant to have a reduction of the temperature.

The movement of the two fluids around the exchanger produces a physical interaction with the structure which translates into a series of repetitive vibrations (Grant, 1980). After some operating time of the HCHE, these structural vibrations around the coil can produce fatigue phenomena in the system. If these vibrations are not reduced, they can produce serious damage in the structure managing to break it after long periods of time (Yuan et al., 2017)

Furthermore, another important problem related to the possible damage of the structure due to the structural vibrations is that in some systems of HCHE, the external fluid and the internal one can react chemically. One example of this reaction happens with the use of water as refrigerating fluid and liquid sodium (Na). These two fluids could come into direct contact if any fissure in the structure is created, for example due to fatigue. The consequences of this contact produce an exothermic reaction that damages the exchanger making it totally useless, with no operating capacity.

1.3 Objectives of the project

In order to study the phenomenon of the vibrations produced in the tubes of the helical coil heat exchangers, this project has two main objectives:

- i. To design a valid model of helical coil heat exchanger and to manufacture it in order to test it experimentally.
- ii. To study the flow-induced vibrations produced in the structure due to the external flow, using the designed models.

In the first objective, in order to design and manufacture the helical coil model, a wide bibliographical study has been performed to understand better the necessary conditions to produce flow-induced vibrations. In this way, it has been necessary to choose several characteristics as the material or the manufacturing process as well as to design the helical support structure to firmly hold it inside the test chamber. Then, different prototypes have been made with different geometrical parameters to be able to analyse how the flow-induced vibrations vary. Another important part of this first objective has been to select the flow-channel to perform the experimental tests in order to determine the geometrical parameters of the prototypes.

Once the first objective was achieved, the designed prototypes have been studied experimentally to achieve the second main objective of the project. The natural frequencies have been first analysed and then tested in the selected flow channel to study the flow-induced vibrations produced in the structure. A photoelectric sensor and a high-speed camera have been used as experimental analysis devices. A MATLAB code has been developed in order to analyse the images from the flow-induced vibrations taken by the high-speed camera.

Both objectives are closely related and the correct achievement of one of them allowed to succeed in the other one and vice-versa.

2. Background – Study of the phenomenon

To get closer to the origin of the fluid-structure interactions phenomena in the HCHE, first, it is necessary to do a bibliographic research to understand better how it works and the conditions that must be applied. A fluid-structure interaction (FSI) is the interaction produced between a movable or deformable structure which is in contact with a fluid flow (Païdoussis et al., 2011). These interactions are very diverse, and they can be stable or oscillatory. The encounter between the fluid and the structure produces a series of forces and stresses in this last one that can carry out deformations of different degrees. Thus, an FSI considers the laws from the fluid dynamics that describes the motion of fluids, such as liquids or gases and couples them with the laws of structural mechanics.

In fluid-structure interactions, the forces applied on the body can make the structure behave as a single rigid body or in the other hand it can produce deformation in some parts or along the entire body (Zienkiewicz et al., 2014). In the domain of aerodynamics, the clear example of this type of interactions is the aero-elasticity theory which considers the relation between the air and a solid, like a wing of a plane.

In the domain of this project, as said in the introductory part, the experimental study is on the external fluid of the heat exchanger that passes through the coil at a certain velocity. Considering this fact, it is possible to observe different phenomena related to fluid-structure interactions (Kaneko et al., 2013). The first possible phenomenon is the vortex shedding, which is, as its name indicates, the interactions produced by the creation of vortices or eddies in the fluid due to the existence of a structure in the flow. Other phenomenon is the fluid-elastic instability which is a type of instability that occurs after a certain point of cross flow velocity. This last instability tends to produce an oscillatory response that increases exponentially the vibrations on the structure. There exist other types of phenomena related to FSI as for example: turbulent buffeting, parallel-flow eddy formation, and acoustic vibration.

Nevertheless, the different interactions named above are diverse and completely different in terms of the type of influence that they exert on the structure. This project is focused on the first phenomena, the vortex shedding one. This selection of the focus has been chosen since the conditions applied during the experiment are the ones close to the vortex shedding. In the case of the fluid-elastic instability phenomenon it is required a higher flow velocity in order to produce it.



Figure 4: Experimental case of Vortex shedding in a cylindrical tube

In this way, the bibliographic research has been focused on the interactions between a structure and a crossflow. If the Reynolds Number is considered:

$$Re = \frac{(\rho * U * L)}{\mu}$$

On one side for low Reynolds Numbers the boundary layer tends to adapt to the geometry of the object through which flows. On the other side if the Reynolds Number is large enough the dynamic effect of the flow has a greater influence on these interactions than the viscosity effect. When the dynamic effect of the flow takes a major importance, it produces a series of vortices with the passage of the fluid around the structure, due to the detachment of the boundary layer in some regions.

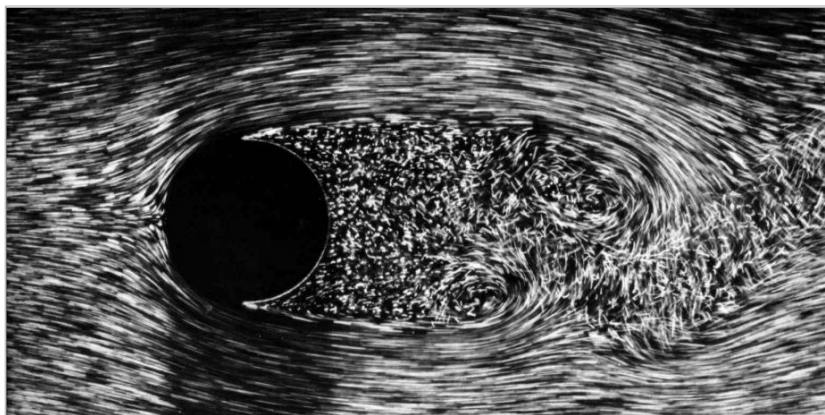


Figure 5: Detachment of the Boundary layer in a cylinder

One of these interactions is the vortex shedding phenomenon. Analysing the case of one unique cylinder studied by the mathematician and engineer Theodore von Kármán among

others (NASA archives, 2016), the cylinder tends to move towards the low-pressure zones created by the vortices. In the vortex shedding it is important to differentiate between two variations of this phenomenon. These variations are related to how vortices break off. The most common one is the Kármán vortex shedding in which the vortices are detached from the rear part of the object alternatively from each of its sides. The other type of vortex shedding is the symmetrical one, in which the vortices are detached at the same time from both sides, giving way to a symmetrical shape (Figure 6).

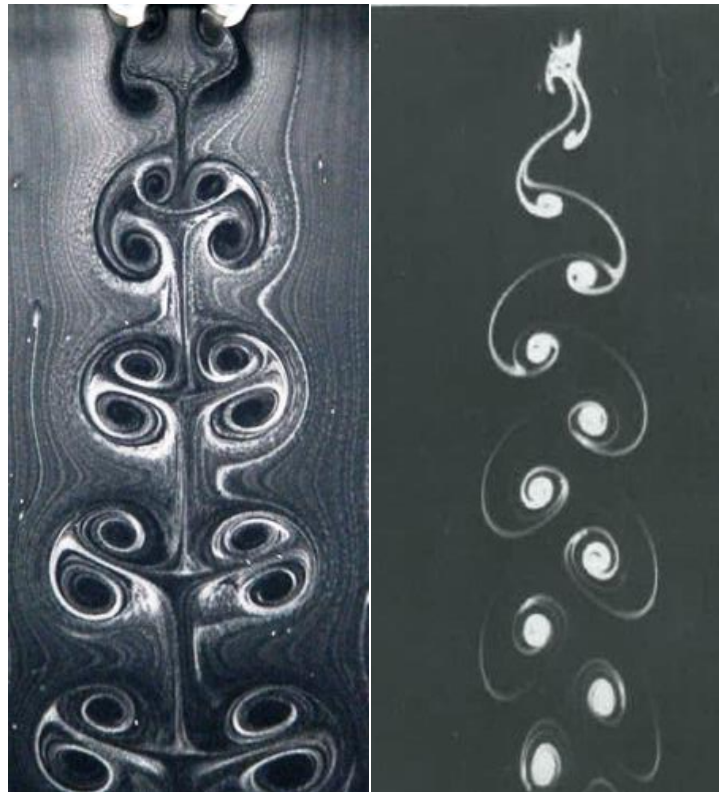


Figure 6: Two variations of Vortex Shedding: Symmetric (on the left) and Kármán (on the right)

There is a well-defined type of forced vibrations produced by vortex shedding which normally can act in two different directions, traverse and parallel to the flow. In the transverse direction the vibration is led by a frequency called the Kármán vortex shedding frequency (f_w). In other words, this last frequency is the one at which the vortices detach from the tube walls. In the same way, for the parallel direction of the flow there is a frequency which normally is twice the Kármán vortex shedding frequency (Kaneko et al., 2013). These two frequencies are clear in a simple experiment with a single tube. In the case of this project, the experimental tests are trying to show a similar relation between the frequencies of the helical structure and the direction of the flow.

$$f_w = St * \frac{U}{L}$$

This Kármán vortex shedding frequency is defined by the dimensionless Strouhal number (St). As shown above the frequency is proportional to the flow velocity (U) and the characteristic length (L) of the object. In this case, the characteristic length for a tube is the diameter. The Strouhal number is important in all fluid-structure interactions since it is proportional to the frequency. Furthermore, the Strouhal number has a direct relation with the Reynolds Number, since in both numbers, the flow velocity and the diameter of the tubes are present. If the definition of the Reynolds number is considered, it is easy to see that for the same tube, if the flow velocity increases, the Reynolds increases proportionally to it. As it is shown in the next graphic the relation between Reynolds and Strouhal numbers has different phases well differentiated.

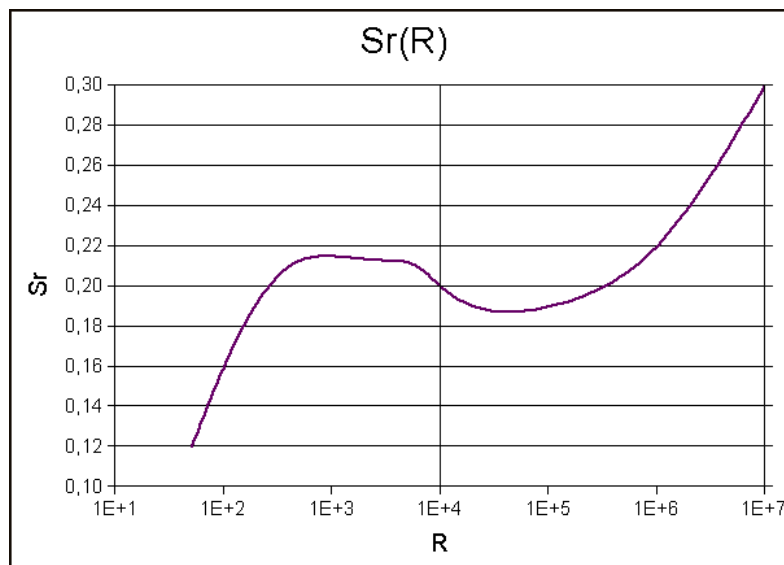


Figure 7: Strouhal number (Sr) as a function of the Reynolds number (R) for a cylinder

From this last relation between both dimensionless numbers, it is deduced the next important fact: the frequency of the vortex shedding should vary in a similar way as it does the Strouhal number, since it is proportional to it. The behaviour of the Strouhal number at low Reynolds it could be considered linear but after some point (0.22), it is not linear along all the spectrum. As it is shown in the Figure 8, the vortex shedding phenomenon appears at a certain velocity and it increases the vibration till a peak where the vibration amplitude is maximum (Païdoussis et al., 2011). If the velocity continues to increase after this peak, the vibratory effect decreases considerably to a lower amplitude where it remains constant for a range of velocities. Along this interval of velocities, a new phenomenon of fluid-structure interactions begins to have much more importance than the vortex shedding. This new phenomenon is the one mentioned before called fluid-elastic instability. This last instability is produced at a higher flow velocity than the vortex shedding and as it shown in the graphic, it produces an exponential increase in the vibration of the structure while increasing velocity.

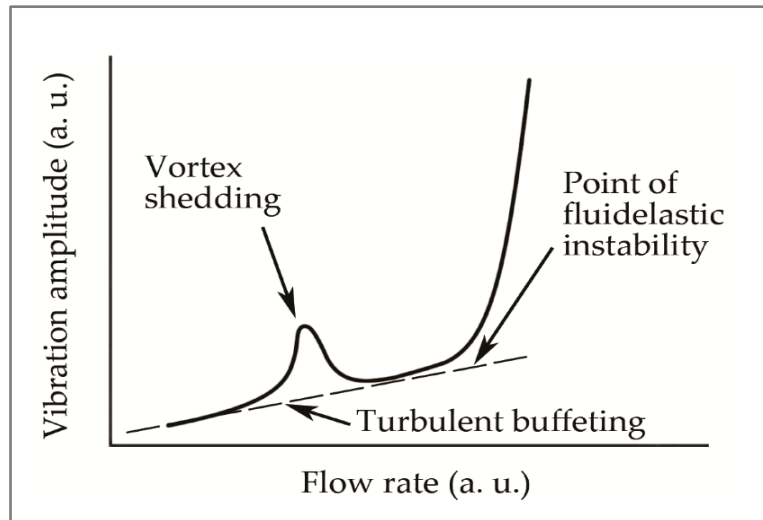


Figure 8: Vibration amplitude of a tube in a bundle as a function of flow-rate (Païdoussis et al., 2011)

As it is shown above, the fluid-elastic instability could be a really damaging disturbance since the vibration amplitudes can become much higher than those produced by the vortex shedding if the velocity continues increasing. This can cause a break in the structure in a short period of time. Nevertheless, to reach the point of fluid-elastic instability it is necessary a high flow velocity (flow rate in the Figure 8). In this project, the maximum velocity applied is going to be smaller than the one necessary to produce this last instability.

Refocusing on the vortex shedding effect, which is the one present in the experiment, it doesn't always behave in the same way. An important variety of the vortex shedding phenomenon is the synchronization of the natural frequency of the structure, in this case the helical structure, with the frequency of the vortex shedding; this frequency matching phenomenon is known as 'Lock-in' (Ziada, 2006). In the same way as for the standard phenomenon of vortex shedding it can occur for the two directions compared with the sense of the flow. It is important to mention that this synchronization is related to the density of the moving fluid. If this density is low, for example a gas, the effect of synchronization may not occur. This fact is quite important when choosing the type of flow channel before performing the experiment.

The Lock-in phase starts at a flow velocity known as critical flow velocity. At this flow velocity, the vortex shedding frequency is quite close (a little bit lower) to the natural frequency of the structure. The synchronization of both frequencies remains during an interval of velocities known as Lock-in range, where both frequencies are quite similar (Païdoussis et al., 2011). During this interval there is a coupling between the two frequencies that produces an even greater vibration than with the simple vortex shedding phenomenon. If this phenomenon of synchronization is exerted on a real case of helical coil heat exchanger, the structure could develop long-term fatigue problems due to the vibrations on it.

3. Project methodology

3.1 Applied hypothesis

In order to perform this project, some hypothesis have been considered:

- Due to the particularity of the helical shape of the heat exchangers, the knowledge applied to study the fluid-structure interactions is based on simple shapes such as cylindrical tubes. Thus, in order to understand how the helical structure reacts to the flow, the theories and equations are the ones previously used on cylindrical tubes in other experimental studies.
- In order to perform the experimental study in this type of devices, it is assumed that the flow of the test chamber has similar characteristics to the external flow of a helical coil heat exchanger.
- The influence of the temperature changes inside the heat exchanger on the flow-induced vibrations is neglected.
- The influence of the movement of the internal flow inside the tube of the helical coil is not considered in the calculations, the design of the prototypes or the experimental results.

3.2 Theoretical knowledge and first calculations

As explained in the background, the main phenomena of flow-induced vibration that appears in this study is the vortex shedding. Considering the synchronization of the natural frequency of the object with the frequency of the vortex shedding (f_w), larger vibrations are produced. This last frequency, as shown before, is calculated with the Strouhal number. Using the theory of vortex shedding for a circular cylinder it is known that the strouhal number should have a value between 0.20 and 0.22 (Païdoussis et al., 2011). As shown in the Figure 7 with the relation between the Strouhal and the Reynolds number, this value of the Strouhal number corresponds to an interval of the Reynolds number between 40 and 10^6 .

Thus, to assure that the phenomenon of synchronization of frequencies is produced there are two necessary conditions that must be satisfied (Kaneko et al., 2013). The first condition is the one related with the natural frequency of the object. This natural frequency (f_n) should be like the vortex shedding frequency (f_w) to produce the effect of resonance. The second condition to make frequency synchronization possible and to produce the explained Lock-in phenomenon is related with a dimensionless parameter called Beta. This last parameter can be understood as a reduced damping and it is composed by the product of a constant and two other parameters, one of them related to the mass of the system (χ) and the other related to the damping (ζ) of it. In order to study the synchronization phenomenon and to produce the resonance conditions, this Beta must have a value smaller than 0.4. So, the two necessary conditions that have to be accomplished are:

- 1) $f_n \approx f_w$
- 2) $\beta = \gamma * 2\pi * \zeta \leq 0.4$

The second condition is quite important in order to design a valid structure to study the phenomenon. First, if the mass parameter Gamma (γ) of the Beta is considered:

$$\gamma = \frac{\text{Structural Mass}}{\text{Fluid Mass}} = \frac{m_s}{\rho_f * D_t^2}$$

This last one is a ratio of the structural mass to the fluid mass. In the formula, the ' ρ_f ' is the fluid density and the ' D_t ' the exterior diameter of the tube. The parameter ' m_s ' is the longitudinal mass of the structure and its units are [Kg/m]. This longitudinal mass is calculated dividing the total mass of structure by the total length of it:

$$m_s = \frac{m}{L}$$

The other parameter that composes 'Beta' is Zeta (ζ), the one related with the damping phenomenon of the vibration:

$$\zeta = \frac{C}{2 * m_s * w_n}$$

Where the ' C ' is the damping constant for the system and ' w_n ' is the natural frequency of the structure:

$$w_n = \sqrt{\frac{k}{m}}$$

Being ' k ' the rigidity constant and ' m ' the mass of the tube. If this method is applied to the helical structure, there are some parameters that are unknown. For example, to obtain the damping coefficient Zeta, the value of ' C ' is unknown due to the complexity of the structure of the helical heat exchanger model, which is not such standard as it could be a simple tube. Looking in the bibliography for a good value of Zeta it is possible to find that a good assumption for the damping coefficient is between 0.5% and 1%, so it is taken 0.75% (Jong Chull Jo and Myung Jo Jhung, 2006). This value considers that the structure has a good fixation and that all the support points of the structure are well designed. In this case, it is possible to consider this low value of damping. For this reason, the design and manufacturing of the structure, it is an important factor to get correct results.

Now, the parameter left to obtain the Beta is the one related with the mass, the Gamma. This Gamma has a part related with the mass of the object and another part related with the fluid.

This last factor is the one that helps to choose the type of fluid used in the experiment, the type of structural material as well as to define geometrically the model.

Starting with the mass of the helical structure, the next formula of the length of a helicoid is applied in order to obtain the mass:

$$L_{hel} = N * \sqrt{h^2 + (2\pi * R_h)^2}$$

Where 'N' is the number of revolutions of the helicoid, 'h' is the height of a revolution and 'R_h' is the helical radius. Then, applying the next formula is calculated the mass of the helicoid considering that it has a tubular section with a hole in the centre where the fluid would flow through as it would have a real heat interchanger:

$$m_{hel} = \rho_m * L_{hel} * \pi * \frac{D_{tExt}^2 - D_{tInt}^2}{4}$$

Where 'ρ_m' is the density of the helicoid material and the 'D_{tExt}' and D_{tInt}' are respectively the exterior and interior diameters of the tube. Using this last two formulas about the length and mass of a helicoid, and substituting them in the original formula of Beta, the next equation for the Beta on a helicoid with cylindrical section is obtained. It is interesting the fact that the variable of the helical length disappears when simplified with the last two formulas obtained. This fact reduces the parameters of the helicoid that influence the value of Beta, since for example the total height of the helicoid or the helical radius are simplified:

$$\beta = \gamma * 2\pi * \zeta = \frac{2\pi * \zeta}{\rho_f * D_t^2} * \frac{m_{hel}}{L_{hel}}$$

$$\beta = \frac{\zeta * \pi^2}{2} * \frac{\rho_m}{\rho_f} * \frac{D_{tExt}^2 - D_{tInt}^2}{D_{tExt}^2}$$

As it is easy to see, the Beta parameter depends in the diameters of the tube and the densities of the fluid and the material. This last formula is useful to choose the type of flow channel that is going to be used. In the laboratory there are two possible fluids, air and water. Each flow channel has completely different dimensions being the wind tunnel bigger than the water tunnel, what means that if the experiment is performed in the wind tunnel the structure should be bigger.

Before proceeding with the next studies, it is important to add a condition related to the comparison hypothesis between a helicoid and a set of tubes. When talking about the interactions between the flow and tube bundle in parallel position, the ratio of the distance among tubes to the tubes diameter is a parameter to consider (Olala, 2016). In order to produce the vortex shedding phenomenon along all the tubes it is required a minimum ratio of 1.75. For the case of the helicoid, this ratio is respected in all the prototypes that are tested

experimentally, considering the distance between tubes as the distance between each revolution of the helicoid.

3.2.1 Parametric Study of Beta

Using MATLAB code to solve the last Beta equation it allows to understand the behaviour of this parameter in relation with geometrical conditions of the helical structure. First, it is used air as a fluid with a density of 1.225 Kg/m^3 . In the next graphic the geometrical parameter that varies is the external tube diameter, remaining constant the tube wall thickness with a value of 4 mm. Furthermore, the Beta equation is solved for two possible materials of construction: copper with a density of 8960 Kg/m^3 and PVC Plastic with a density of 1360 Kg/m^3 .

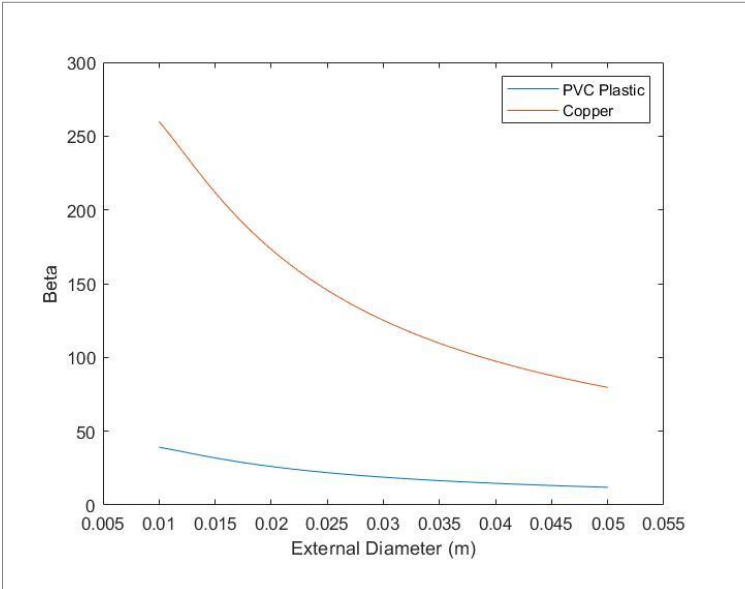


Figure 9: Beta as a function of the external diameter in air flow with constant wall thickness

As seen in the Figure 9, the Beta decreases when the tube diameter increases. Furthermore, the Copper (red line), due to its higher density, has a considerably larger Beta than the PVC.

Another way of analysing the Beta is studying it in relation to the change of the tube wall thickness. Just below, it is presented the graphic for the same two materials. In this case it is considered a helicoid with a constant external tube diameter of 15 mm and again using air as a fluid. The interval of the wall thickness considered is between 1.5 mm and 7.5 mm.

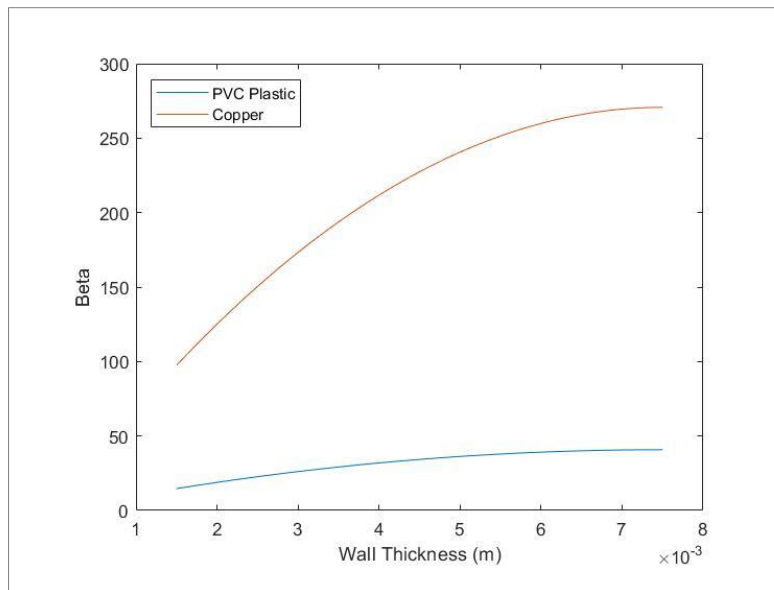


Figure 10: Beta as a function of the wall thickness in air flow

As it shows the Figure 10, the increase in the wall thickness produces an increase in the Beta parameter too, till the point where the tube is completely solid with no interior hole in the centre. In the graphic, this point is reached when the wall thickness is the maximum (7.5 mm), since the internal diameter of the tube is 0.

After seeing these two variations of Beta using air, Beta is still too high. As said before, the second condition for the frequency synchronization phenomenon to occur is that Beta should be lower than 0.4. However, for the analysed cases, the copper has a Beta value between 50 and 300 and the PVC plastic between 10 and 50. So these calculations are still two orders of magnitude above the target value (0.4). This means that using air as the experimental flow it wouldn't let the phenomenon of synchronization occurs, since the second condition is not reached.

Now, the same calculations are shown using water, considering the water density as 997 Kg/m³. Using the same geometrical relations of the helicoid as for the air, the next graphics are obtained. First, taking the external diameter as independent variable and then taking the wall thickness as the independent one:

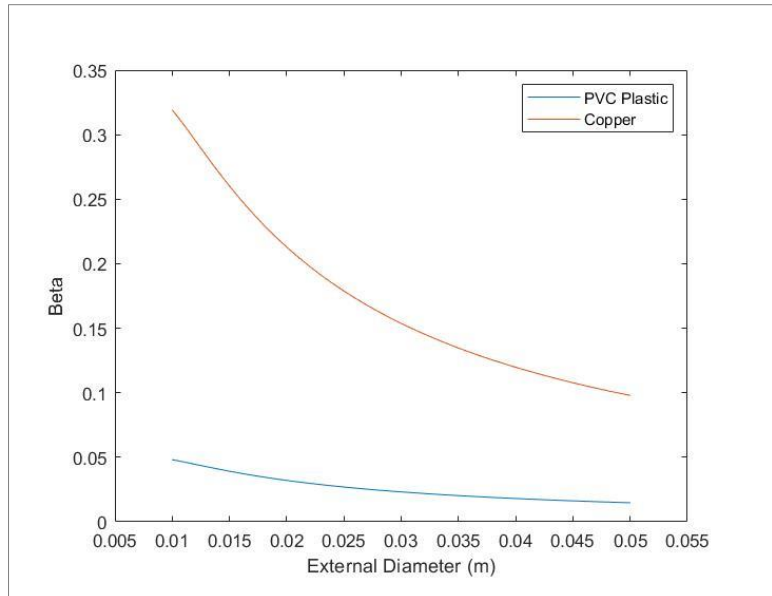


Figure 11: Beta as a function of the external diameter in water flow with constant wall thickness

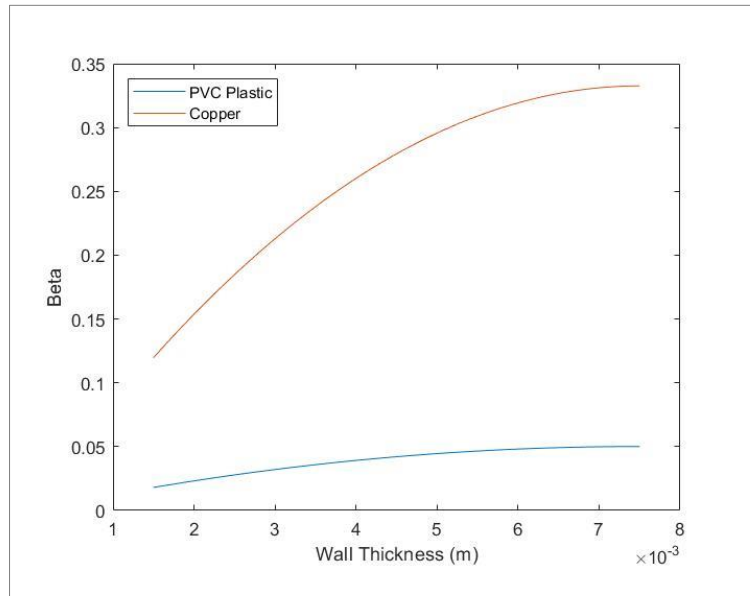


Figure 12: Beta as a function of the wall thickness in water flow

The shape of the graphics is similar to those calculated in water since the Beta parameter varies in the same way. However, if the attention is focused in the vertical axis, the interval of Beta for both materials is under the threshold value of 0.4. This fact allows to predict that conducting the experiment in water, due to its higher density, it facilitates the study of the phenomenon of synchronization of vortex shedding in a correct way. In the corresponding section, all the details about the water channel and the test chamber used in the experiment are given.

3.2.2 Natural Frequency of the Helicoid

As said above, the first necessary condition for the synchronization of the Vortex Shedding frequency with the natural frequency of the helicoid is that both must be similar. Then the lock-in phenomenon appears, and the vibrations of the structure are increased considerably. In this part of the report, the goal is to know how to accomplish this condition through a relation with the natural frequency of the structure and the flow velocity.

As it has been explained in the previous subsection, the fluid where the experiment is performed is water, since the second condition related with the calculation of the Beta is satisfied. Now, talking about the first condition, different calculations have been performed using the corresponding formulas (Kaneko et al., 2013). In this book it appears the next graphic which it relates the normalized amplitude of the vibrations with a reduced velocity (V_r) during the synchronization phenomenon for the case of a cylinder:

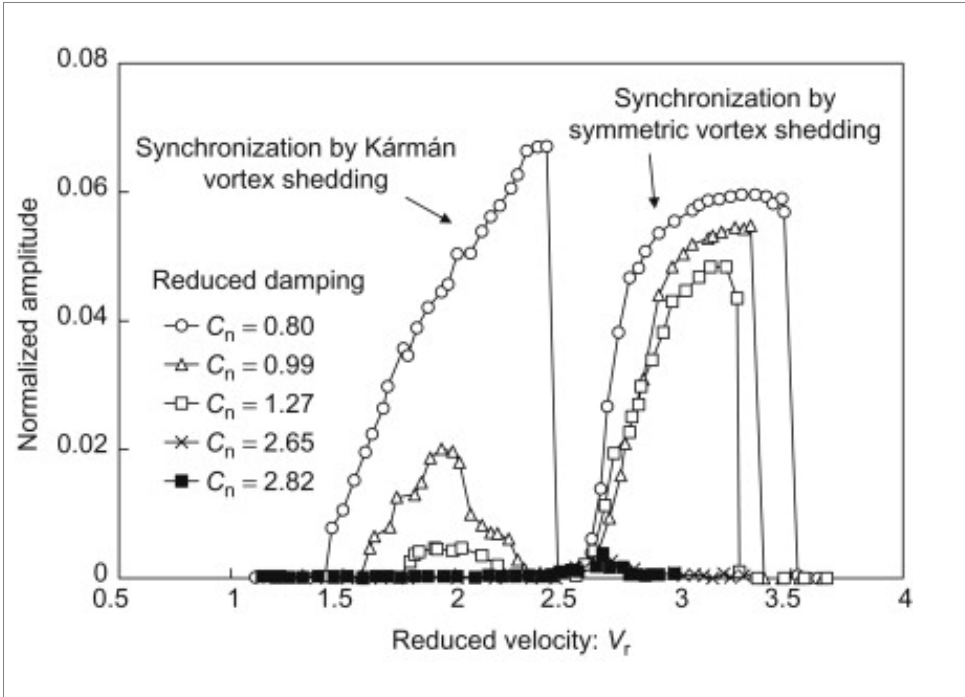


Figure 13: Relation between the normalized amplitude of the vibration and the reduced velocity (Kaneko et al., 2013)

On the left of the graph, it appears a parameter called reduced damping (C_n) which is twice the Beta parameter obtained before. The graphic differentiates between two types of synchronizations. As it is shown, for a Beta equal to 0.4 (C_n equal to 0.8) the amplitude is maximum for both cases. The first type is the synchronization by Kármán vortex shedding. As explained in the introduction, this type alternates the shedding of vortices each time from one side of the cylinder to the other side. This synchronization starts at a reduced velocity of 1.5 and the maximum is achieved before 2.5. The second type of synchronization is produced with the Symmetric vortex shedding. This last type of synchronization needs a higher reduced velocity and its maximum goes from 3 to 3.5 for the case of C_n equals 0.8. To have a better understanding of this last graphic it is necessary to show the definition of the reduced velocity V_r :

$$V_r = \frac{V}{f_n * D_{ext}}$$

Where the 'V' is the velocity of the flow and 'f_n' the natural frequency of the tubes. So here it is shown a useful relation with the natural frequency of the object that is helpful with the purpose of designing a valid helical coil.

Using the SolidWorks software, different helicoids have been designed applying the two different materials used before for the Beta study, copper and PVC plastic. In each design test, some parameters of the helicoid have been modified as for example, the number of revolutions (N) or the tube diameter (D_t), keeping constant other parameters like the total length or the helical diameter. Then, with the same software, it has been performed a frequency study with the purpose of obtaining the natural frequency for each design. To perform this frequency study, the constraints of movement limitation have been applied in the extremities of the helicoid and an automatic mesh has been created before performing each simulation. This software gives information, not only about the first natural frequency, but also from the second vibrating mode till the fifth, including a representation of the vibratory response of the structure for each frequency (Figure 14). The more relevant cases are in the Appendix 3.

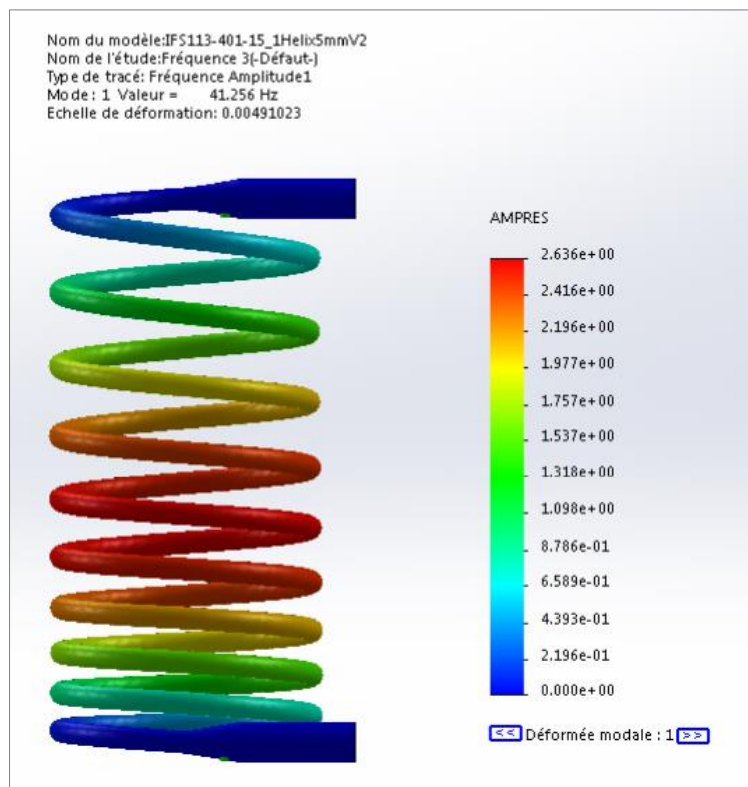


Figure 14: : Example of natural frequency simulation with SolidWorks

Once the computed natural frequency is obtained it can be replaced in the last formula of the reduced velocity in order to know the flow velocity required to produce the synchronization

phenomenon with symmetric or Kármán vortex shedding. In the next table, some of the most representative cases of helicoid designs made with SolidWorks are shown. To calculate the flow velocities, the optimal values of the reduced velocity have been extracted from the last graphic (Figure 13), using a value of 2.4 for Kármán synchronization and a value of 3.2 for symmetric synchronization.

As it is shown in the Table 1, there is a big difference in the frequencies between copper models and plastic models. The frequencies are much higher in the copper ones, partly due to the higher density. This contrast in the frequency also produces a difference in the required flow velocity to reach the two types of synchronizations. The flow velocities are required to be higher in the copper models. This fact is quite important when selecting the definitive material for the prototypes, since the flow velocity is a limiting factor given by the water pump used in the experiment. Thus, as it is shown later in the section 4, the manufacturing material is a plastic like PVC, since the required flow velocities for a metal like copper are above the limit of the available water pump.

Table 1: Different SolidWorks helicoid designs frequencies and flow velocities

| MATERIAL | N | D _t (mm) | Frequency (Hz) | FLOW VELOCITY (m/s) | |
|----------|-----|---------------------|----------------|---------------------|--------------|
| | | | | Kármán VS | Symmetric VS |
| Copper | 5.5 | 7 | 97.09 | 1.63 | 2.17 |
| PVC | 5.5 | 7 | 37.44 | 0.63 | 0.84 |
| Copper | 5.5 | 5 | 70.25 | 0.84 | 1.12 |
| PVC | 5.5 | 5 | 27.08 | 0.32 | 0.43 |
| Copper | 7.5 | 5 | 63.15 | 0.76 | 1.01 |
| PVC | 7.5 | 5 | 24.00 | 0.29 | 0.38 |
| Copper | 9.5 | 5 | 41.26 | 0.50 | 0.66 |
| PVC | 9.5 | 5 | 15.91 | 0.19 | 0.25 |

From this study, it is observed that there is a decreasing in the natural frequency when decreasing the tube diameter. Which allows to predict that to have synchronization of both frequencies, the tube diameter is an important factor to consider. Another important geometrical parameter it seems to be the number of revolutions, since there is a reduction in the natural frequency when increasing this last one. These two parameters are studied in the design section of the prototypes.

3.3 The water tunnel

At the beginning of the project, the initial idea was to test the experiment in a wind tunnel, but after the work and the calculations explained in the last section, the project is performed in water. This is because the water density is high enough to induce the phenomenon of synchronization of the helicoid's natural frequency with the frequency of the vortex shedding. This initial change in the project planning has meant an adaptation of the measures of the experiment to the ones of the water tunnel.

One of the main parts of the water tunnel is the test section where the designed prototype remains attached during the experiment:

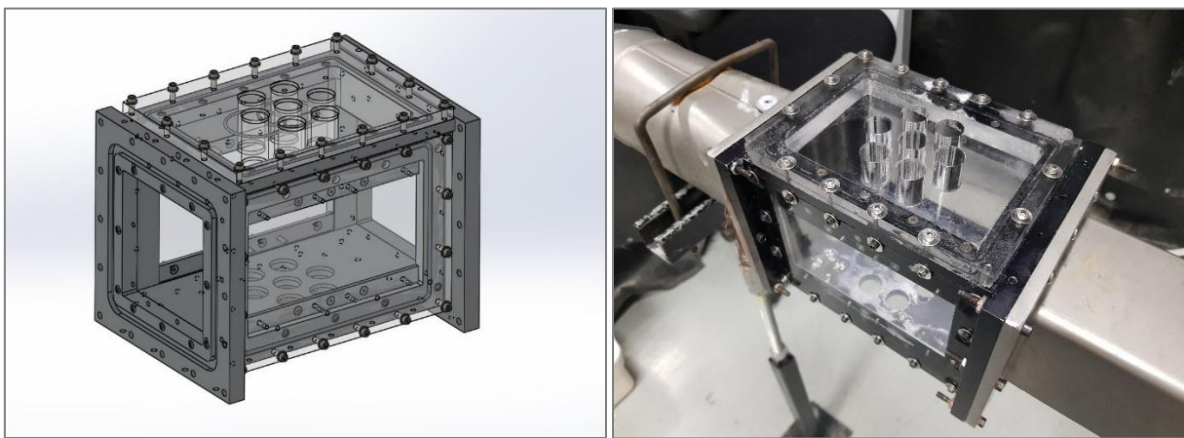


Figure 15: SolidWorks design of the test chamber and real test chamber

As it is seen in the model of the test chamber, the core structure is a metal box open on all sides except the bottom part. It is made of aluminium to avoid any possible deformation or leaks due to high internal pressures during the experiments. The inlet and the outlet of the chamber have a square section of 100 mm each side. Then, there are two transparent side walls and a top one that close the system, all three rectangular and made of PMMA or Plexiglass. In the upper and lower sides there are 7 coaxial holes. These 7 cylindrical holes were part of a previous experiment. Because of this, it is necessary to adapt the design of the prototypes and to avoid water leaks from the holes. Moreover, as explained below in the prototype design section of this report, 6 of the 7 lower holes are used for the attachment of the support structure.

The measures from the test chamber of the SolidWorks model have been useful for the design of the prototypes. They have been compared with the calliper of the real chamber to assure that they are the same. The rectangular base surface where the helicoid is attached is 100 mm x 155 mm and the lateral transparent walls from which the helicoid is analysed are rectangular windows with the same measures. Each part of the test chamber is well screwed with several bolts and the core metallic structure has a groove in each side (inlet, outlet and the 3 plexiglass walls) to insert a plastic rubber that helps to produce a hermetic closing.



Figure 16: Pump water of the water tunnel

The system is also composed by a water pump. The input of this motor is introduced in Hz in order to measure the revolutions of it and it goes from 6 Hz to 60 Hz. Just after the power unit, there is a flowmeter that shows the volumetric flow rate in litres per second (L/s). For the maximum value of revolutions (60 Hz), the flowmeter shows a maximum flow rate of 5.2 L/s. Finally, there is a big water tank which contains the water that passes through the motor and through the whole system. All the mentioned components are connected with a series of pipes and valves that prevent any type of water leakage.

3.4 Experimental analysis devices

3.4.1 High-speed camera

The camera model used in the experiment is the 'MotionBlitz Cube', a type of high-speed camera with internal memory. The maximum resolution is 1696 x 1719 pixels and the maximum capture speed with this resolution is 523 fps during a recording time of 13 seconds. However, if the camera resolution is reduced then it is possible to increase the frames per second and the recording time, being possible to change these three parameters depending on the recording needs.

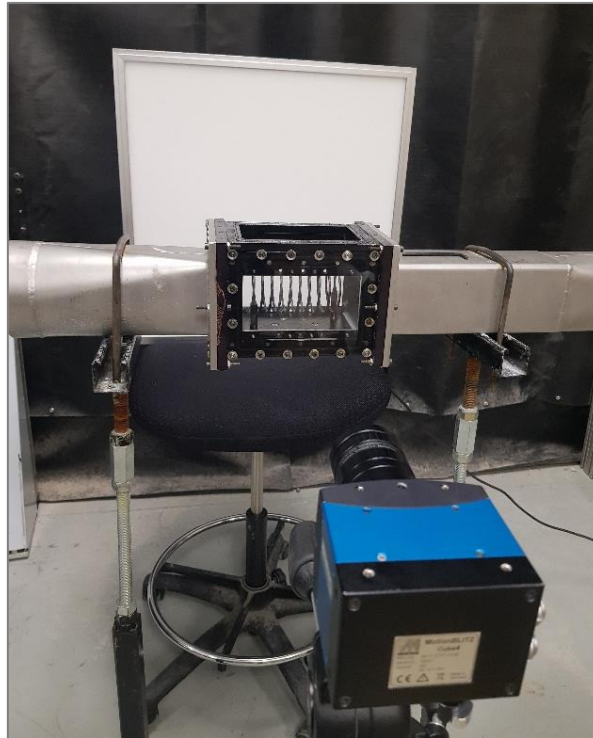


Figure 17: Setting up of the high-speed camera used in the experiment

In the setting up, a dimmed white light is used behind the test chamber to provide enough light level and thus take sharp pictures. The camera is placed just in front of the test chamber and perpendicular to the structure at the same height level. Once the camera is connected to the computer it is possible to use its own software in order to adjust different parameters of the recording such as the fps, the number of pixels or the recording time. Before the recording, the live mode of the camera is used to watch how the images are being taken and to improve the quality of these, selecting the light level and focusing the image as well as possible.

3.4.2 The MATLAB code to analyse the images

The data obtained from the high-speed camera is saved in “.bmp” format which keeps each image separately. A MATLAB code has been written to analyse each one of these images. This code has different sections that are explained just below. The objectives of the code are to visualize each one of the images individually and to define a set of points along the structure in order to obtain different information about the movement and the vibratory behaviour of the helicoid. Finally, with all the images analysed, several descriptive results of the vibrations are obtained, and a video of the movement is created.

Going deeper through the code, first of all, different parameters are defined: the diameter of the helical tube in meters and in pixels (to obtain the ratio between them), the number of pictures analysed and the sampling frequency (FPS) of the camera which is 600 Hz. To choose this sampling frequency, the Nyquist's Theorem has been applied. This theorem states that in order to represent a wave and avoid the aliasing effect, the sampling frequency of the sensor must be twice the signal frequency (Baker, 2013). So, if the sampling frequency selected is 600

Hz, the maximum frequency processed is 300 Hz, which is large enough to cover the frequencies of the designed helicoids.

After that, each image is loaded through a 'for' loop, applying a black and white filter to increase the difference between the white colour of the light and the black colour of the helicoid using the MATLAB command 'imadjust'. The filters used have been the ones tested in other similar experiment done in the lab. In the original image, there is a small enlargement of the tube diameter due to a smaller difference in the shades of grey and also, it has small grey spots that could affect the subsequent analysis of the images.

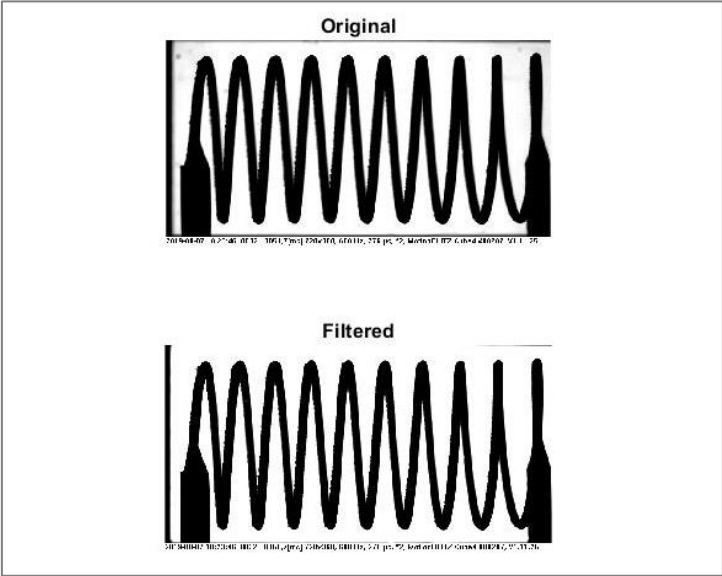


Figure 18: Original image (on the top) and filtered image obtained from the high-speed camera

Then, in the next loop of the code, the analysing method is performed. As explained before, the method is based on determining certain points of the structure. The chosen points are each one of the pixels that form one of the revolutions of the helical silhouette. These troughs have a V-Shape as shown in the following image:

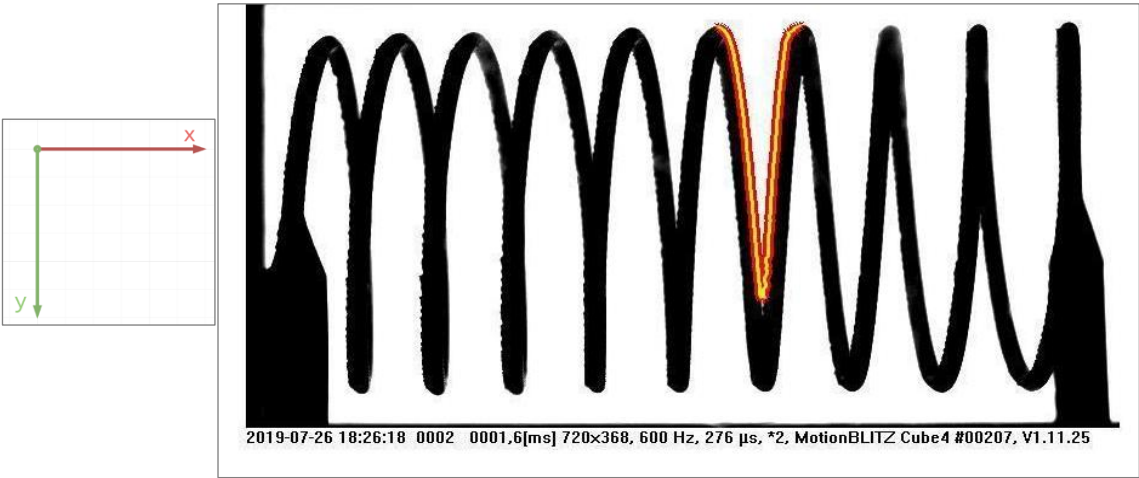


Figure 19: Example of V-shape detected by the MATLAB code along the helicoid

The analysed image is represented as a matrix of pixels where the black colour from the helicoid has the index “0” and the pure white colour from the free space takes the index “255” with all the intermediate numbers as different shades of grey. To define each point of the V-shape it is necessary to set a colour threshold with a certain index. This threshold allows to analyse the image and to choose which points correspond to the structure and which to the free space. For this experiment, the threshold selected (160), has been chosen based on other past experiments and after testing different index.

If the analysed pixel has an index lower than the threshold then the code considers it as part of the structure. On the other hand, if the index is higher than the threshold, then it considers it as free space. The method used to characterize the V-shape is based on a horizontal sweep from an initial point which is defined manually with its coordinates. This initial point must fulfil two conditions. The first condition is that it must always be free space, which means that the point index is over the threshold or simply being white (0). The second condition for this point is that its position must be placed between 2 revolutions. As it is shown in the Figure 20, there are three selected pixels with different grey index. The left one has an index of 112, which is under the threshold, so it is considered as part of the helicoid. The intermediate pixel, which is in the free space (index of 255) and it is between 2 revolutions, so it could be an initial point to perform the method. Finally, the point with an index 0 is completely black and part of the structure too.

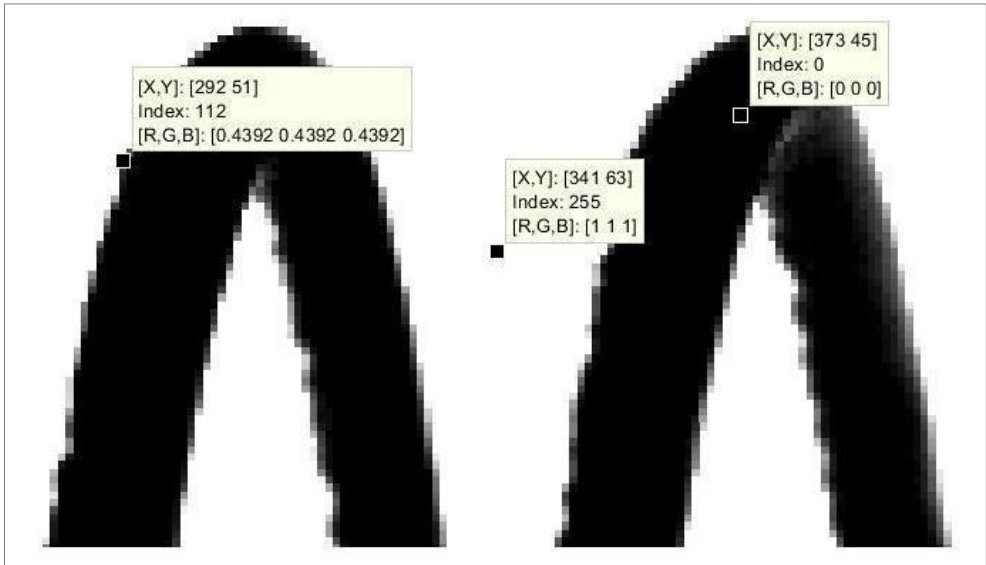


Figure 20: Example of three pixels of a helicoid image with different grey index

In the method to characterize each point of the V-shape, the code is moving horizontally to the left and to the right along the pixels of the image starting from the selected central point. The scanning in both directions is performed until a lower threshold index is reached. So, at the end of this sequence a pair of points are obtained, one on the left and another on the right, each point defining the silhouette of the V-shape. Then, the code does an average to re-centre and recalculate the central starting point and it repeats the same process a row of pixels below. The average done is used in fact to avoid having the central starting point as a

black point from the structure, maintaining the two necessary conditions, explained above, for this point. So, in each iteration one row down, the central point is recalculated in order to reach until the lowest point of the V-shape.

$$Pt_{Central}(y + 1) = Pt_{Left}(y) + \frac{Pt_{Right}(y) - Pt_{Left}(y)}{2}$$

If the last average it wouldn't be applied, when descending each row it could happen that when the analysis is near to the lowest point of the helicoid, the central point could be already part of the helicoid, so the code would act as if the lowest point has been reached. Using this average to recalculate each central point allows not to arrive to a black pixel from the helicoid before finishing the 'V'.

Once the lowest point of the V-shape is reached, what means that the central point has an index under the threshold, the same process is performed but in the other sense, upwards. Starting from the first central point selected at the beginning, the code selects each one of the points from the helicoid, on the left and on the right until it reaches the last two maximum points above the V-shape. In the same way, these two points are the last ones having an index lower than the threshold. These points are the highest points of the structure along the two studied revolutions of the helicoid.

It is important to say that the two last points obtained are being used to calculate the different parameters of displacement, velocity and frequency. The use of these two points instead of any other from the obtained along the 'V' is because of the 3D vibratory movement of the structure. The images taken by the camera are in 2D in a plan parallel to the direction of the flow. If, instead of using these maximum points, two of the central points from the 'V' were used for obtaining the results, they would produce an important error since in each photo of the movement the two points analysed would be different points in the structure in 3D. So, using the maximum points allows to minimize this error since the highest point of the structure remain the same no matter from what angle the picture is taken or in what part of the movement the image is taken.

Before continuing with the last part of the code it is important to show that if the initial central point, that is chosen manually, is selected wrong because it does not meet any of the conditions, an image similar to the following shows up to advice that there has been some problem with the characterization of the points. As the Figure 21 shows, the V-shape is not well created.

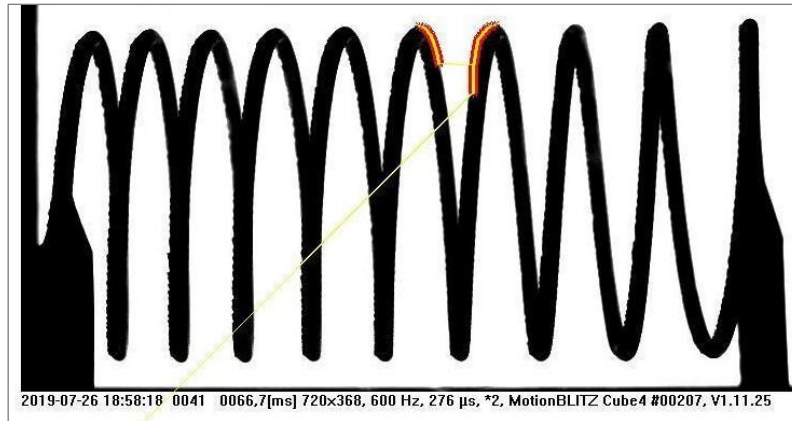


Figure 21: Example of a bad selection of the initial central point in the MATLAB code

To perform the graphic analysis of the structural movement, the position of the two highest points is used in order to obtain the displacement of these points along the time. First, it is necessary to reconvert the measures of the displacement from pixels to meters. Therefore, using the ratio of the diameter of the helicoid in meters to the same parameter in pixels (17 pixels for 3 mm diameter, 29 pixels for 5 mm diameter and 36 pixels for 7 mm diameter), it is possible to obtain the real values for the displacement in meters and to plot the results. To obtain the plot of the displacement velocity the procedure is the same, considering that the value for the displacement in each image is divided by the time step.

Using the obtained displacement, the frequency spectrum of the structure vibration is obtained using the Fourier transform. The displacement function (in the time domain) is transformed to a frequency function with complex values. The magnitudes for the different frequencies are considered as the amount of each frequency in the real displacement function. For this project, it is used a particular type called fast Fourier transform (FFT), which computes the discrete Fourier transform of the displacement variable, using an FFT algorithm ('Fast Fourier transform', n.d.). This algorithm manages to reduce the complexity of the data matrix, increasing the computing speed. To avoid noise problems when using the FFT, it is better to subtract the average of the displacement along the entire movement as it is shown in the MATLAB code in the appendix.

In order to obtain the frequency spectrum in another way and to compare the one obtained with the FFT, it has been applied another method commonly used in this field called 'power spectral density' (PSD). This is a complex method that translates the signal, in this case the displacement along time into a power distribution of the frequencies of this signal. The PSD is generally used when analysing a random vibration signal, for example when turbulent phenomena appears. It takes the amplitude of the FFT and uses the complex conjugate in order to normalize the signal. The units of the PSD generally are the squared signal units over frequency units, in this case squared length units over Hertz (mm^2/Hz) (Bendat, Allan G. Piersol, 1991).

In addition, a last method of analysing the displacement due to the vibrations is the root mean square (RMS) which is a mathematic tool quite used in the turbulence field:

$$x_{RMS} = \sqrt{\frac{1}{N} * (x_1^2 + x_2^2 + \dots + x_n^2)}$$

Where 'N' is the total number of values, and 'x_n' are each of the displacement values obtained from the MATLAB code. The RMS gives a value for the vibrations of each experimental test. This final value is an average number. Furthermore, since each displacement value is squared, the result is bounded only in positive values.

Finally, the last part of the code creates the final video of the movement, using each of the analysed images with each one of the helicoid's detected points highlighted along the V-shape. This way, it is easy to see the vibrations for each experimental test.

3.4.3 The displacement photoelectric sensor

In order to compare and validate the obtained measures of the helicoid's natural frequency from the written MATLAB code for the high-speed camera, it is used the CP08MHT80 photoelectric sensor from Wenglor. This sensor determines the displacement of an object using angular measurement and giving an output from 0 to 10 V. The sensor is connected to a data acquisition system that sends the digital signal to the computer. Thereby, using a simple code in MATLAB it is possible to analyse the signal, to obtain the displacement values and the frequency spectrum.

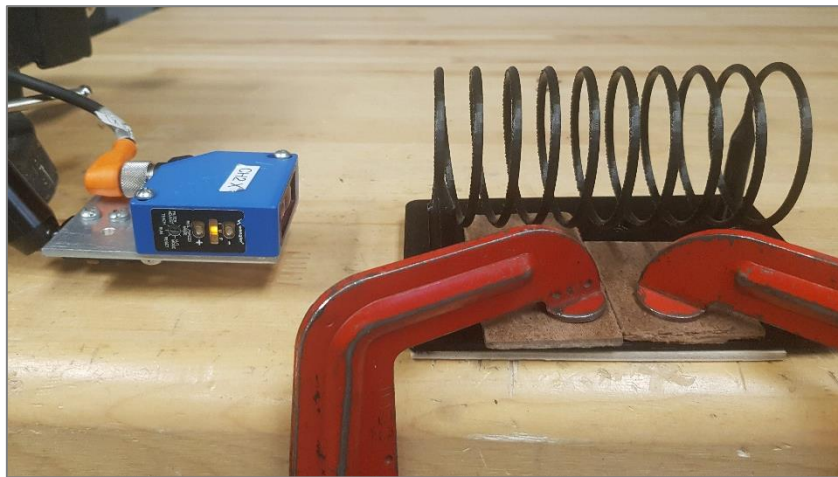


Figure 22: Setting up of the photoelectric sensor with the prototype 3

To perform the frequency test, a clear impact is made on the structure. After analysing the frequency modes of the helical structure using SolidWorks, it has been seen that there are two types of vibrations, the horizontal ones, and the vertical ones. For this reason, two types of frequency test have been performed, each in one of the vibration directions. The horizontal one (Figure 22), from left to right, and the vertical one which is from top to bottom.

4. Design and manufacturing of the Prototypes

One of the main parts of this project is to build a valid model of helical coil heat exchanger. If a real example of HCHE is taken, it would be composed by various tubes overlapped. The different tubes would be separated between them at a constant distance along all the heat exchanger and always keeping the same helical shape. Here it is presented a first example made with Autodesk that clearly shows the shape of the main part of the structure. Specifically, in this design there are 6 rows of tubes, three of them begin their helical turn at 0 sexagesimal degrees and the other three begin the turn at 180 degrees. To design this model, parameters such as the relationship between the diameter of each tube and the separation between have been inspired by real prototypes.

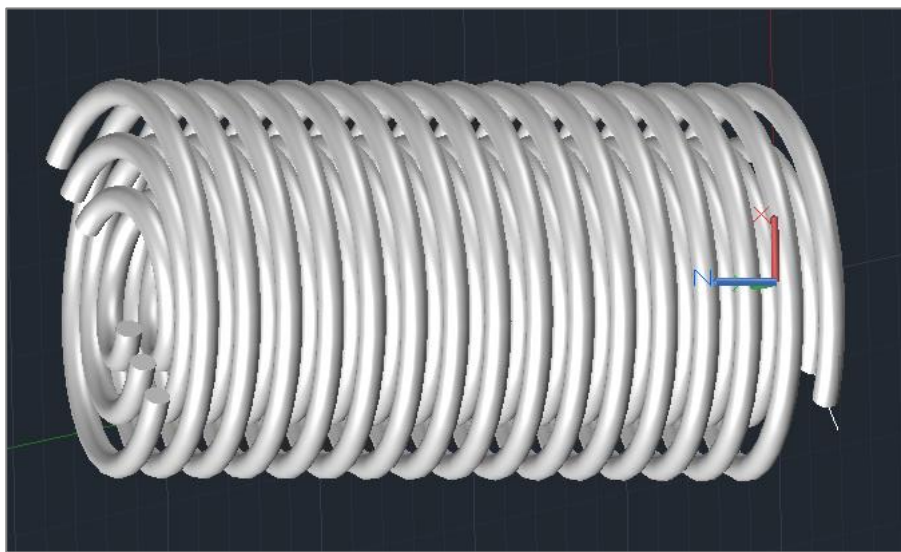


Figure 23: Example of a helicoid model with 6 tubes performed with AutoCAD

In the Figure 23, a diameter of 15 mm was used for all the tubes. The use of different rows of tubes helps to increase the cooling effect of the heat exchanger, since the surface in contact with the coolant is increased. As it can be seen, the proximity between the tubes could produce possible fluid-structure interactions, since the ratio of the space between tubes and the diameter is higher than 1.75 (Olala, 2016).

In order to have a better understanding of the interactions that happen in the prototypes, the developed models only have 1 tube. In this way, the fluid-structure interactions appear much clearer and easier to study. Thus, the simplified model consists of a single solid helical tube with a specific number of revolutions 'N', to try to better understand the interactions of this type of structure with the flow. The helicoid must meet certain geometric conditions to facilitate the study and to allow to see the vibratory phenomenon inside the test chamber. Obviously, another important part is the design and construction of the support for the helical coil, which must be sufficiently rigid and stable in order not to affect the structure of study. This helps avoid external vibrations to the helicoid. To design both, the helicoid and the support structure, it is important to know the geometrical parameters of the test chamber

explained before, to set the whole prototype inside it. The Figure 24 shows one of the final prototypes placed in the test chamber, also showing the sense of the flow.

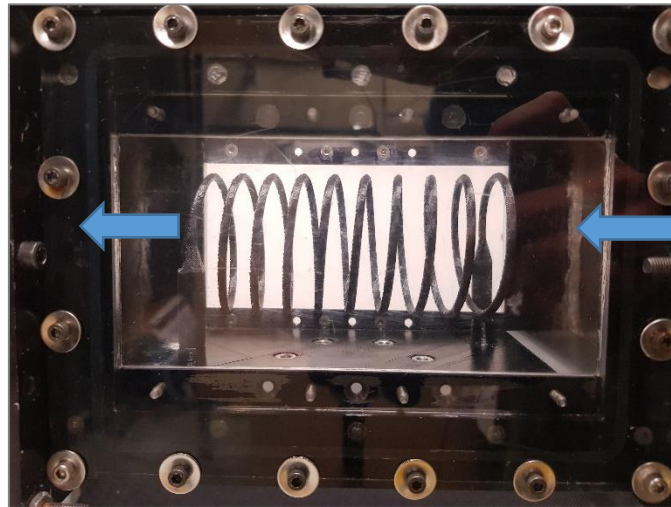


Figure 24: Prototype 3 inside the test section (blue rows represent the direction of the flow)

Although at the beginning of the project the material of construction for each piece wasn't clear, finally all the pieces have been done with 3D Printing. The 3D printer used in the manufacturing has been the Ultimaker 3 with a build volume up to 197 x 215 x 300 mm wide enough for all the components. The printing material used has been PLA Plastic (Polylactic acid), which has a density of 1300 Kg/m³ with an extruder accuracy of 0.1 mm. Using this new printing technology has greatly helped to reduce the production time of each piece since it was possible to do it in the 3D printers from the lab. As it is explained below, this reduction in the manufacturing time has helped to do different design tests, as well as different prototypes. Furthermore, it has reduced the production costs since the PLA Plastic used in the 3D printers is much less expensive than other possible building materials.

4.1 The elements to prevent leaks

In order to avoid leaks in each one of the holes from the top and bottom sides of the test chamber, 2 plug models have been designed with the correct tolerances. The diameter of the holes is 18.97 mm. During the design of these plugs, a small circular groove with internal diameter of 16.94 mm has been performed at the end of each plug in order to install a type of O-ring (small plastic ring with round cross-section). These O-rings have as main objectives to achieve a good fixation of the plugs inside the holes and to avoid any type of leaks. They need to resist a considerable amount of pressure due to the pressure difference between the interior of the chamber and the exterior. As well, they have been designed with a slightly wider cap (diameter of 25.5 mm) at one of the tips to extract them as well as to prevent them from entering the chamber during the experiments.



Figure 25: Plug model from the top part of the test chamber

There are two types of plugs, the ones used in the top wall are 50,8 mm long, as the example shown in the Figure 25. The other ones from the bottom part of the chamber are shorter since the inferior metal plaque of the test chamber where they are placed is thinner. These last ones have a length of 19.4 mm and as they are quite short, they only have space for one O-ring. The infill density of the print for these pieces is 100 % to prevent the water from entering the printing material due to the high pressure, since as seen with lower printing densities, the plugs may produce leaks and drips.

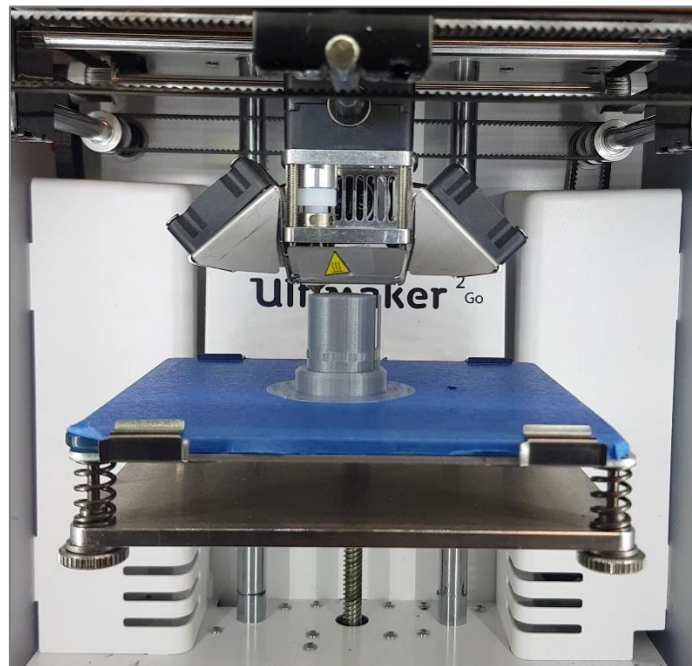


Figure 26: 3D Impression of a plug

These plugs are a simple part of the design but some of the inferior ones are used not only for its main sealing objectives commented above, but also as attachment points for the helical support structure. For this reason, a cylindrical hole has been performed in the centre of them. As explained below, a bolt is passes through this hole in order to attach the support structure.

4.2 The support structure for the helical coil

The helical structure that is tested inside the water channel needs a good support structure in order to avoid any vibration non-related to the flow-induced vibrations produced by the vortex shedding phenomenon. For this reason, the support structure is one of the significant parts of the project design. There are different objectives to fulfil with this design. The first goal, as said, is to produce a clear fixation of the helicoid. As well, it is necessary to reduce the influence the support structure could produce, in the form of turbulence, to the flow due to its shape or size. Furthermore, the support plate is designed to introduce it together in the test chamber with the helical structure already screwed into it, since it is easier than screwing it inside the test chamber due to the small space of this last one.

At first different support methods have been thought for the design but finally, after several tests the next method is the one that has been used. The support structure is based on a thin plate that is placed on the base of the test chamber. This plate is held in the test chamber by 6 pairs of bolts and nuts that passes through 6 of the inferior plugs mentioned above.

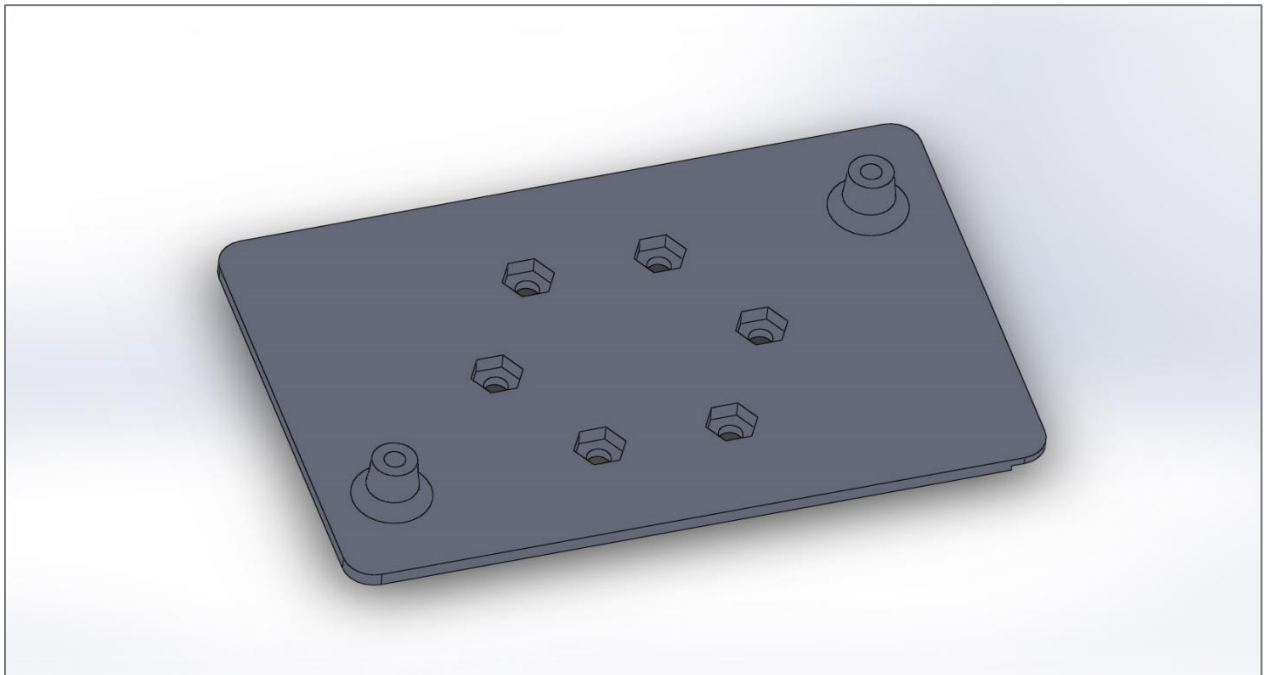


Figure 27: SolidWorks final design of the support plate

To perform the design of the support plate it has been used a small space or step between the inlet pipe and the entrance of the test chamber. This little step down is 3 mm height. The main idea is using this step in order to build the plate. On one hand, the plate is quite thin, which means that the influence of the plate on the water flow is minimum. On the other hand, it could seem that using only 3 mm of thickness for a plate that is 3D printed it is not such a right choice for the structural support. Nevertheless, since the fill density of the 3D printing is 100% the plate is rigid enough to assure the correct attachment of the helicoid, avoiding any type of secondary vibration.



Figure 28: Bolt type used to attach the plate to the chamber test

The 6 bolts that are used to hold firmly the support plate to the test chamber are sealing bolts (Figure 28). These ones have between the head and the shank a small O-ring to prevent leaks. These 6 bolts pass through 6 of the plugs in the inferior part of the chamber keeping the head down, outside of the chamber, and the tip of the screw inside the test section without going beyond the thickness of the support plate. To prevent the bolt movement and reach a good stiffens, a hole with the nut shape is created on the superior part of the support plate. In this way, when the screws are turned from outside to tighten the plate, the nuts are not moving so the screw nut system works correctly. Different design tests have been performed with the 3D printers in order to print the correct geometrical parameters of the hexagonal nut to achieve a good nut fit in the hexagonal hole and to avoid clearance when screwing from outside.

In the bottom of the support plate, where the 7 inferior holes of the test chamber are located, 7 extruded cylinders 2.8 mm high with the same diameters of the chamber holes have been designed underneath in order to fit the plate on the base of the test chamber.

The plate, besides being well attached to the chamber test, it also must fulfil its function of holding the helical structure. With this last purpose, in the design of the plate, two cylinders with a diameter like the helical tube have been extruded. Two wood screws are passed through the two cylinders to connect the plate with each of the extremities of the helicoid. To keep a good attachment between the helicoid and the plate, it has been created the same shape of the conical head of the screws (with an angle of 82°) to introduce it completely in the bottom part of the support plate. Thereby, when the screws are introduced inside the two extremities of the helicoid, the screw heads are the ones that maintain the plate and the helicoid attached together exerting all the pressure on the extruded cylinders of the plate. Since the system should be completely rigid, some 3D printed tests have been performed, in the same way as for the holes of the hexagonal nuts to have a good final design. In the case of these cylinders, the problem is that the contact force between the helicoid and the plate is so high that the cylinders collapse. After doing different design test with different cylinders diameters (Figure 29) this problem has been avoided.



Figure 29: Support cylinders tests for the screws (on the left) and hexagonal holes tests for the nuts (on the right)

Finally, a valid model of support plate has been designed and used in the experiment with good results. An important fact of this plate is that the helical coil is screwed once outside the test chamber and then the whole system (the support plate and the helicoid) remains joined forever, so that a plate is needed for each helicoid. This is because if only one plate were used for the different prototypes of helical coil, screwing and unscrewing the system would cause wear that could result in a worse fixation and rigidity.

This design makes the process to introduce the support plate with the screwed helicoid inside the test chamber quite efficient. Once the system is introduced from the top part of the test chamber, it is placed on the base of it and simply it is necessary to screw the 6 sealing bolts into the 6 nuts, being this last ones in their respective holes of the support plate. The system remains firmly attached to the water channel.

4.3 The helical model of the heat exchanger

In this part, the design of the main object of study is analysed. As explained in the subsection 3.2 from this report, the helicoid needs to meet some geometrical conditions to be valid to study the vortex shedding phenomenon. Although the helicoid has different geometrical parameters, the ones that are the most important in order to produce the synchronization of the vortex shedding are the external diameter of the tube and the construction material. Specially, the first parameter has been the focus of attention and 3 different prototypes have been tested to understand the influence of this parameter. When talking about the building material, it has been already explained that using a metal as copper to build the helicoid it is not the best idea, since the natural frequency is too high to produce a synchronization with the vortex shedding frequency. Because of that, the material used has been also PLA which is a plastic material with similar properties (almost equal density) to the PVC plastic used on the first calculation of section 3.2.



Figure 30: Support plate and helicoid from prototype 3

The helicoid has been the most difficult piece to 3D print due to its shape. It is important to mention that black colour has been chosen for the printing material in order to achieve a better colour difference with the white background of the light. In this way, each one of the taken photos with the high-speed camera clearly shows the image of the helicoid. Thanks to the help of the laboratory technicians, it has been printed using a tree-shaped support structure that is printed at the same time as the helicoid. This tree-shaped structure has the function of keeping the printing material of the helicoid, which is deposited at high temperature and still without being in solid-state, in the correct position. Once the printing is finished, the support material is removed easily using small pliers.



Figure 31: Helicoid with the tree-shaped support structure of the 3D printing and after removing the support structure

To be able to introduce the helicoid inside the test chamber and to have a good visualization of the vibrations, the first parameters that have been set in the design are the total length and the helical diameter. The chosen values have been respectively 120 mm and 55 mm. Once these parameters have been chosen the number of revolutions has changed as explained later in this section. Additionally, the helicoid has been designed with a solid tube due to the small tube diameters selected, obtaining valid results for the Beta parameter in order to produce the vortex shedding synchronization ($\text{Beta} < 0.4$), as explained in the theoretical knowledge section.

The helicoid is attached to the support plate through the two extremities as explained in the last subsection. Each extremity is a straight cylindrical tube with a diameter of 9 mm and with a hole in the centre of 2.4 mm where the screw goes through. The interior hole has been designed in order to reach the end of each cylindrical extremity and the screw has been selected to occupy almost all the longitudinal length of the hole. Thus, the fixation of the helicoid with the screw is done just in the extremity's region just before the helical revolutions start.

The first prototype has been designed with a tube diameter of 7 mm and 5.5 revolutions. After designing and manufacturing this first prototype it has been seen that the stiffness of the helicoid is quite large, since the vibrations produced inside the water tunnel are minimal and difficult to study. For this reason, it has been thought that it would be necessary to decrease the rigidity of the structure. To do so, the second and the third prototypes have been designed using the next formula. Since the helical structure behaves as a spring, as it has the same shape, the next mechanical law from a spring have been used where 'k' is the well-known stiffness parameter (Savaresi et al., 2011):

$$k = \frac{G * D_t^4}{64 * N * R_h^3}$$

The new parameter in this formula is the shear modulus of the material 'G'. As said before, the other parameters in the formula are the tube diameter 'D_t', the number of revolutions 'N' and the helical radius 'R_h'. It is easy to see in the formula that the tube diameter and the helical coil radius have a crucial influence in the stiffness or rigidity of the structure since D_t is to the fourth power and the R_h to the third power. The helical radius is kept constant since the change in this parameter could cause problems related with space inside the test chamber. For this reason, the tube diameter of the second and the third prototypes are reduced by 2 mm and 4 mm respectively. From tube diameter of 7 mm in the first prototype to 5 mm in the second and 3 mm in the third. This means that the stiffness is reduced considerably to 26.03% from the original in the second prototype and to 3.37% for the third prototype.

In order to design the second and the third prototype the number of revolutions has also been increased from 5.5 to 9.5 for both cases. With this second change of parameter, the final stiffness has been further reduced with the respective values of 15.07 % and 1.95 %.

5. Experimental results

First, the graphics for the natural frequency for each prototype are going to be presented in order to validate the written MATLAB code. Secondly, the experimental results of the water induced vibration are shown using the information obtained exclusively from the high-speed camera and the written MATLAB code.

5.1 Natural frequency in air

The natural frequency in air is obtained by two different sensors, the photoelectric sensor and the high-speed camera. In this way, the two results are shown in the next pages and after they will be compared in a table. To produce the vibration, a small impact on the structure has been made. The next graphic is an example of the displacement of the helicoid after the impact:

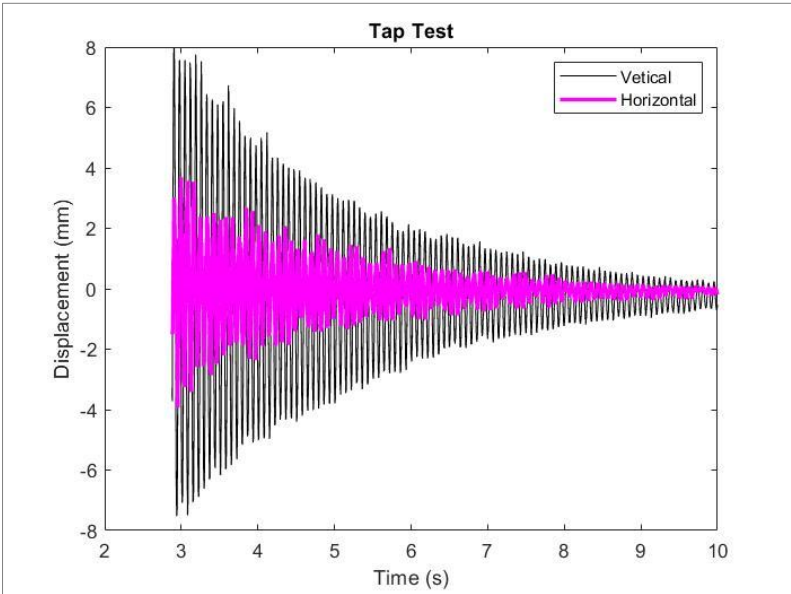


Figure 32: Vertical and horizontal displacement of the proto 3 from the photoelectric sensor

From the displacement data as shown in the example above and using the fast Fourier transform (FFT) in MATLAB, the next graphics of the frequency spectrum are obtained for each prototype, using both sensors:

The Photoelectric Sensor.

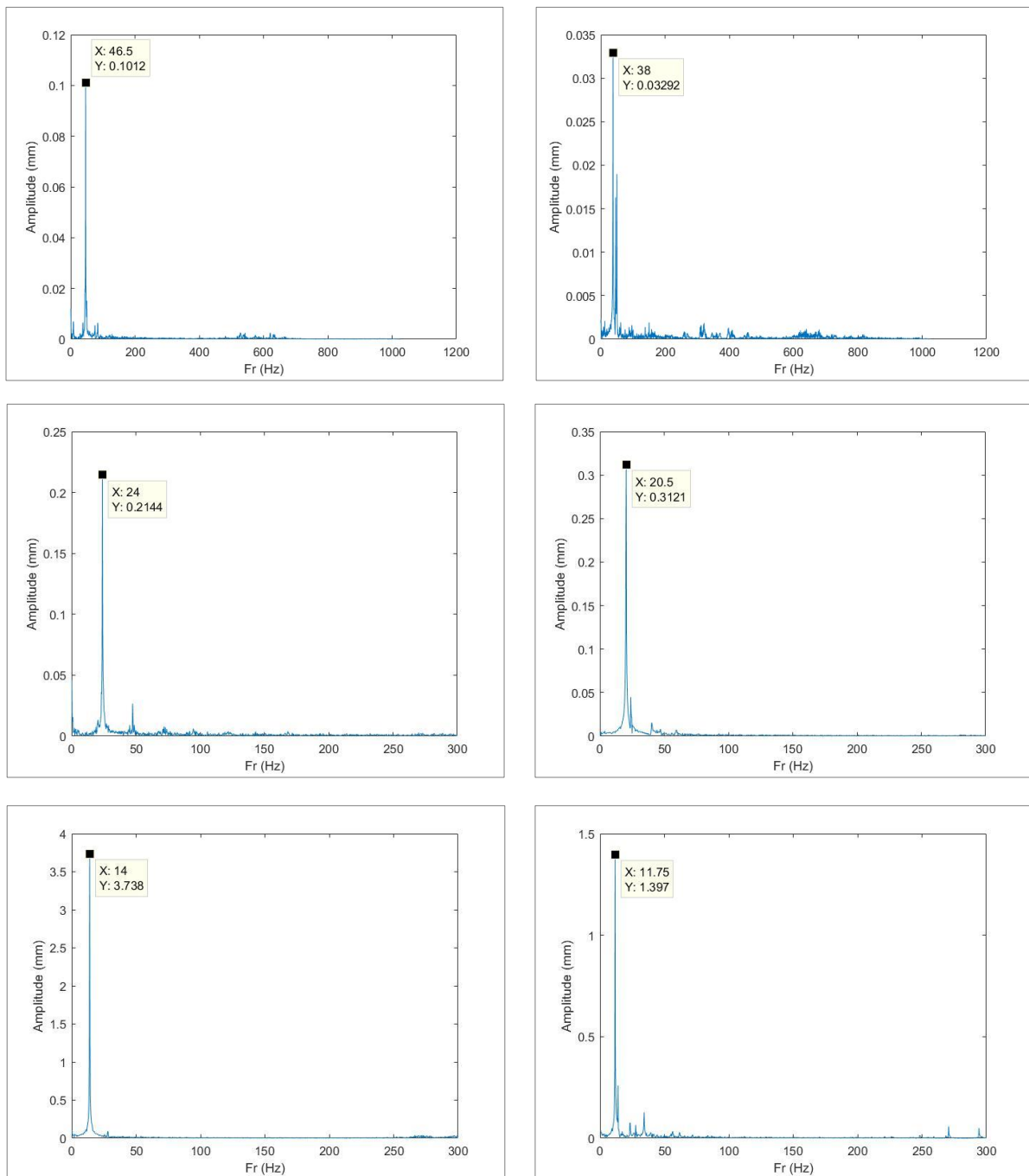


Figure 33: Laser frequency spectrums for the 3 prototypes: vertical for proto 1 (Top Left), horizontal for proto 1 (Top right), vertical for proto 2 (centre left), horizontal for proto 2 (centre right), vertical for proto 1 (down left), horizontal for proto 1 (down right)

The High-Speed Camera.

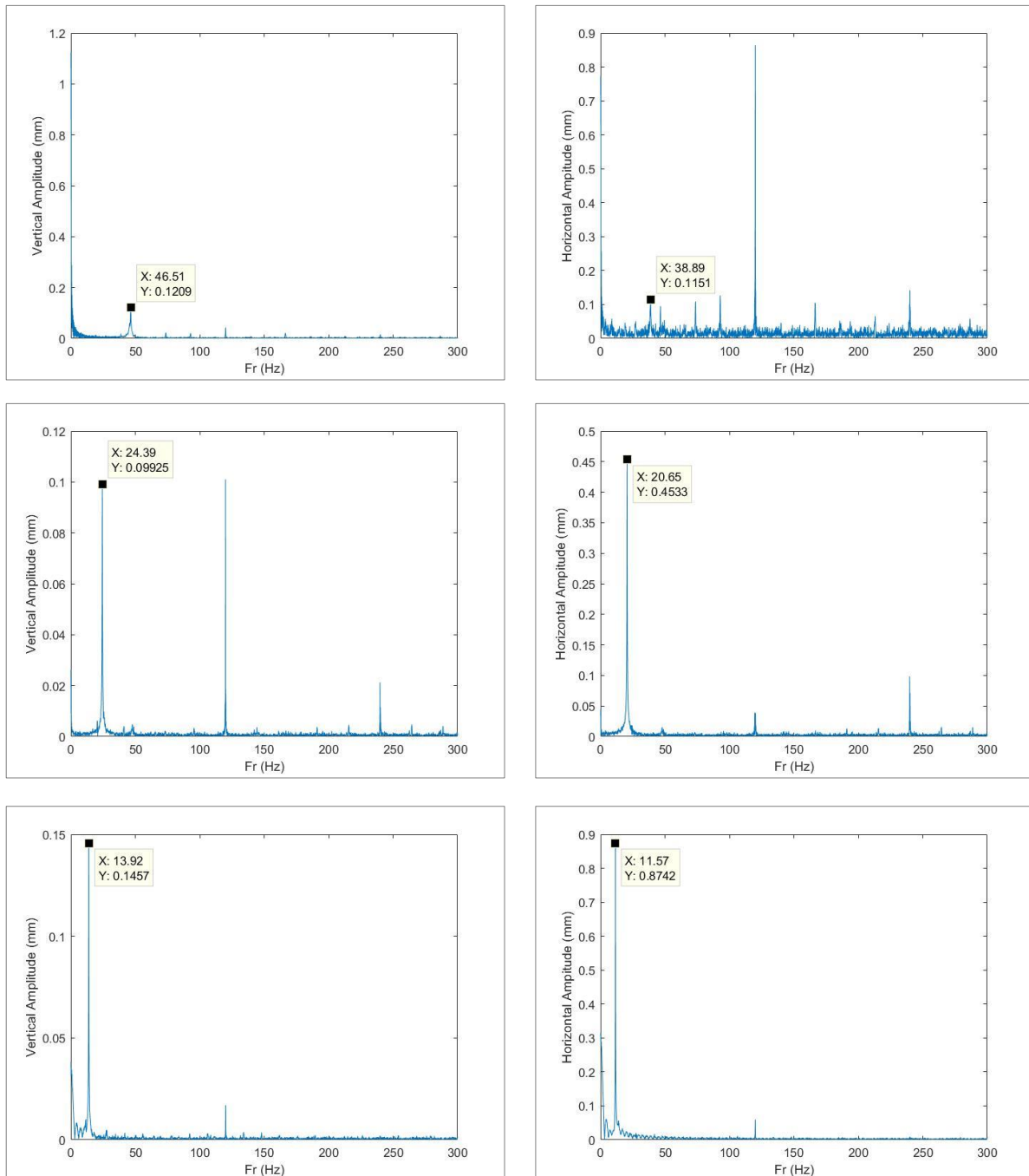


Figure 34: High-speed camera frequency spectrums for the 3 prototypes: vertical for proto 1 (Top Left), horizontal for proto 1 (Top right), vertical for proto 2 (centre left), horizontal for proto 2 (centre right), vertical for proto 1 (down left), horizontal for proto 1 (down right)

From the graphics of the photoelectric sensor, the vertical and horizontal frequencies obtained by the fast Fourier transform are quite clear since they are shown as peaks with a greater amplitude than the rest of the frequency spectrum. From the graphics of the high-speed camera, similar frequencies are obtained. It is important to mention that the natural frequency peak for the prototype 1 (Figure 24) is harder to see it, possibly due to a greater stiffness of the helicoid that decreases the amplitude of vibration. Furthermore, in all the graphics from the camera, there is a peak at 120 Hz (appearing with lower amplitudes at 60 Hz and at 240 Hz) produced by the electrical supply, since here in Canada the electric current is supplied at 60 Hz.

In the Table 2 the different natural frequencies obtained with both sensors are presented for each prototype:

Table 2: Comparison of natural frequencies between sensors

| SENSOR | PROTOTYPE | TUBE DIAMETER (mm) | VERTICAL FREQ. (Hz) | HORIZONTAL FREQ. (Hz) |
|----------------|-----------|--------------------|---------------------|-----------------------|
| PHOTO-ELECTRIC | 1 | 7 | 46.50 | 38.00 |
| | 2 | 5 | 24.00 | 20.50 |
| | 3 | 3 | 14.00 | 11.75 |
| CAMERA | 1 | 7 | 46.51 | 38.89 |
| | 2 | 5 | 24.39 | 20.65 |
| | 3 | 3 | 13.92 | 11.57 |

It is possible to see a reduction of both frequencies when the diameter decreases. This fact matches with the SolidWorks simulations presented above, since in the preliminary SolidWorks tests, this reduction in frequency was also clear.

5.2 Water induced vibration

5.2.1 Prototype 1

All the results presented in this section have been obtained with the high-speed camera. When the several prototypes have been introduced inside the water channel, it was clear that the most affected prototype by the water flow, was the third, with the smallest diameter and as explained in the design section with the smallest stiffness. The first prototype (diameter of 7 mm) is the most rigid, and it doesn't vibrate until the maximum flow velocity of the water channel was reached (0.520 m/s). Due to this fact, the deeply studied prototypes in this section are the second and the third, which are the ones that have a truly induced vibration by the water flow.

5.2.2 Prototype 2

The Displacement.

The second prototype is less rigid than the first prototype, and as shown in the Figure 35 some vibrations are induced in the helicoid by the water flow. These vibrations are mainly in the vertical direction:

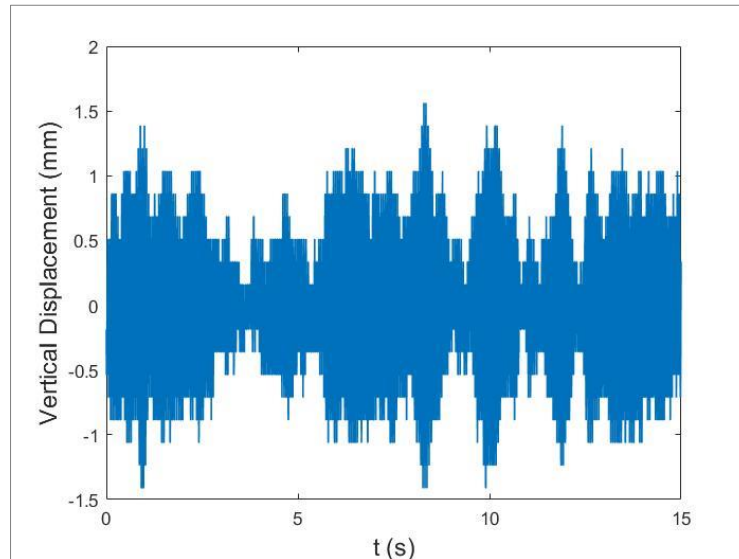


Figure 35: Vertical displacement at a velocity 0.497m/s for proto 2

The maximum amplitude of displacement for this prototype is of 3 mm in the vertical direction and it occurs at a velocity of 0.497.

The Spectrum of Frequencies.

Using the fast Fourier transform (FFT) and the power spectral density (PSD) methods, as explained in the MATLAB code's subsection 3.4.2, it is possible to obtain the 3D graphics below in order to see a global view of the frequency spectrum. In the 'x' axis the different velocities (21 different tested velocities equally spaced from 0.078 m/s to 0.520 m/s) are presented. In the 'y' axis, the frequencies interval shown is from 5 to 30 Hz and in the 'z' axis the respective amplitude of the FFT or the PSD in mm.

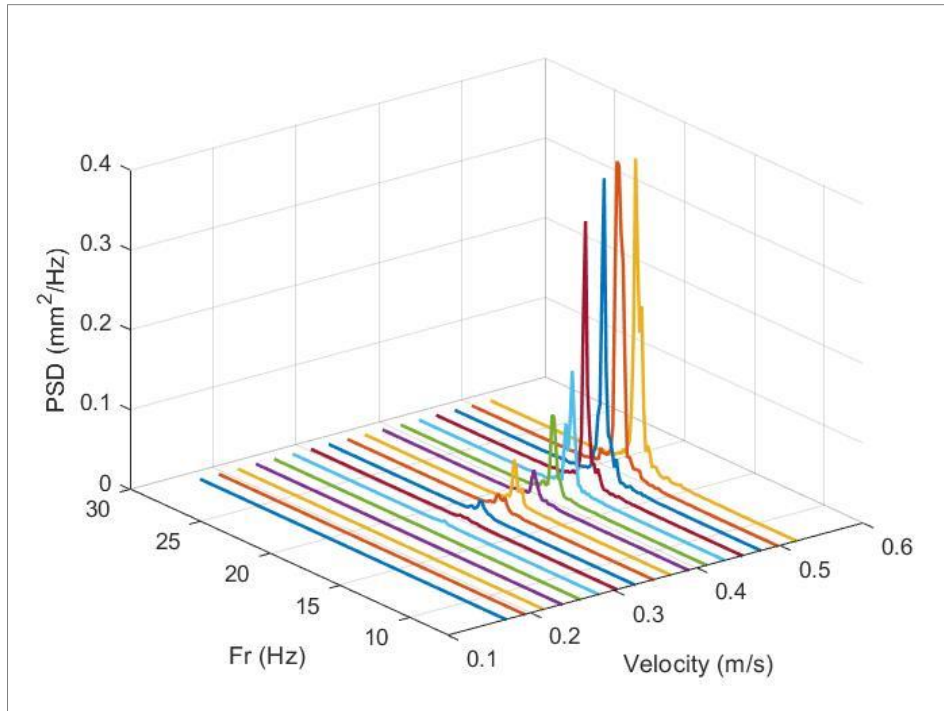


Figure 36: PSD 3D graphic of the vertical movement for proto 2

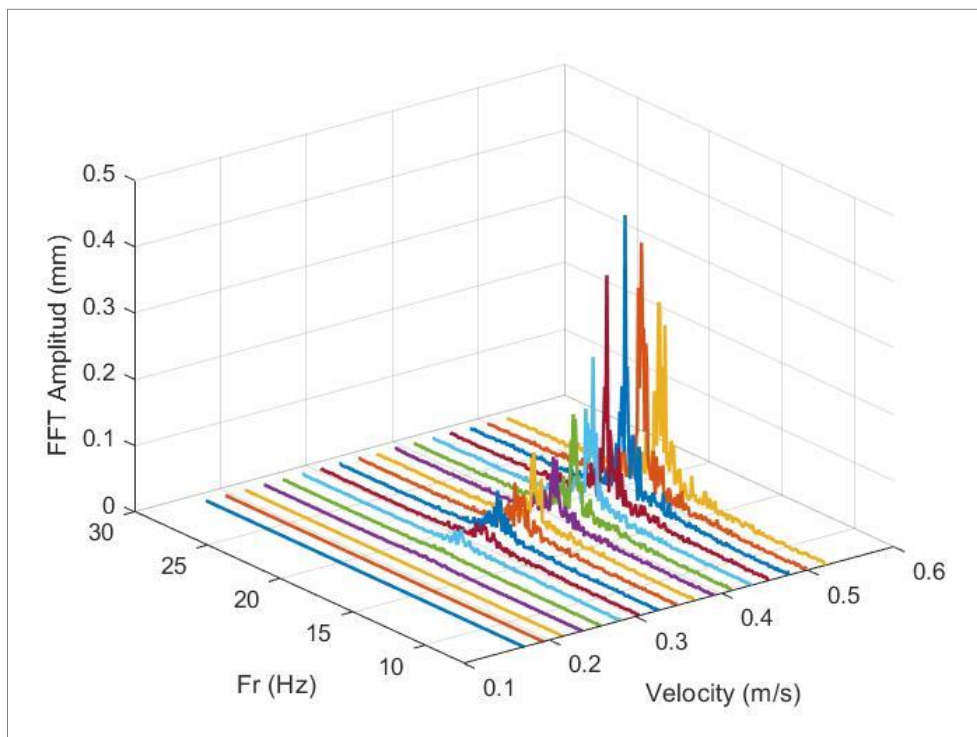


Figure 37: FFT 3D graphic of the vertical movement for proto 2

The 3D graphic of the PSD (Figure 36) shows that the maximum peak is at a velocity of 0.497 m/s with a frequency of 18.75 Hz. In the Figure 38, it is presented this case individually:

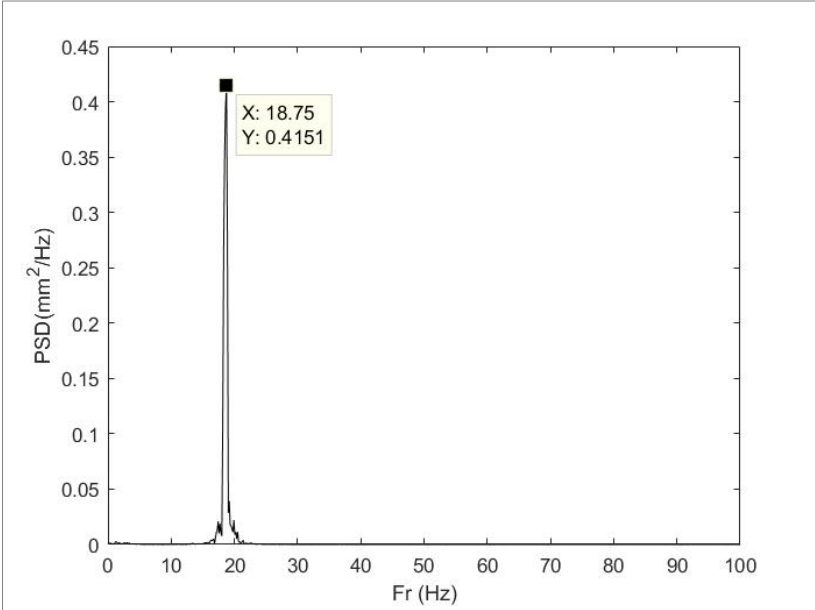


Figure 38: PSD Vertical frequency spectrum at a velocity of 0.497 for proto 2

In the 3D graphic of the FFT (Figure 37), it is shown that the maximum peak is reached at a velocity of 0.477 m/s with a frequency 18.53 Hz. The Figure 39 represents the FFT for this particular case:

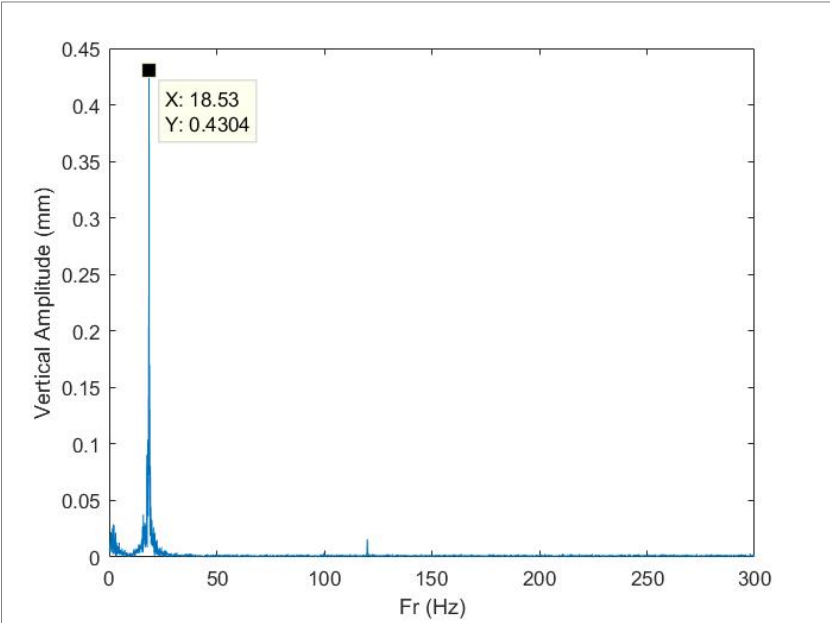


Figure 39: FFT Vertical frequency spectrum at a velocity of 0.477 m/s for proto 2

The RMS Graphic

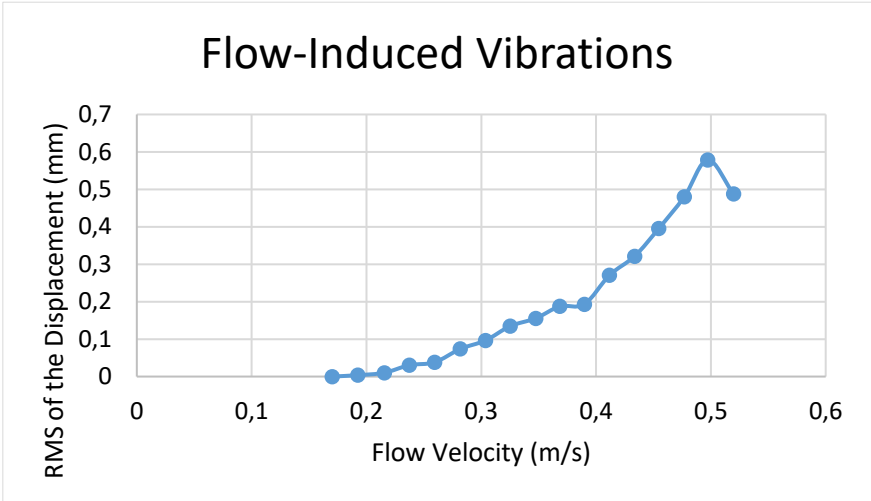


Figure 40: Flow-induced vibrations using RMS for proto 27.2.2 Prototype 3

Finally, the root mean square (RMS) of the displacement for each velocity is shown (Figure 40). In this graphic it appears the amplitude peak at 0.497 m/s.

5.2.3 Prototype 3

The results obtained for the third prototype are quite different from the other two. The first noticed vibrations start at a velocity of 0.147 m/s which is the 28.3 % of the maximum water flow velocity of the water channel. This leads to think that there is a sufficiently long range of speeds available in order to study the vortex shedding synchronization phenomenon in all its phases. Furthermore, there are two well defined types of vibrations, in the vertical and horizontal directions.

The Displacement.

In the prototype 3, the displacement graphics have been divided in two types of movement, since the vortex shedding interaction occurs in the horizontal direction of the flow and on the vertical direction. For the vertical displacement, the maximum vibration amplitude is produced at a velocity of 0.304 m/s, it is shown in the Figure 41:

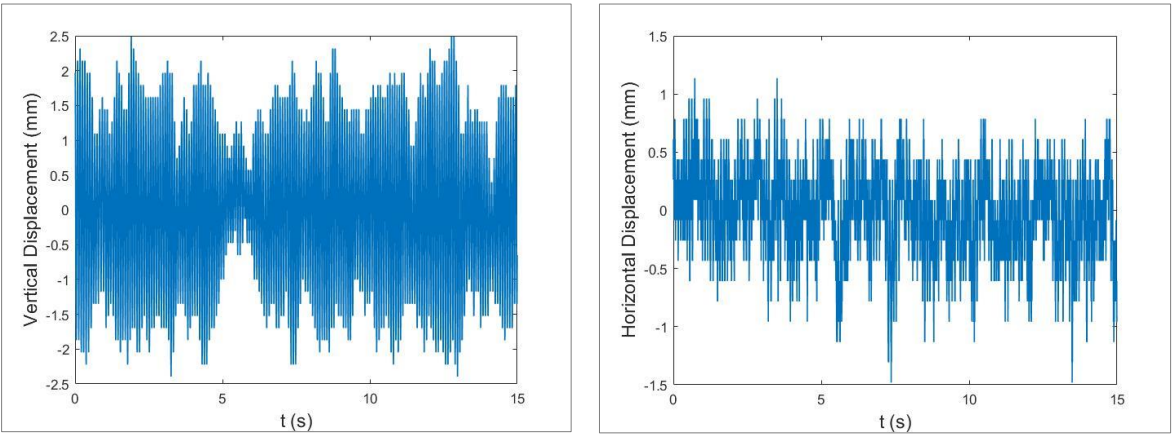


Figure 41: Vertical and horizontal displacement at a velocity 0.304 m/s for proto 3

An example of intermediate velocity is at 0.412 m/s with intermediate vibrations in both directions. It is shown in the Figure 42:

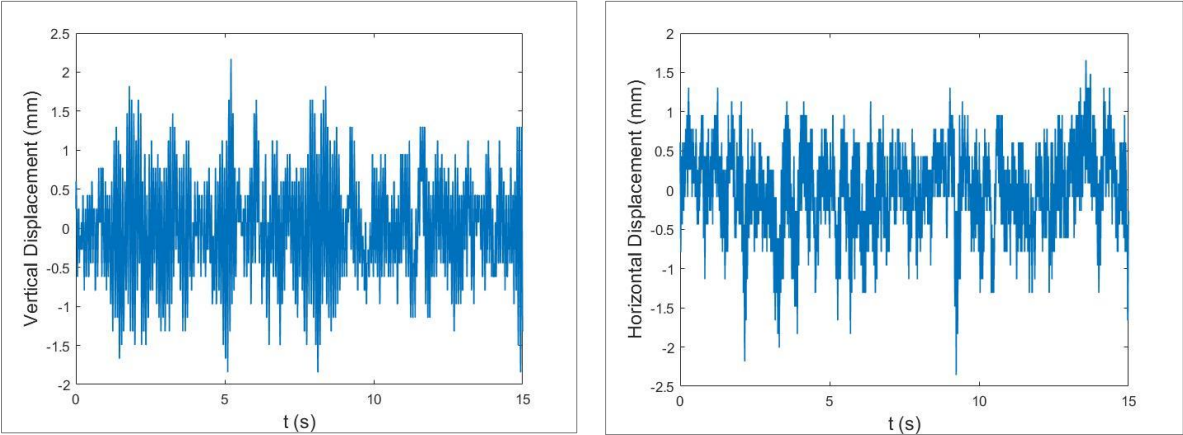


Figure 42: Vertical and horizontal displacement at a velocity 0.412 m/s for proto 3

For the horizontal displacement, the maximum vibration amplitude is obtained at a velocity of 0.477 m/s (Figure 43):

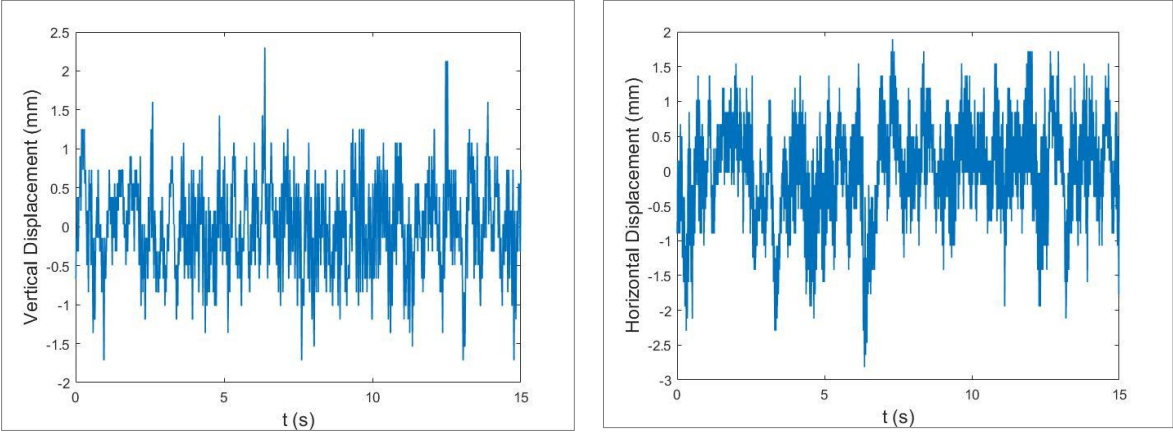


Figure 43: Vertical and horizontal displacement at a velocity 0.477 m/s for proto 3

The Spectrum of Frequencies.

Once obtained the displacement of the vibrations, the frequency spectrums are shown in the same way as for the prototype 2 but considering the two directions of vibration. First the two PSD 3D graphics are shown, each one in one of the analysed directions, vertical and parallel to the flow.

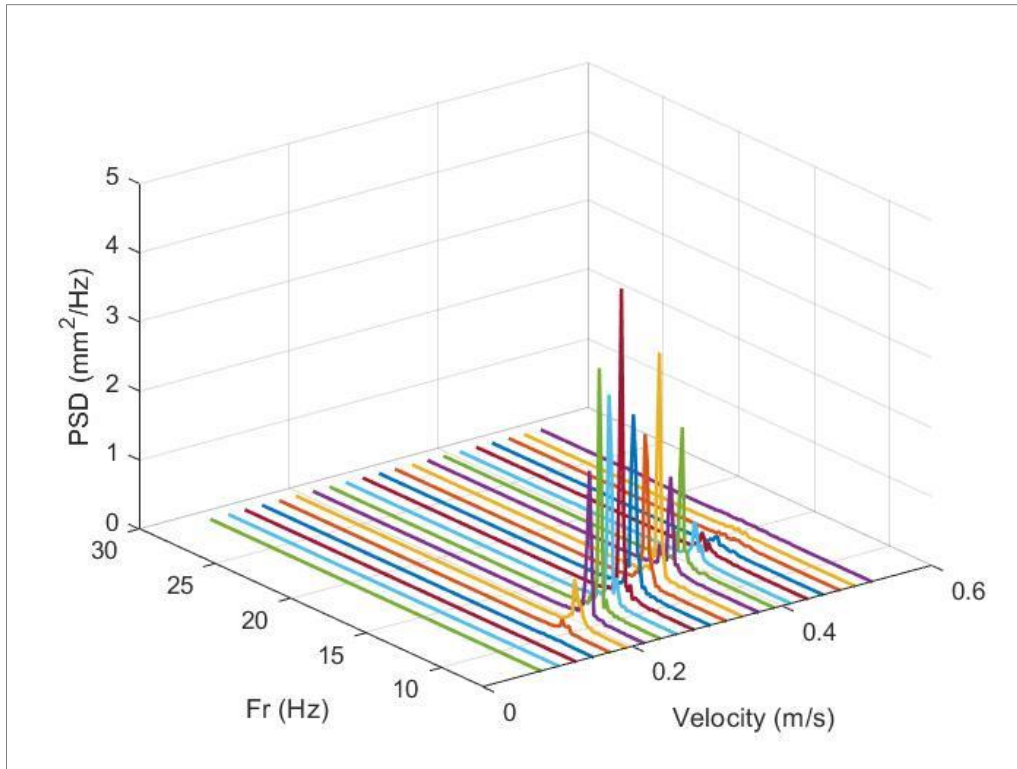


Figure 44: PSD 3D graphic of the vertical movement for proto 3

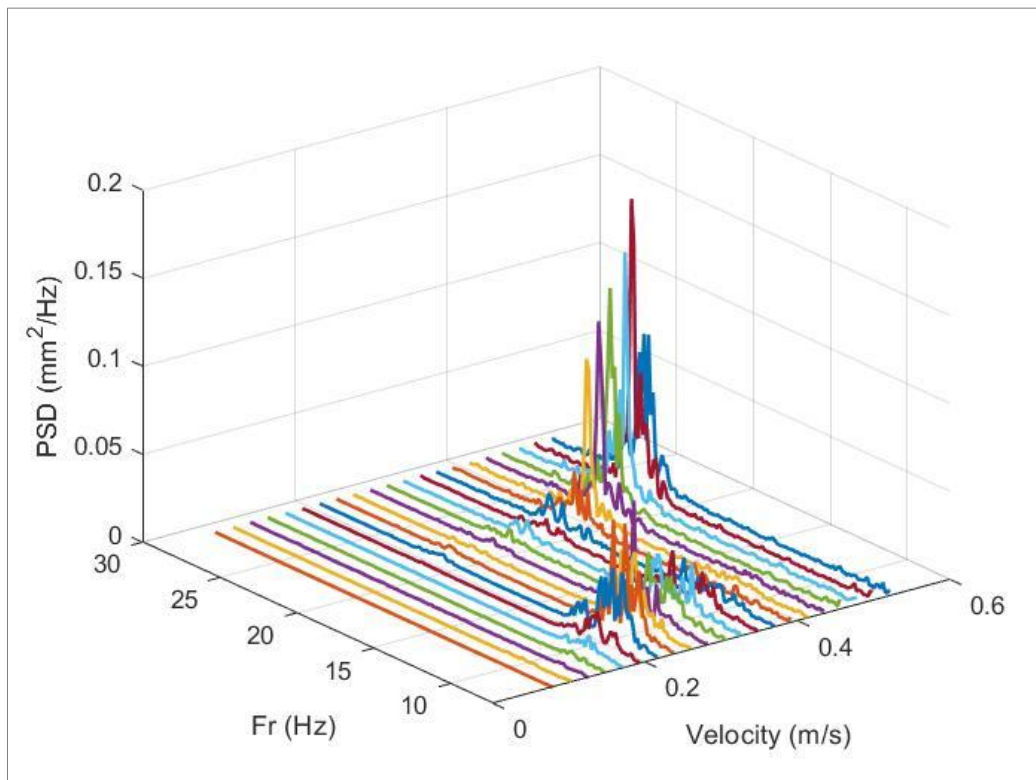


Figure 45: PSD 3D graphic of the horizontal movement for proto 3

These graphics show important relations with the vortex shedding phenomenon that are analysed in the analysis section. In the two 3D graphics for the PSD the maximum peaks are: for the vertical displacement (Figure 44) at a velocity of 0.282 m/s with a frequency of 12.01 Hz and for the horizontal displacement (Figure 45) at a velocity of 0.497 m/s with a frequency of 22.85 Hz. These two particular cases are shown in the graphics (Figure 46, Figure 47):

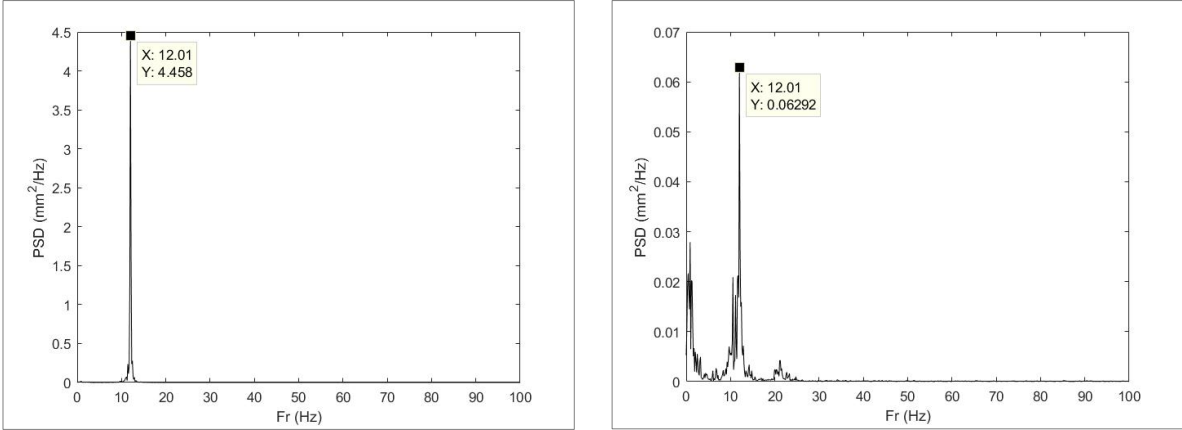


Figure 46: PSD vertical and horizontal frequency spectrum at a velocity of 0.282 m/s for proto 3

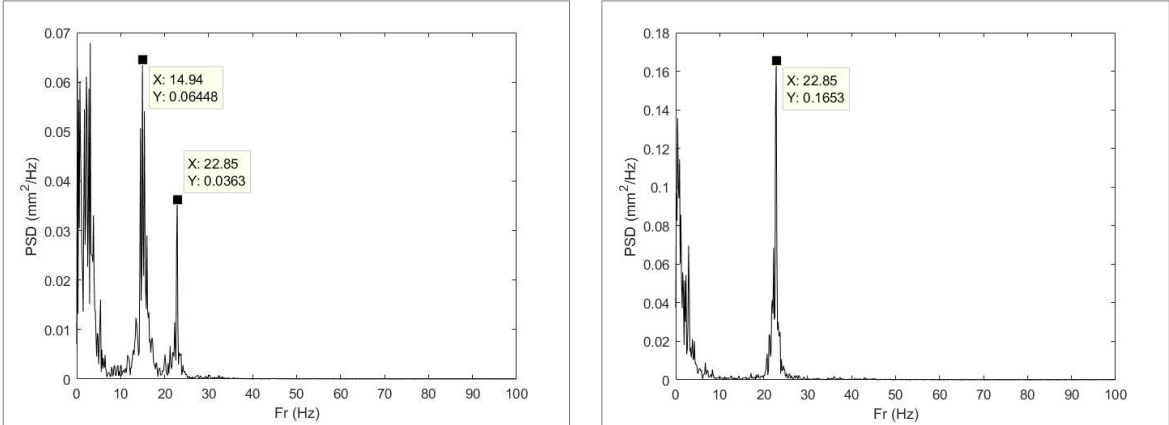


Figure 47: PSD vertical and horizontal frequency spectrum at a velocity of 0.497 m/s for proto 3

The 3D graphs of the frequency spectrum calculated with the FFT are shown below. It is important to remark that to better understand the graphics from the FFT, half of the velocities in the 'x' axis have been removed in order to see the graphs more clearly, the original FFT 3D graphics with all the velocities are shown in the Appendix 2.

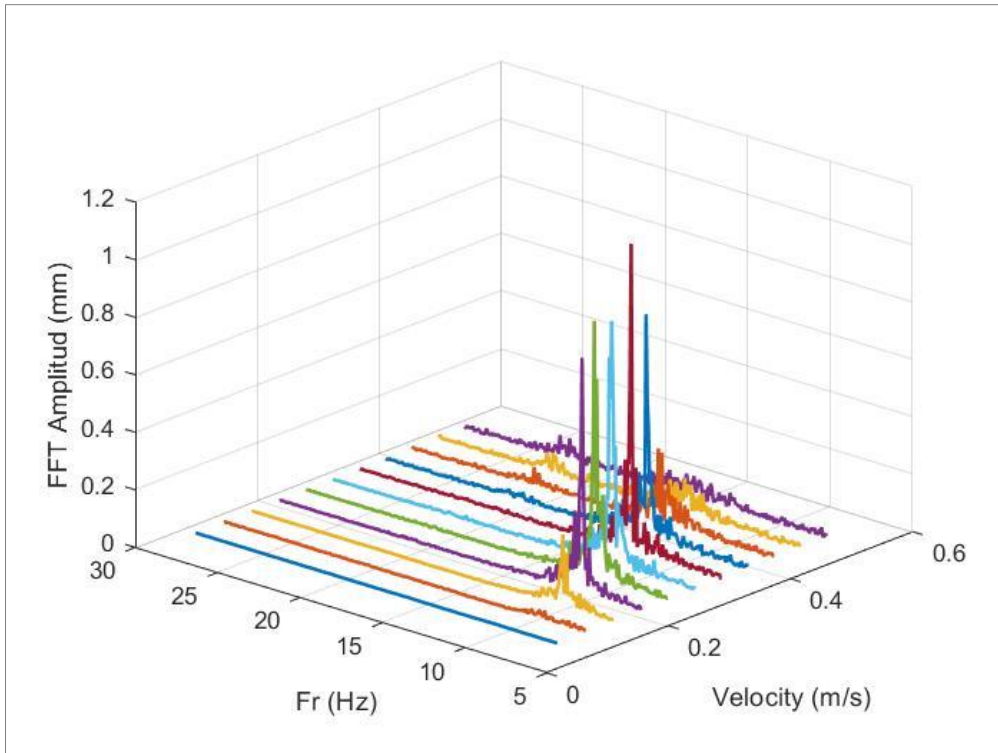


Figure 48: FFT 3D graphic of the vertical movement for proto 3

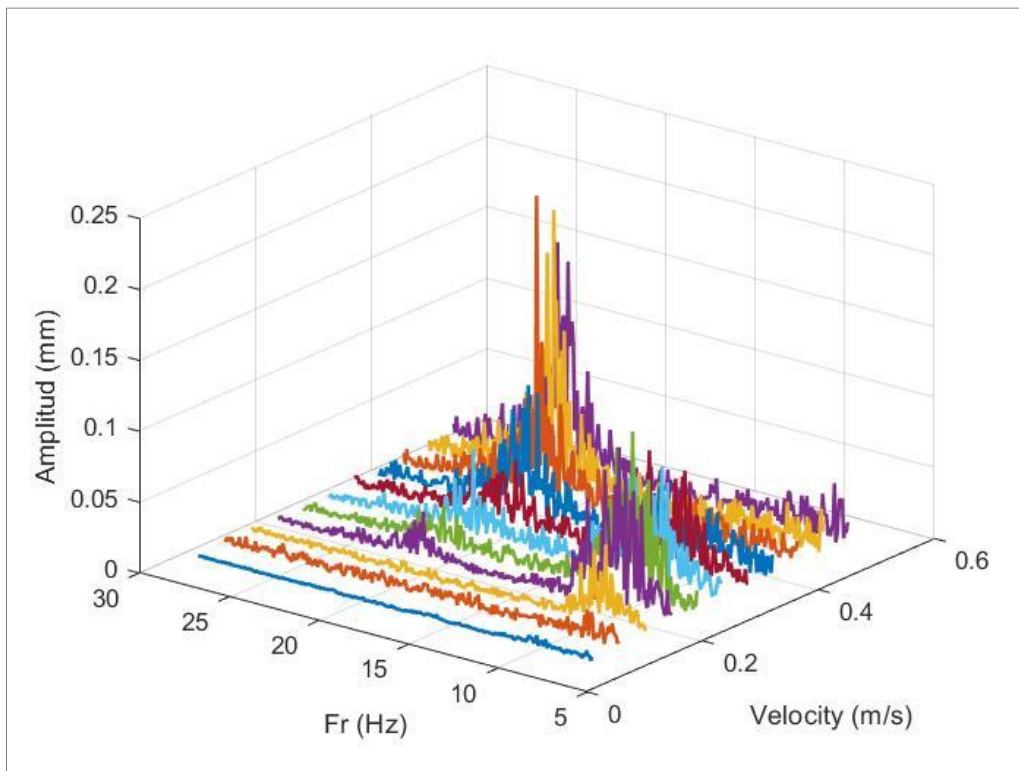


Figure 49: FFT 3D graphic of the horizontal movement for proto 3

In the first 3D graphic (Figure 48) obtained with the FFT from the vertical movement, there is a clear frequency peak at a velocity of 0.282 m/s. In the second graphic (Figure 49), obtained from the FFT of the horizontal displacement, it appears two peaks at different frequencies, one of them it is the same peak as in the first graphic from the vertical displacement and the other peak emerges at a higher velocity (0.434 m/s) which is the true peak from the horizontal displacement. These two peaks can be seen clearly if the particular FFT frequency spectra for these velocities are shown:

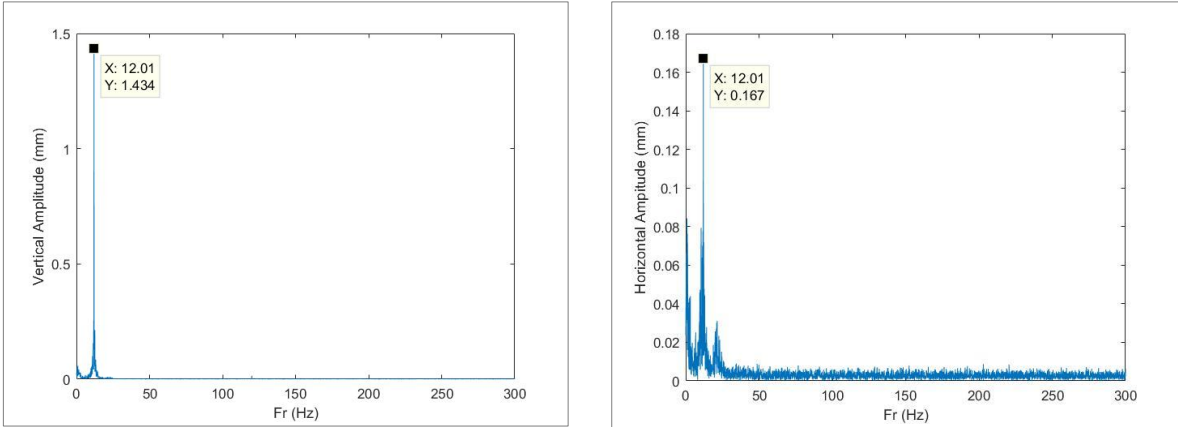


Figure 50: Vertical and horizontal frequency spectrum at a velocity of 0.282 m/s for proto 3

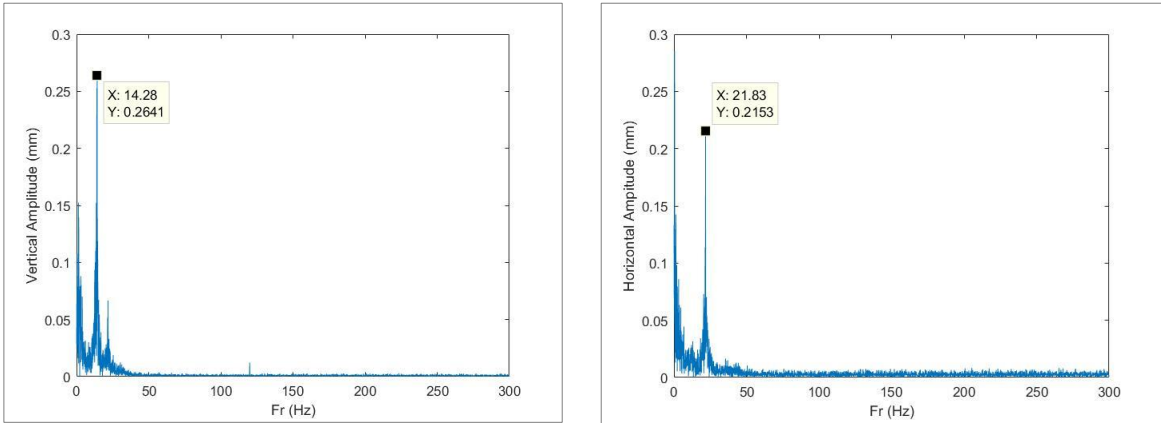


Figure 51: Vertical and horizontal frequency spectrum at a velocity of 0.434 m/s for proto 3

In the first two graphics (Figure 50), at a velocity of 0.282 m/s, it appears the clear peak at 12.01 Hz, with a higher amplitude at the spectrum of the vertical movement. In the other two graphics, at a velocity of 0.434 m/s (Figure 51), it still appears the same peak at a frequency a little bit higher (14.28 Hz), from the vertical spectrum. On the other hand, in the horizontal spectrum the second frequency (21.83 Hz) shows up.

An important phenomenon that can be extrapolated also from the 3D graphics is the 3D increase in the vortex shedding frequency with velocity maintaining a linear relationship. In the Figure 52 the first vertical frequency of vibration is plotted in function of the velocity increase:

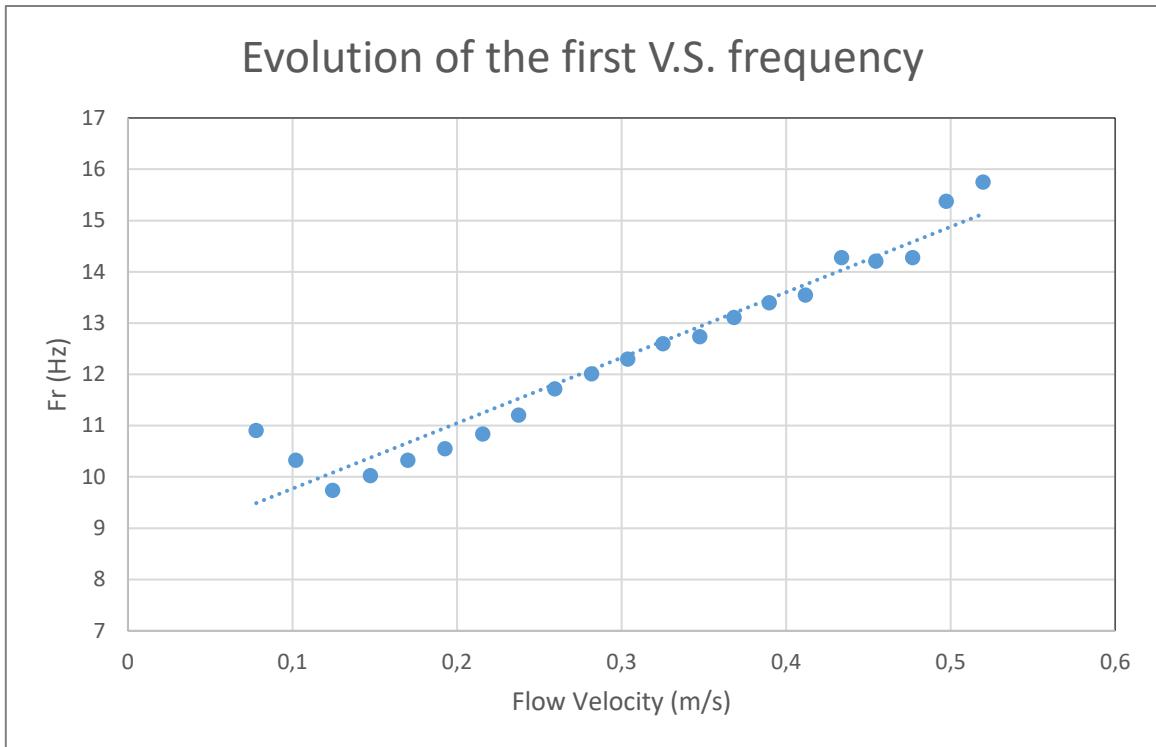


Figure 52: Evolution of the first vortex shedding frequency for proto 3

The RMS graphic.

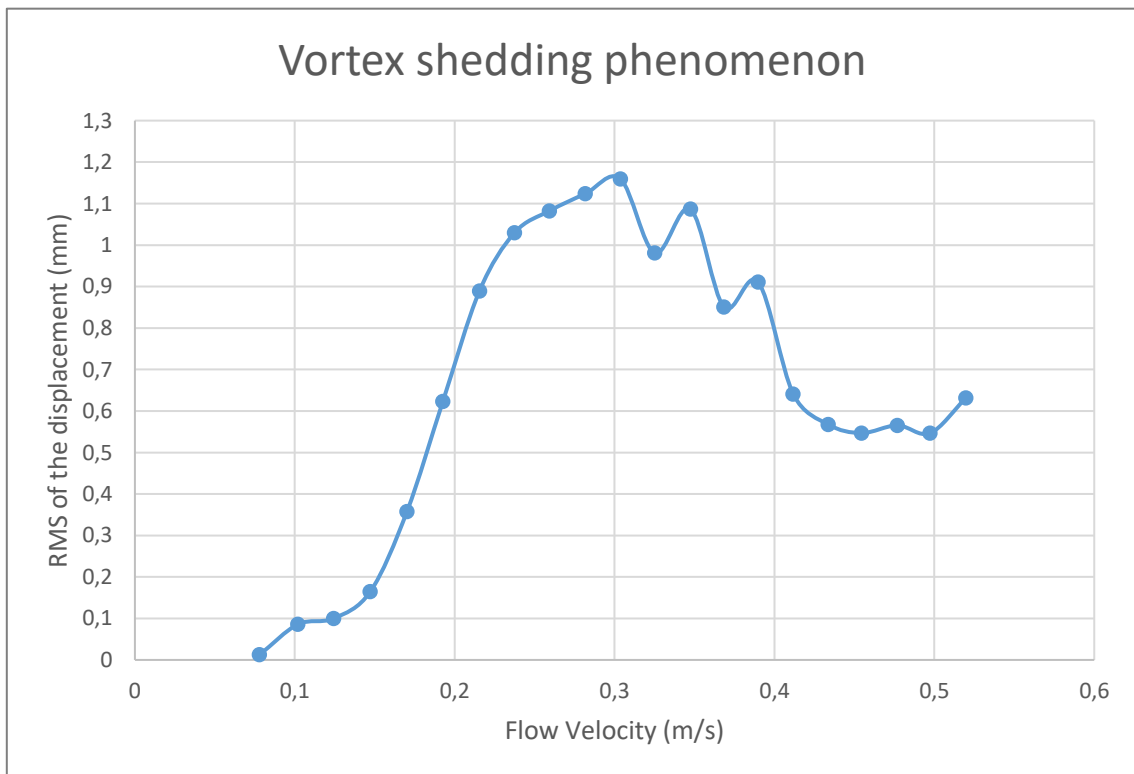


Figure 53: Vortex shedding phenomenon using RMS of the displacement for proto 3

Finally, using the data obtained from the Root Mean Square (RMS) in the MATLAB code the Figure 53 has been obtained in order to better describe the vortex shedding phenomenon in the helical structures. It is represented the displacement of the vibration in function of the tested flow velocities. First, there is a clear increase of the displacement till the maximum point (1.16 mm) at a flow velocity of 0.304 m/s. After that, the displacement decreases considerably with some fluctuations without reaching 0, and it sets constant after a flow velocity of 0.434 (at an RMS of the displacement value of 0.55 mm) during the last interval of velocities.

6. Analysis of the experimental results

This section analyses the results previously presented. First, it is discussed the validation of the high-speed camera using the measures from the photoelectric sensor. Secondly, the results obtained for the flow-induced vibrations are analysed in a global way among the 3 prototypes. Then, second and third are analysed separately, commenting on the important particularities of each one and highlighting the third prototype, in which the flow-induced vibrations have been manifested more clearly.

The Data analysis for the validation of the frequencies obtained by the camera shows that the different natural frequencies obtained by both sensors (photoelectric sensor and high-speed camera) are quite similar. The natural frequency of the vertical mode shows a very low maximum error of 1.62 % (0.39 Hz) in the prototype 2. In the horizontal frequency mode, the highest difference between both sensors is 2.34 % (0.89 Hz) in the prototype 1, being also a sufficiently low value. Thereby, it is possible to confirm that the obtained values from the MATLAB code used to analyse the images of the high-speed camera are reliable enough to study the flow-induced vibrations of the helicoid.

In a global comparison of the flow-induced vibrations between the prototypes, it is observed that the stiffness of the helicoid is an important parameter to consider. As explained in the design section, the stiffness is directly related to the tube diameters. For this reason, in the prototype 1, with a diameter of 7 mm, the flow-induced vibrations are not noticed till the maximum velocity of the experiment at 0.520 m/s. This result indicates that higher flow velocity is required in order to obtain analysable data from this first prototype. The decrease in stiffness of 85 % and 98 % in prototypes 2 and 3 respectively, obtained with a reduction of the tube diameter and an increase of the revolutions of the helicoid, has favoured considerably the production of analysable flow-induced vibrations. These details can be seen in the results presented.

An induced vibration in the vertical direction is produced in the prototype 2. This can be seen in the 3D graphics of the frequency spectrum from the power spectral density and the fast Fourier transform of the second prototype. The vibration starts after a velocity for the PSD (0.325 m/s) and a little bit earlier on the FFT (0.282 m/s). Showing in both very similar frequencies (18.75 and 18.53 respectively). Although both graphics are valid, the results obtained with the PSD are much clearer because there is a reduction of the noise compared to the FFT graphic.

The results obtained in the prototype 3 show clear fluid-structure interactions. The maximum amplitudes of vibration (5 mm) among the 3 prototypes are shown in this third prototype. The diameter of the tube (3 mm) has played an important role in the flow-induced vibrations for two reasons; the first reason is the explained above related with the stiffness of this helicoid. The second reason it's related to the reduced velocity parameter (explained in the section 3.2.2), where the small diameter reduces the velocity needed to produce synchronization with the vortex-shedding.

In the third prototype two types of vibrations have been obtained (shown in the 3D graphics for the PSD and FFT). These vibrations occur at different flow velocities, in the direction transverse to the flow (vertical displacement) and in the parallel direction (horizontal displacement). The existence of two vibrations in this experiment is a typical peculiarity of the vortex shedding phenomenon (Païdoussis et al., 2011). Considering the vertical vibration as the first vorticity shedding frequency, the horizontal frequency (second vortex shedding frequency) has a value which is twice as much as the first vorticity shedding frequency. This relation between first and second frequencies appears in other experimental studies about the vortex shedding in tube bundles (Ziada, 2006), which means that the helical structures behaves in a similar way.

When the first vorticity shedding frequency of the third prototype, the vertical one, is deeply analysed, it is shown that the vertical vibration appears at lower velocities (0.193 m/s at the PSD and 0.170 m/s at the FFT) and increases until it reaches the maximum peak of both graphs (PSD and FFT). This means that with this first frequency, there is a synchronization phenomenon of the vortex shedding with the natural frequency of the helicoid. This synchronization phenomenon occurs between the lowest velocities commented above and the velocity of 0.412 m/s that matches in the FFT and the PSD. During this interval, it appears the Lock-in phenomenon with the natural frequency of the helicoid. Both required conditions (explained in the section 3.2) in order to produce the vortex shedding synchronization are achieved. First, the vortex shedding frequency is quite similar to the natural frequency of the helicoid. During all the Lock-in interval of velocities, the frequency of the vibrations is between the vertical and the horizontal natural frequencies of the helicoid obtained in the first part of the results (Table 2). The second condition related with the Beta parameter is also matched. In this way, there is a coupling between the natural frequency of the helicoid and the vortex shedding frequency that produces the highest amplitudes of vibration (Kaneko et al., 2013).

Finally, it has been obtained (using root mean square) the graphic of the vortex shedding phenomenon (Figure 53), since it represents clearly the curve of the vibration amplitude in function of the flow velocity. Before analysing this last graphic, it is important to explain a relation obtained between the PSD and the RMS. In this last graphic, it appears the vibration peak at a velocity of 0.304 m/s. Nevertheless, in the PSD results, the maximum amplitude is obtained at a velocity of 0.282 m/s and a frequency of 12.01 Hz. This small difference of velocity between the peaks can be explained calculating the RMS of the displacement, integrating the surface under the PSD curve and applying the square root. In other words, despite being lower than the highest peak of the PSD at 0.282 m/s, the peak at 0.304 m/s yields a larger surface after integration.

In order to better explain the phenomenon of flow-induced vibrations, the Figure 53 is a clear representation of the vortex shedding phenomenon for the helical structures. The interval of velocities where the peak rises represents the Lock-in interval of velocities (from 0.304 to 0.434 m/s) that produces a vortex shedding frequency similar to the natural frequency of the helicoid. When this graphic is compared with the theoretical vortex shedding effect of a tube (Païdoussis et al., 2011) it shows a similar relation. This final result shows a clear peak of maximum vibrations. Furthermore, when the velocity is increased after this peak, the

vibration amplitude decreases till a constant level of displacement where the vibrations remains constant for some velocity interval.

Although in the present study, the maximum velocity is not enough to notice the fluid-elastic phenomenon, at this maximum velocity, the final result (Figure 53) shows a considerable increase of the vibrations. This could represent the start of the vibration exponential growth characteristic of the fluid-elastic instability.

7. Conclusions and recommendations

Conclusions:

Along the whole project, several tasks have been performed in different fields in order to achieve the established objectives. The conclusions of this report are:

- The 3 different designed prototypes have been useful to understand how the flow-induced vibrations vary with the geometrical parameters of the helical coil. The reduction of the tube diameter has been an important factor in order to obtain analysable fluid-structural phenomena. The third prototype, with the smallest tube diameter (3 mm), has been the most valid of the 3 helicoids in order to study the flow-induced vibrations.
- The support plate for the helicoids, in the design of the structure, has been ingeniously designed to minimize the influence of this plate on the helical structure and to assure a good fixation inside the test chamber. Furthermore, the whole set (helicoid and support plate) has turned out to be a clearly stiff and durable system to ease the experimental setup.
- The MATLAB code created for the high-speed camera images has been improved until the definitive image analysis code is able to provide good enough results of the vibrations induced by the flow.
- Reasonable results of flow-induced vibrations in helical coils, related with the vortex shedding phenomenon, have been reached. This has been possible due to a good initial planning and a methodical execution of the experiments while maintaining constant external conditions.
- A graphic relation between the vibration amplitude and the flow-velocity has been obtained for the vortex shedding phenomenon in the helical structures.

Recommendations for future research:

This project has been quite innovative inside the field of fluid-structure interactions since the helical shape is not a common shape of study of these types of interactions. In order to continue the research and to increase the knowledge in this field, there are different paths that can be studied and tested in future research. One of these research paths could be to study the flow-induced vibrations using higher velocities than the ones applied for this project in order to have more flexibility when choosing the geometrical parameters to design the helical coil model. Furthermore, using a higher flow-velocity would help to study other related phenomena like the fluid-elastic instability.

In addition, a good way to increase the knowledge about the vibrations produced in the helical structure would be to use other experimental methods to analyse the movement. An example for this is the particle image velocimetry (PIV) which is commonly used in experimental studies of flow and turbulence. Furthermore, a useful way to compare the flow-induced phenomena that occur in the helical coil heat exchangers could be performing CFD simulations. This will help to better understand the interactions between the flow and the helical structure.

Bibliography

- Baker M. 2003. 'Demystifying Mixed Signal Test Methods'. Ed. Newnes, Ch.5: Frequency Domain Testing and the FFT, pp. 115-146.
- Bendat J.S and Allan G. Piersol. 1991. 'Random data analysis and measurement procedures'. John Wiley & Sons, Second ed., pp. 120-136.
- Grant G. 1980. 'Design and development of a once-through helical coil steam generator for large LMFBR plants'. ASME, pp. 1-7.
- Jong Chull Jo and Myung Jo Jhung. 2006. 'Flow-induced vibration and fretting-wear predictions of steam generator helical tubes'. Elsevier, Nuc. Eng. Des. 238, pp. 890-903.
- Jong Chull Jo, Myung Jo Jhung, Woong Sik Kim, Hho Jung Kim. 2004. 'Fluid elastic Instability and Fretting-Wear Characteristics of Steam Generator Helical Tubes Subjected to Single-Phase External Flow and Two-Phase Internal Flow', pp.1-16.
- Kaneko S., Tomomichi Nakamura, Fumio Inada, Minoru Kato, Kunihiko Ishihara and Takashi Nishihara. 2013. 'Flow-Induced Vibrations'. Elsevier, Second ed., pp. 28-50.
- NASA archives. 2016. 'Various Views of von Karman Vortices', pp. 1-12.
http://oceancolor.gsfc.nasa.gov/cmsdocs/educational_material/VariousViewsofvonKarmanVortices.pdf
- Olala S.O. 2016. 'Streamwise fluid elastic instability of tube arrays subjected to two-phase flow' (Doctoral dissertation), Polytechnique Montréal, Montréal, Canada, pp. 6-7.
- Païdoussis M.P., Stuart J. Price and Emmanuel de Langre. 2011. 'Fluid-Structure Interactions', Cross-Flow-Induced Instabilities. Cambridge, pp. 105-124; 215-218.
- Savaresi S.M., C. Poussot-Vassal, Cristiano Spelta, Oliver Sename and Luc Dugard. 2011. 'Semi-Active Suspension Control Design for Vehicles', Butterworth-Heinemann pp. 15-39.
- Wikipedia contributors, n.d., 'Fast Fourier transform'. In Wikipedia, The Free Encyclopedia. Retrieved 19:43, August 27, 2019, from:
https://en.wikipedia.org/wiki/Fast_Fourier_transform#Algorithms
- Yuan H., Jarome Solberg, Elia Merzari, Adam Kraus and Iulian Grindeanu. 2017. 'Flow-induced vibration analysis of a helical coil steam generator experiment using large eddy simulation', Nuclear Engineering Design. Elsevier, pp.
- Ziada S. 2006. 'Vorticity Shedding and Acoustic Resonance in Tube Bundles', J. of the Braz. Soc. Of Mech. Sci. & Eng. ABCM. Vol. XXVIII, No. 2, pp. 1-7.
- Zienkiewicz O.C, R.L. Taylor and P. Nithiarasu. 2014., 'The Finite Element Method for Fluid Dynamics', Butterworth-Heinemann (Elsevier), Seventh ed., Introduction, pp 1-4.

Appendices

Appendix 1: MATLAB codes

High-speed camera code:

```
%% Initial Parameters %%
format long
N=30; % Numbers of pictures
initial=1; % Premiere photo a analyser
Fs= 600; % »» Sampling frequency (Hz) ««
dt= 1/Fs; % »» Time between the two picture ««
D= 0.003; % »» Diameter of the object (m) ««
Dp= 17.19; % »» Radius of the object (pixel) «« 3mm ->17.19; 5mm-
>28.57; 7mm->35.65
t= 0:dt:(N-1)*dt; % Time origin
len= D/Dp; % »» Lenght of a pixel (m) ««
rgb= cell(1,N); % Original pictures
RGB1= cell(1,N); % Filred pictures
folder= 'C:\Users\Ferran\Desktop\PFE\Eau\40Hz3mm600FPS\';
Imadjust_option= {[0; 0.33],[0; 1]}; % maps the intensity values of the image in
greyscale

%% Loading pictures %%
for i=1:N

    baseFileName= '15Hz3mm00000'; % The name of the pictures to be loaded
    im_ind= sprintf('%d', i+initial); % to format the data in arrays in column
order, and returns the results to str.
    fullFileName= [baseFileName(1:end-length(im_ind)) im_ind '.bmp'];
    rgb{i} = imread(sprintf('%s%s', folder, fullFileName));
    RGB1{i} = imadjust(rgb{i},Imadjust_option{1}, Imadjust_option{2}); % Imadjust
[low_in; high_in],[low_out; high_out]

    % figure(1)
    % subplot(2,1,1), imshow(rgb{i}); title('Original') % To show the comparison of
figures
    % subplot(2,1,2), imshow(RGB1{i}); title('Filtered')
    % figure(2), imshow(RGB1{i}); % To show the filtered figure
    % clf

end

%% Processing Pictures %%
for i=1:N
    methode= 2; % For other methods
    if methode == 1

    else
        file_name= 'Object_info.mat';
        threshold= 160; % Threshold

        helicoid= 1; % For other future cases
    end
end
```



```

switch helicoid

case 1

    i_coord = 57;                % »» Vertical Coordinate
    j_coord = 431;              % »» Horizontal Coordinate

    i_haut = i_coord;
    j_centr = j_coord;

    % For the lower points %
    r=1;
    countInf=0;
    True= true;

    while True

        InfR= RGB1{i}((i_haut+r), j_centr:(j_centr+200));
        InfL= RGB1{i}((i_haut+r), j_centr:-1:(j_centr-200));
        indR= find(InfR <=threshold);
        indL= find(InfL <=threshold);
        indDefR= indR(1);
        indDefL= indL(1);
        ptInfR(r,1:2) = [i_haut+r, j_centr+indDefR-1];
        ptInfL(r,1:2) = [i_haut+r, j_centr-indDefL+1];
        countInf=countInf+1;
        j_centr = ptInfL(r,2) + round((ptInfR(r,2) - ptInfL(r,2))/2); %
centre origin point
        r=r+1; % Vertical Displacement
        BreakC = RGB1{i}((i_haut+r), j_centr);
        if BreakC <= threshold
            True= false;
        end
    end

    % For the upper points %
    i_haut = i_coord;
    j_centr = j_coord;
    r=0;
    countSup=0;
    True = true;

    while True

        SupR= RGB1{i}((i_haut-r), j_centr:(j_centr+200));
        SupL= RGB1{i}((i_haut-r), j_centr:-1:(j_centr-200));
        indR= find(SupR <=threshold);
        indL= find(SupL <=threshold);
        indDefR= indR(1);
        indDefL= indL(1);
        ptSupR(r+1,1:2) = [i_haut-r, j_centr+indDefR-1];
        ptSupL(r+1,1:2) = [i_haut-r, j_centr-indDefL+1];
        r=r+1; % Vertical Displacement
        countSup=countSup+1;
    end
end

```

```

        j_centr = ptSupL(r,2) + round((ptSupR(r,2) - ptSupL(r,2))/2); %
centre origin point
        % For testing if the last upper point has been achieved
        % 80 Pixels have been chosen to analyze it
        SupR= RGB1{i}((i_haut-r), j_centr:(j_centr+80));
        SupL= RGB1{i}((i_haut-r), j_centr:-1:(j_centr-80));
        indR= find(SupR <=threshold);
        indL= find(SupL <=threshold);
        emptyR = isempty(indR);
        emptyL = isempty(indL);
        if emptyR==1 && emptyL==1
            True= false;

        elseif emptyL==1
            while True
                SupR= RGB1{i}((i_haut-r), j_centr:(j_centr+80));
                indR= find(SupR <=threshold);
                indDefR= indR(1);
                ptSupR(r+1,1:2) = [i_haut-r, j_centr+indDefR-1];
                r=r+1; % Vertical Displacement
                countSup=countSup+1;
                SupR= RGB1{i}((i_haut-r), j_centr:(j_centr+80)); % >>>
i_haut-r==0 error

                indR= find(SupR <=threshold);
                emptyR = isempty(indR);
                if emptyR == 1
                    True=false;
                end
            end

        elseif emptyR==1
            while True
                SupL= RGB1{i}((i_haut-r), j_centr:-1:(j_centr-80));
                indL= find(SupL <=threshold);
                indDefL= indL(1);
                ptSupL(r+1,1:2) = [i_haut-r, j_centr-indDefL+1];
                r=r+1; % Vertical Displacement
                countSup=countSup+1;
                SupL= RGB1{i}((i_haut-r), j_centr:-1:(j_centr-80));
                indL= find(SupL <=threshold);
                emptyL = isempty(indL);
                if emptyL == 1
                    True=false;
                end
            end
        end
    end
end

end
ptSupLRev = flip(ptSupL);
ptInfRRev = flip(ptInfR);
Pts = double([ptSupLRev; ptInfL; ptInfRRev; ptSupR]);

Xo_first(i)= Pts(1,1); %First Max Point
Yo_first(i)= Pts(1,2);

```

```

        Xo_end(i)= Pts(end,1); %Last Max Point
        Yo_end(i)= Pts(end,2);

%% Highlighted points
        hg= figure(5);

        clf

        imshow(RGB1{i})

        hold on
        plot(Pts(:,2), Pts(:,1), 'r*')
        plot(Pts(:,2), Pts(:,1), 'y.-')
        Fa2(i) = getframe(hg); % Video images
    end
clear ptSupR ptSupL ptInfR ptInfL ptSupLRev ptInfRRev
end

%% Obtaining Graphics
% X --> Vertical Movement

% Y --> Horizontal Movement

X_oFirst= zeros(1, N-1);

Y_oFirst= zeros(1, N-1);

X_oEnd= zeros(1, N-1);

Y_oEnd= zeros(1, N-1);

for i=2:N
    X_oFirst(i)= Xo_first(i)-Xo_first(1); % (pixel)
    Y_oFirst(i)= Yo_first(i)-Yo_first(1); % (pixel)
    X_oEnd(i)= Xo_end(i)-Xo_end(1); % (pixel)
    Y_oEnd(i)= Yo_end(i)-Yo_end(1); % (pixel)
end
X_oFirst= X_oFirst*D/Dp*1000; % (mm) % First Maximum
Y_oFirst= Y_oFirst*D/Dp*1000; % (mm)
X_oEnd= X_oEnd*D/Dp*1000; % (mm) % Second Maximum
Y_oEnd= Y_oEnd*D/Dp*1000; % (mm)
VX_oFirst= diff(X_oFirst)/dt; % (mm/s)
VY_oFirst= diff(Y_oFirst)/dt; % (mm/s)
VX_oEnd= diff(X_oEnd)/dt; % (mm/s)
VY_oEnd= diff(Y_oEnd)/dt; % (mm/s)

% Displacement Graphics
figure(7)
plot(dt*(0:length(X_oFirst)-1), X_oFirst-mean(X_oFirst), 'LineWidth', 1); xlabel('t
(s)', 'FontSize', 14); ylabel('Vertical Displacement (mm)', 'FontSize', 14);

figure(8)

```

```

plot(dt*(0:length(Y_oFirst)-1), Y_oFirst-mean(Y_oFirst), 'LineWidth', 1); xlabel('t
(s)', 'FontSize', 14); ylabel('Horizontal Displacement (mm)', 'FontSize', 14);

% Root Mean Square
rmsXFirst = rms(X_oFirst-mean(X_oFirst)); % Vertical Disp Root mean Square
rmsVXFirst = rms(VX_oFirst-mean(VX_oFirst));
rmsYFirst = rms(Y_oFirst-mean(Y_oFirst)); % Horizontal Disp Root Mean Square
rmsVYFirst = rms(VY_oFirst-mean(VY_oFirst));

%% FFT and PSD parameters %%
Fs;

t;

DispV1=X_oFirst;

DispH1=Y_oFirst;

DispV2=X_oEnd;

DispH2=Y_oEnd;

DispV=detrend(DispV1, 'constant');
DispH=detrend(DispH1, 'constant');
dispV1=transpose(DispV);
dispH1=transpose(DispH);
DF=0.25; % Frequency Resolution (Hz)
BlockTime=1/DF;
BlockLength=BlockTime*Fs;
Percent_overlap=0;
NWin=BlockLength;
NOVERLAP=floor(Percent_overlap*NWin/100);

[PFLFLV, FREQ] = pwelch(dispV1, rectwin(NWin),NOVERLAP, [], Fs);
[PFLFLH, FREQ] = pwelch(dispH1, rectwin(NWin),NOVERLAP, [], Fs);

figure(100)
plot(FREQ,PFLFLV,'k');
xlim([0 100]);
set(gca, 'FontSize', 16)
xlabel('Fr (Hz)', 'FontSize', 14)
ylabel('PSD(mm^2/Hz)', 'FontSize', 14)

figure(101)
plot(FREQ,PFLFLH,'k');
xlim([0 100]);
set(gca, 'FontSize', 16)
xlabel('Fr (Hz)', 'FontSize', 14)
ylabel('PSD(mm^2/Hz)', 'FontSize', 14)

NFFT= 1024*2^3; % Total Sampling Points
delta_f= (Fs)/(NFFT);
f3 = 0:delta_f:Fs/2;
tin_1= 0*dt; % The first analysed point

```

```

indFFT= find(t>= tin_1);

FFTV1 = fft(DispV1(indFFT(1): end)-mean(DispV1), NFFT);
FFTH1 = fft(DispH1(indFFT(1): end)-mean(DispH1), NFFT);
FFTV2 = fft(DispV2(indFFT(1): end)-mean(DispV2), NFFT);
FFTH2 = fft(DispH2(indFFT(1): end)-mean(DispH2), NFFT);

AmplitudeV1= 2*abs(FFTV1(1:NFFT/2+1))/NFFT;
AmplitudeH1= 2*abs(FFTH1(1:NFFT/2+1))/NFFT;
AmplitudeV2= 2*abs(FFTV2(1:NFFT/2+1))/NFFT;
AmplitudeH2= 2*abs(FFTH2(1:NFFT/2+1))/NFFT;

figure (13) % Vertical Amplitude
plot(f3(2:end), AmplitudeV1(2:end))
xlabel('Fr (Hz)'); ylabel('Vertical Amplitude (mm)');

figure(14) % Horizontal Amplitude
plot(f3(2:end), AmplitudeH1(2:end))
xlabel('Fr (Hz)'); ylabel('Horizontal Amplitude (mm)');

%% Video creation %%
v = VideoWriter('15Hz3mm.avi','uncompressed AVI');
open (v)
writeVideo(v,Fa2)

```

Beta in function of the external diameter:

```
%% Initial Parameters %%
%rhof=1.225;           % Fluid Density: Air
rhof=997;             % Fluid Density: Water
%rhos=1350;           % Material density: Plastic PVC
rhos=8960             % Material Density: Copper
zeta=0.0075;         % Damping Coefficient
sigma=2*pi*zeta;
ep=0.004              % Wall thickness
Dext=[0.01:0.001:0.05] % External diameter
Dint=Dext-ep*2;      % Internal diameter

%% Beta is independent from these parameters:
Dhx=0.3;             % Helicoidal Diameter
H=0.7;              % Total Height
N=7.5;              % Number of revolution

%% Calculation of the total length 'T':
h=H/N;              % Height per revolution
C=pi*Dhx;           % Circle Perimetre
L=(h^2+C^2)^0.5;    % Length of 1 Revolution
T=L*N;              % Total length

%% Mass calculation:
m=rhos*T*pi*(Dext.^2-Dint.^2)/4;

%% Beta calculation:
beta = m.*sigma./(rhof.*Dext.^2*T)

%% The plot
plot(Dext,beta)

xlabel('External Diameter (m)')
ylabel('Beta')
xlim([0.005 0.055])
hold on
```

Beta in function of the wall thickness

```
%rhof=1.225; % Fluid Density: Air
rhof=997; % Fluid Density: Water
%rhos=1350; % Material density: Plastic PVC
rhos=8960 % Material Density: Copper
zeta=0.0075; % Damping Coefficient
sigma=2*pi*zeta;
Dext=0.015; % External diameter
ep=[0.0015:0.0001:0.0075]; % Wall thickness
Dint=Dext-ep*2; % Internal Diameter

%% Beta is independent from these parameters:
Dhx=0.3; % Helicoidal Diameter
H=0.7; % Total Height
N=7.5; % Number of revolutions

% Calculation of the total length 'T':
h=H/N; % Height per revolution
C=pi*Dhx; % Circle perimetre
L=(h^2+C^2)^0.5; % Length of 1 Revolution
T=L*N; % Total length

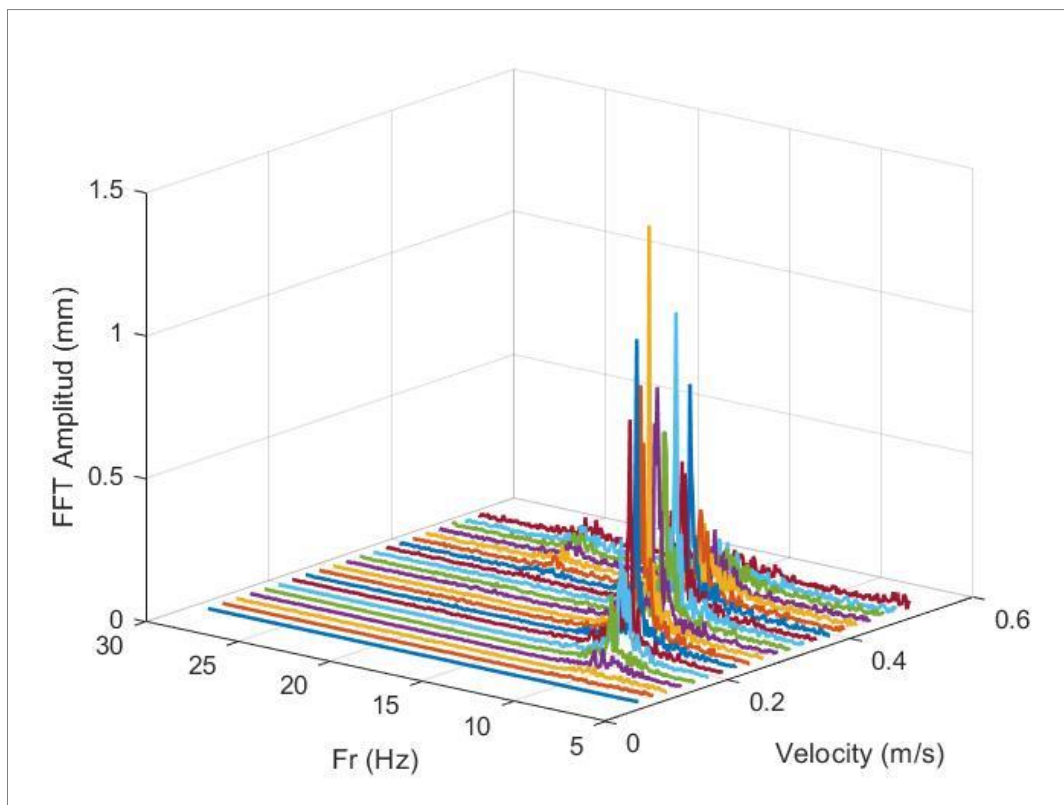
% Mass calculation:
m=rhos*T*pi*(Dext.^2-Dint.^2)/4;

% Beta calculation:
beta = m.*sigma./(rhof.*Dext.^2*T)

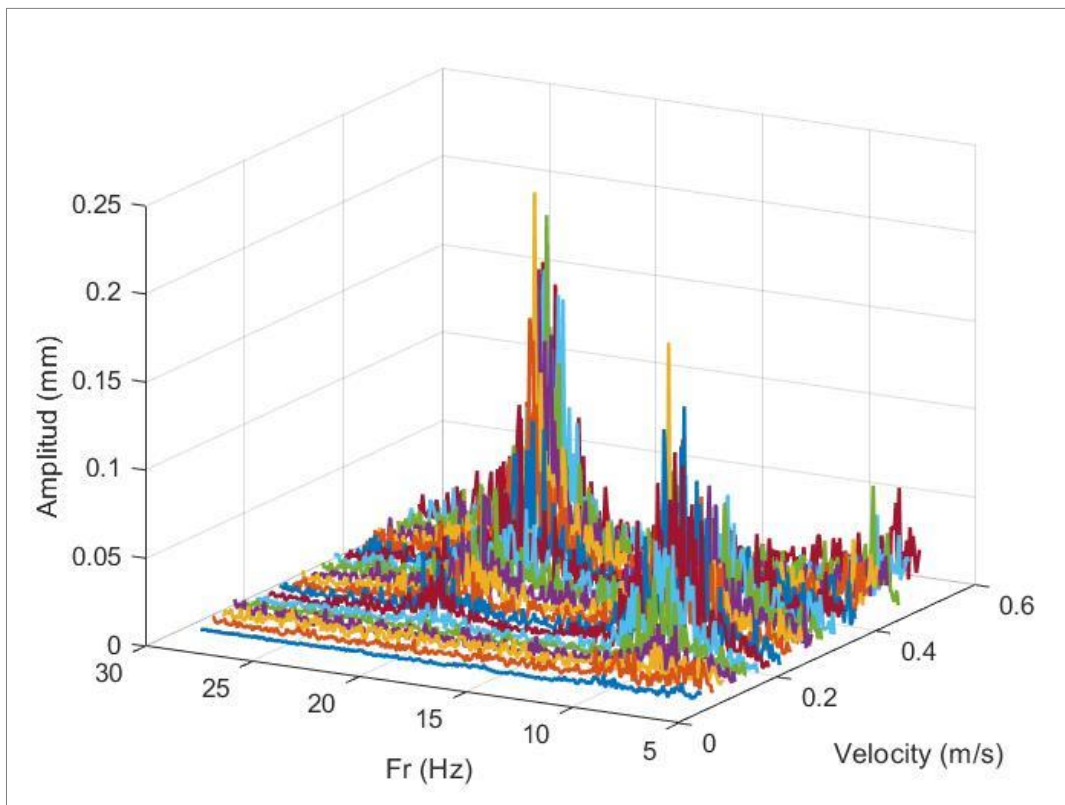
% The plot
plot(ep,beta)

xlabel('Wall Thickness (m)')
ylabel('Beta')
hold on
```

Appendix 2: Additional graphics

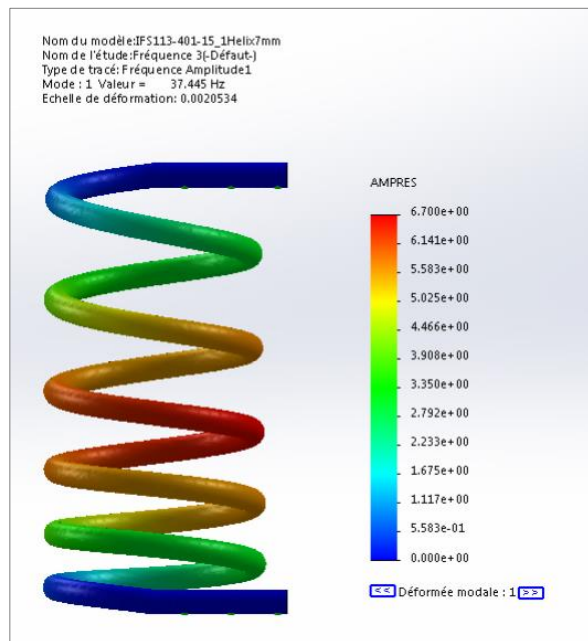
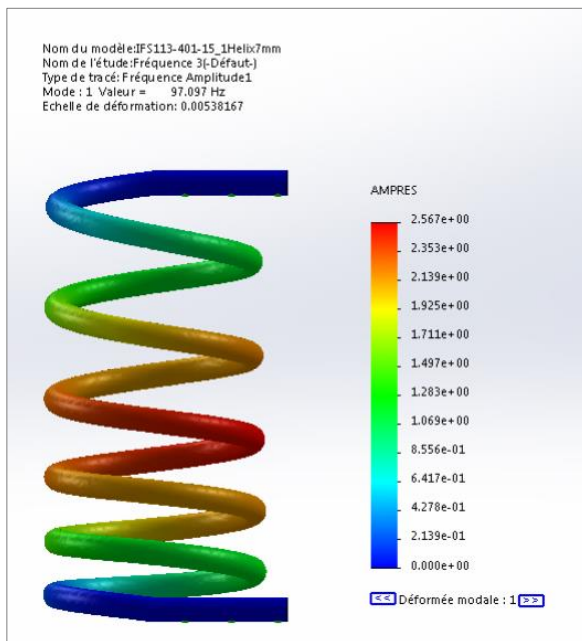


Original FFT 3D graphic of the vertical movement for proto 3 (with all the velocities)

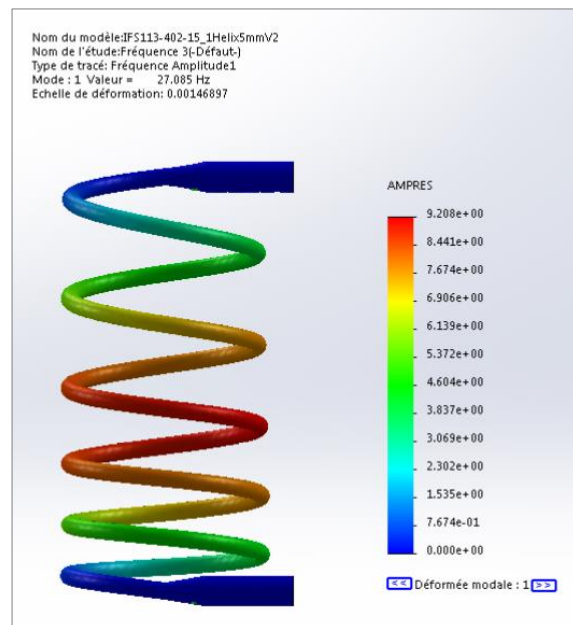
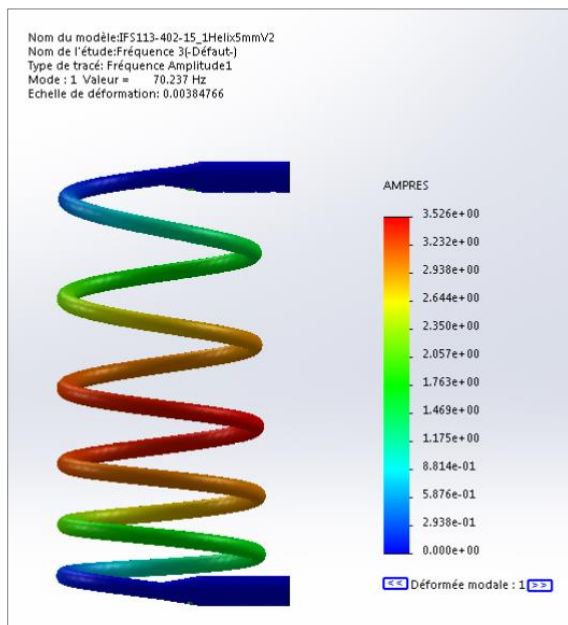


Original FFT 3D graphic of the horizontal movement for proto 3 (with all the velocities)

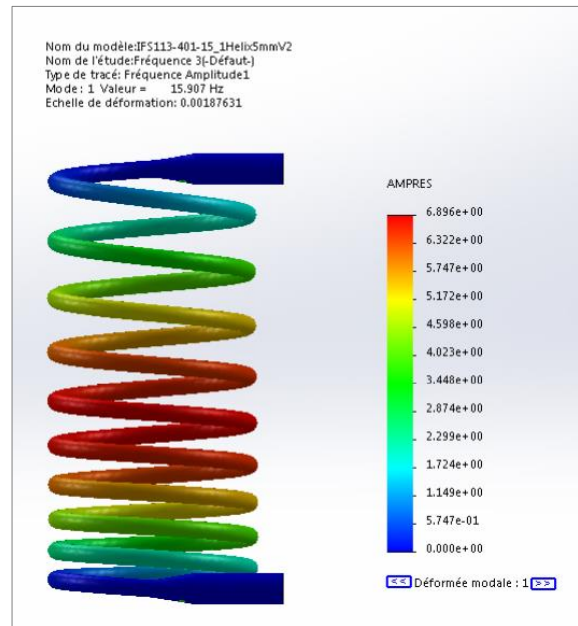
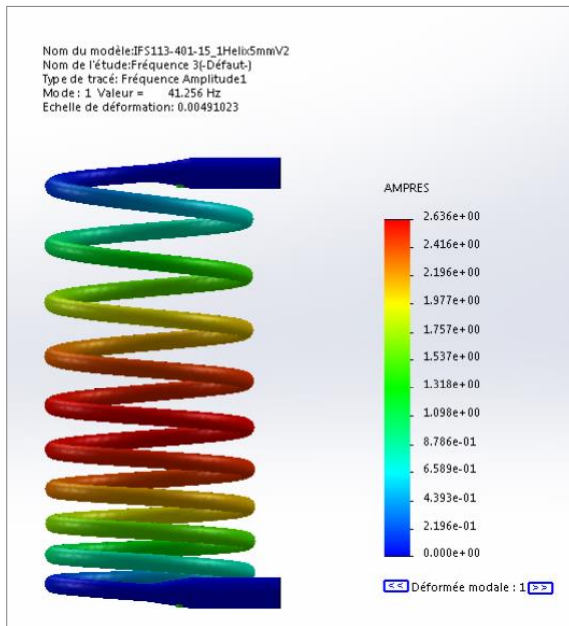
Appendix 3: SolidWorks simulated frequencies



SolidWorks model with 7 mm of tube diameter and 5.5 revolutions, copper (on the left) and PVC plastic (on the right)

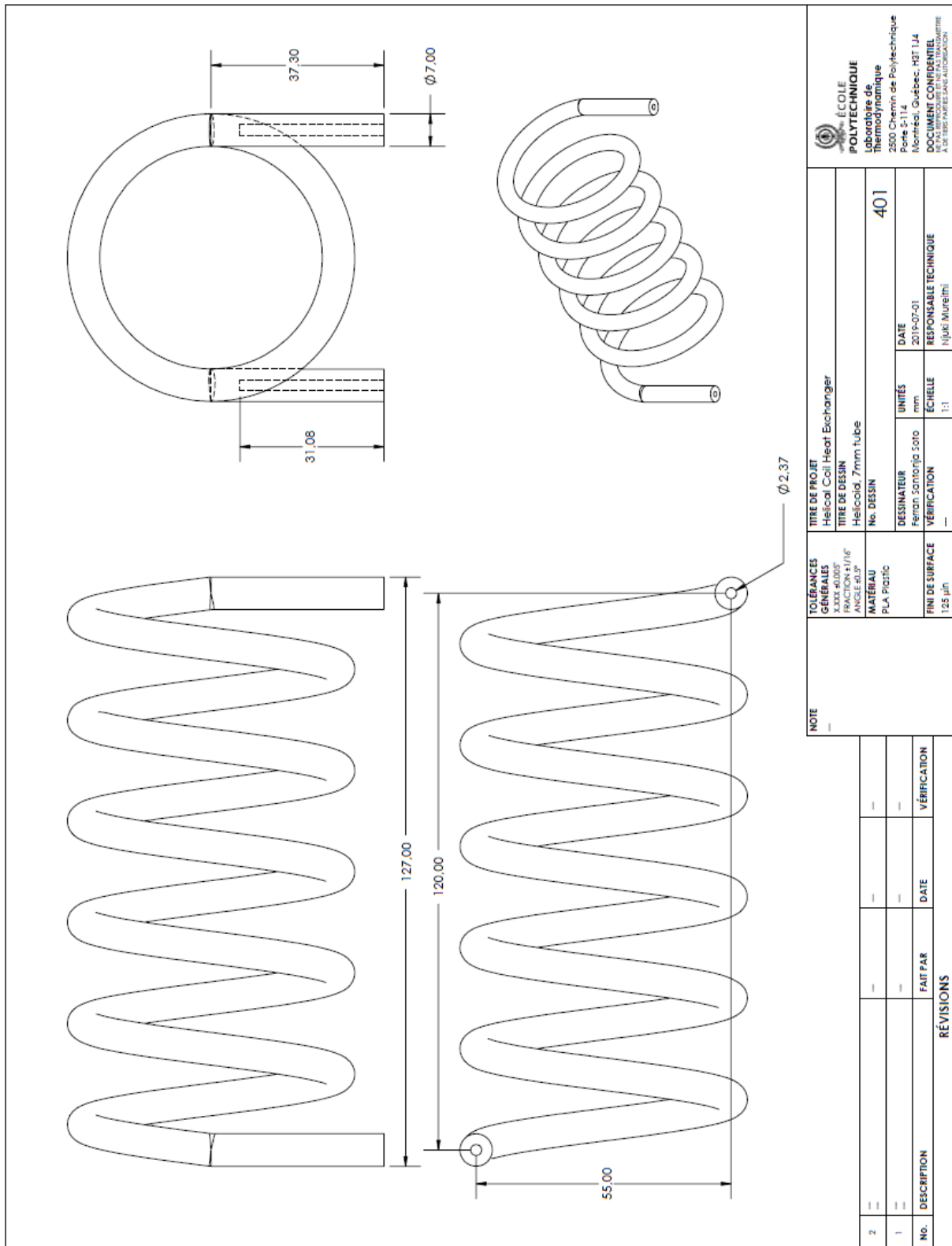


SolidWorks model with 5 mm of tube diameter and 5.5 revolutions, copper (on the left) and PVC plastic (on the right)

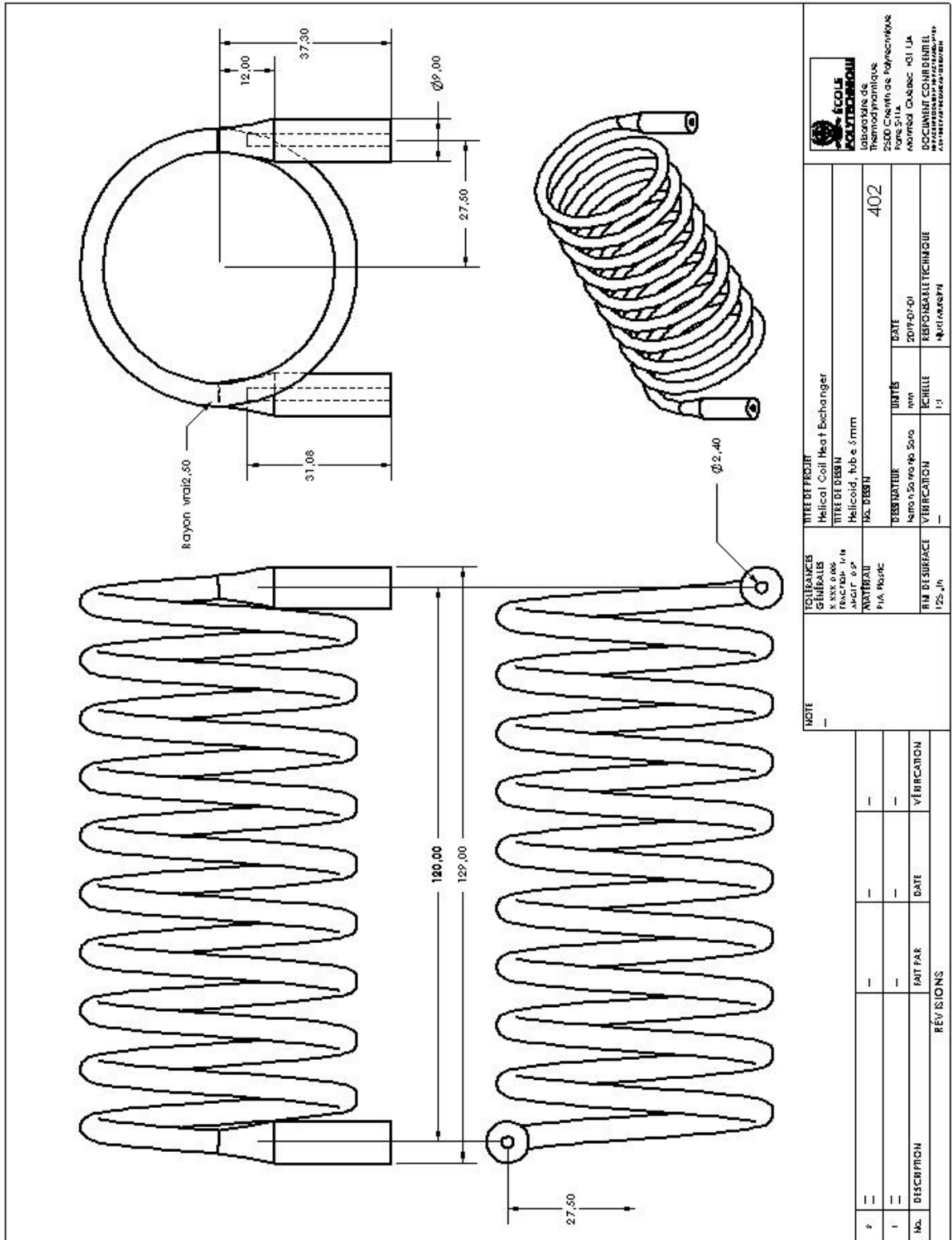


SolidWorks model with 5 mm of tube diameter and 9.5 revolutions, copper (on the left) and PVC plastic (on the right)

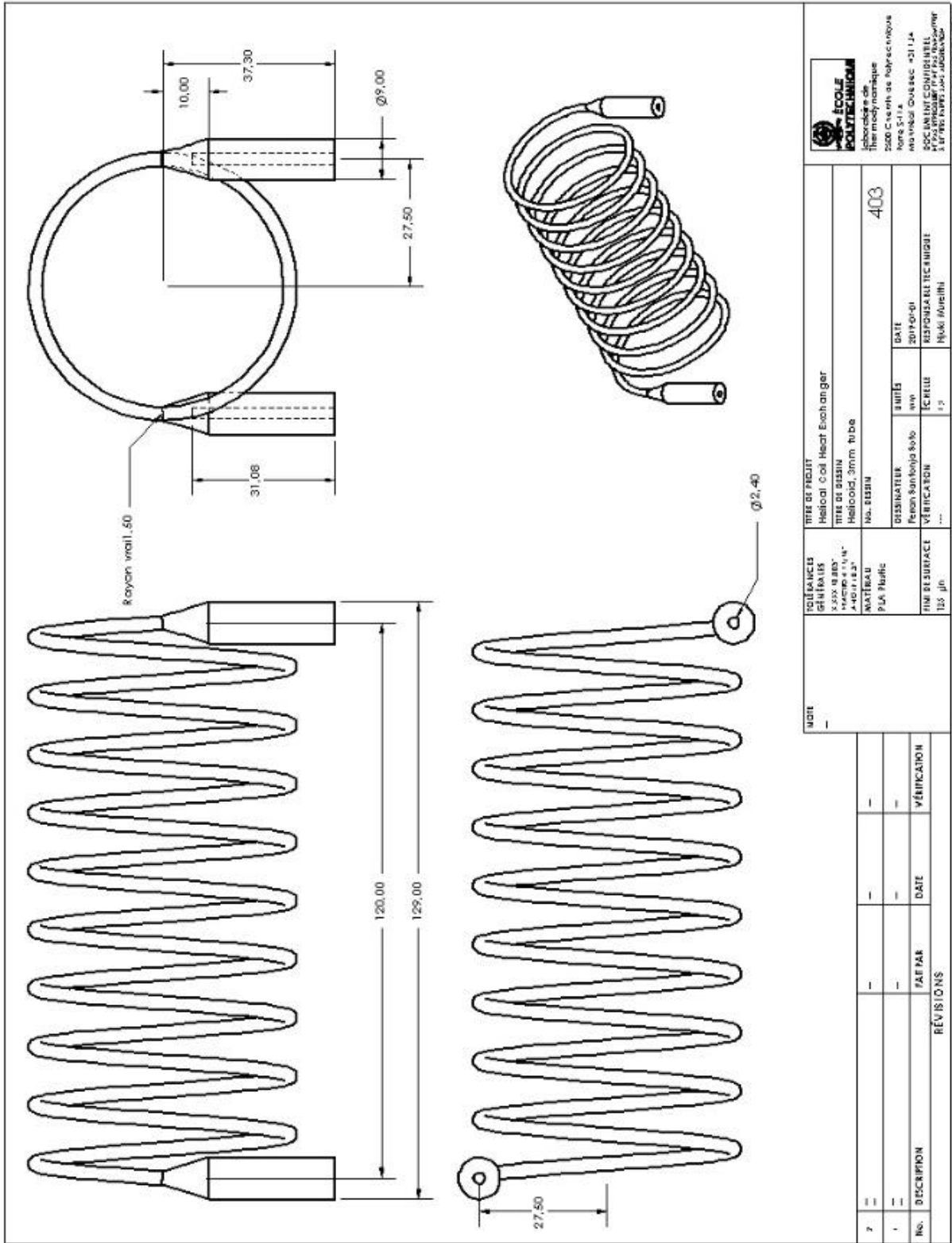
Appendix 4: Parts drawings



Helical coil prototype number 1



Helical coil prototype number 2



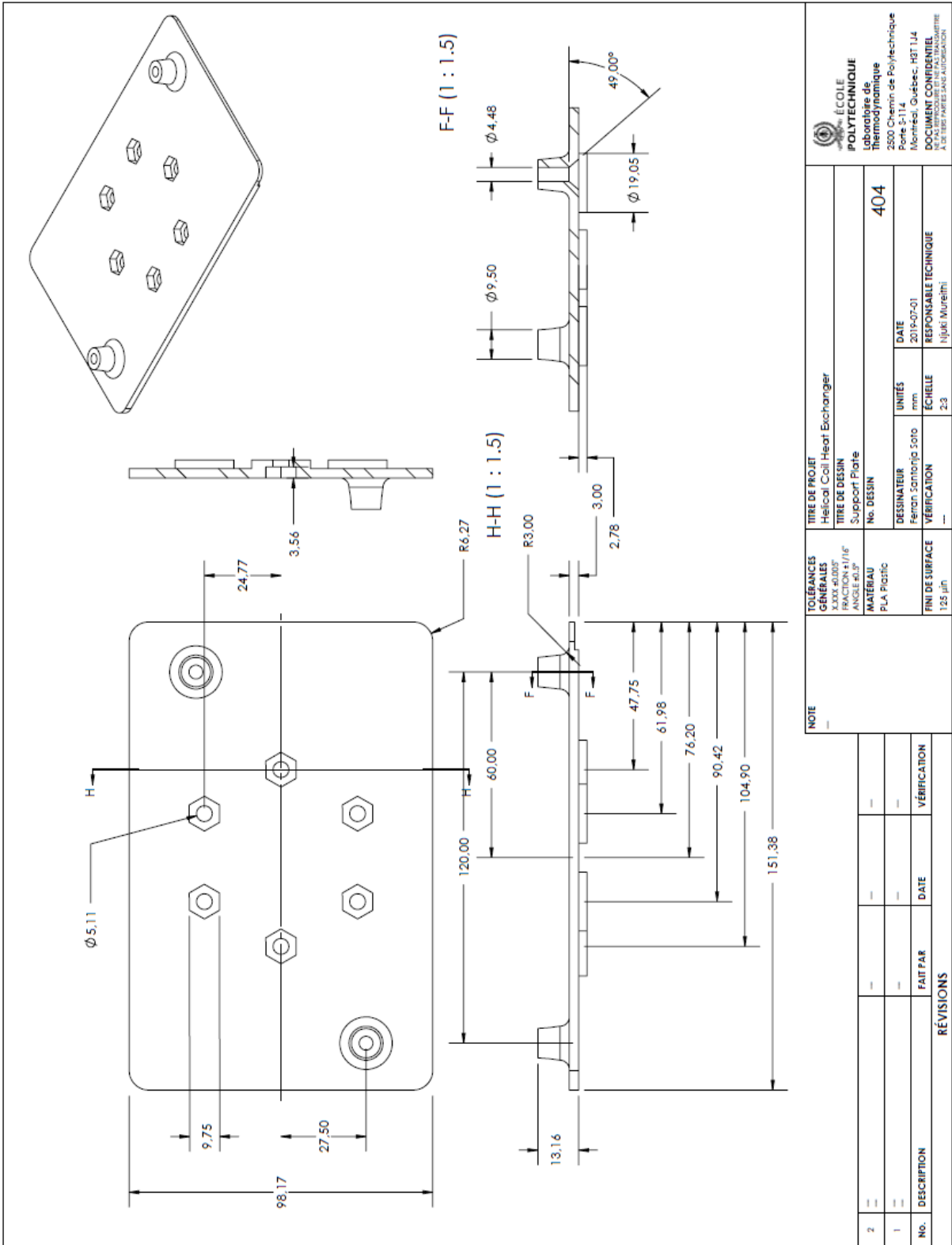
Helical coil prototype number 3

| REVISIONS | | REVISIONS | |
|-----------|-------------|-----------|------|
| No. | DESCRIPTION | FAIT PAR | DATE |
| 1 | | | |
| 2 | | | |

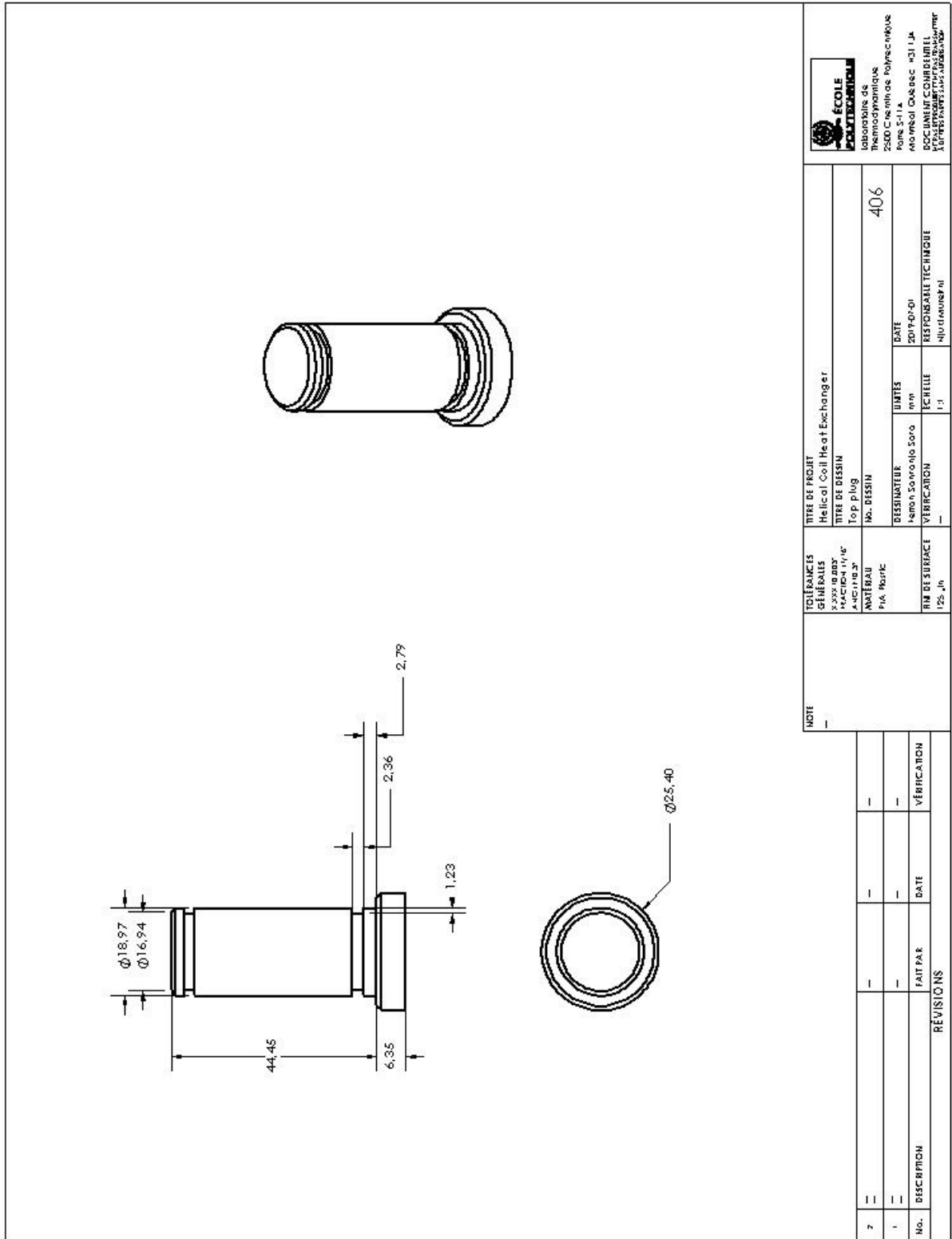
| | | | |
|-----------------|--|-----------------------------|--|
| NOTE | | TITRE DE PROJET | |
| | | Helical Coil Heat Exchanger | |
| SOLlicitANTS | | TITRE DE BUREAU | |
| GILFILLIS | | HEELOOD, 30mm tube | |
| X 55X 8.80" | | No. 81831 | |
| "MACHO 4 1/4" | | DISSEMINATEUR | |
| "A-10118.2" | | FRENCH SCHOOL 806 | |
| MATERIAU | | VERIFICATION | |
| PLA Plastic | | E.CHELLE | |
| FINI DE SURFACE | | RESPONSABIL TECHNIQUE | |
| 125 µm | | No. 403 | |
| | | DATE | |
| | | 2014-09-01 | |
| | | SIGNATURE | |
| | | No. 403 | |



École Polytechnique
 2500 Ch. de Ste-Jérôme
 Montréal, Québec H3T 1J4
 Téléphone: (514) 393-2111
 Télécopieur: (514) 393-2114
 Site Web: www.etsmtl.ca



Support plate for the helioids



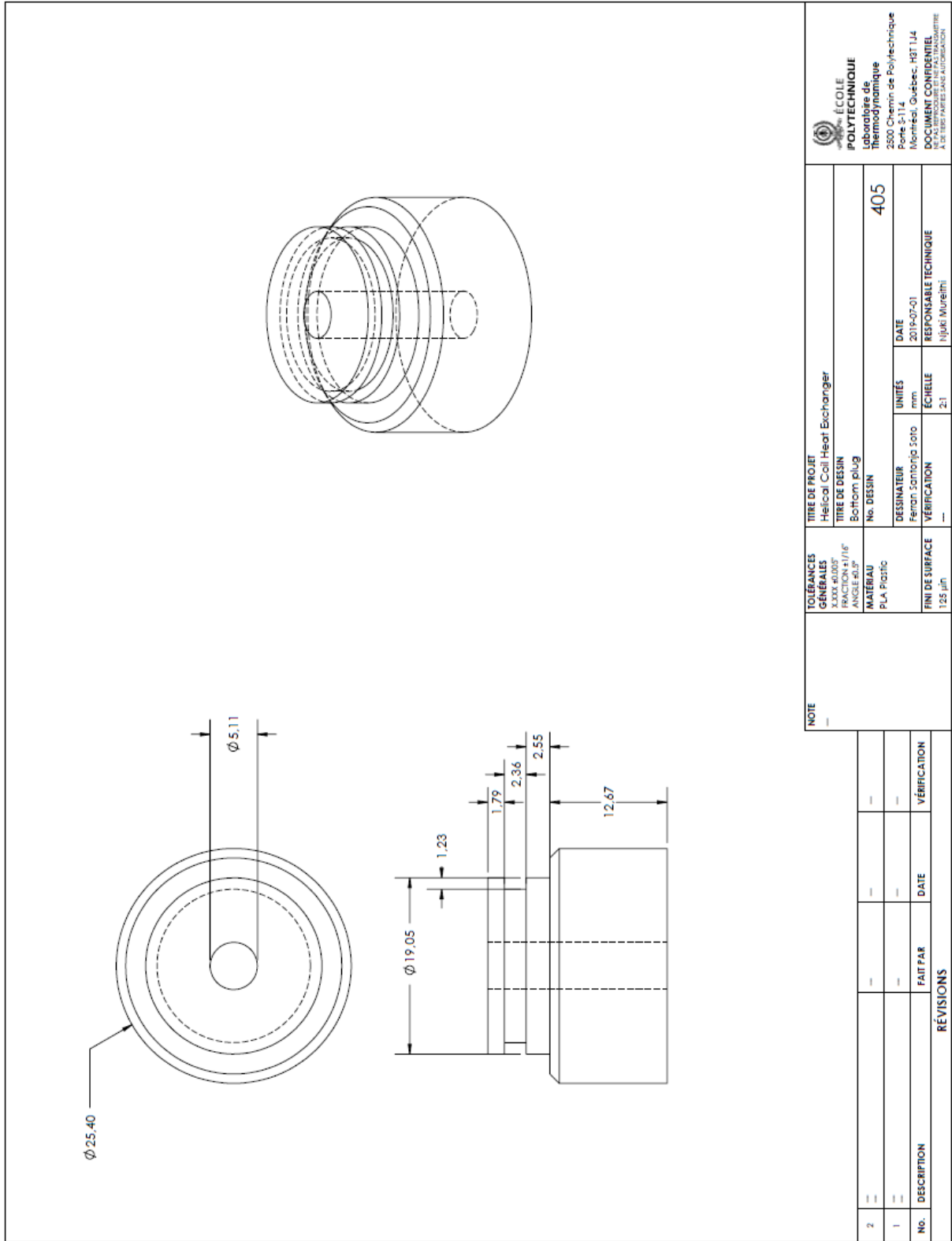
Top plug of the test chamber

| REVISIONS | | VERIFICATION | |
|-----------|-------------|--------------|------|
| No. | DESCRIPTION | FAIT PAR | DATE |
| 7 | | | |
| 1 | | | |

| | | | |
|----------------------|--|-----------------------------|--|
| NOTE | | | |
| — | | | |
| TOLERANCES GÉNÉRALES | | TITRE DE PROJET | |
| X.255 la 0.025 | | Helical Coil Heat Exchanger | |
| X.255 la 0.025 | | TITRE DE BASSIN | |
| X.255 la 0.025 | | Top Plug | |
| MATERIAU | | No. BASSIN | |
| PVA, Pastic | | 406 | |
| RM DE SURFACE | | DESTINATEUR | |
| 125, Jn | | Amao, Soomnio Sara | |
| | | DATE | |
| | | 2019-01-01 | |
| | | UNITE | |
| | | mm | |
| | | ECHELLE | |
| | | 1:1 | |
| | | RESPONSABLE TECHNIQUE | |
| | | Mouhammad Ali | |



laboratoire de
Thermodynamique
2500, rue de la polytechnique
Montréal, Québec H3J 1J4
BOCQUET, C. DANIEL
11, rue des Pères, Montréal
Québec H2T 1S6



Bottom plug of the test chamber

| NOTE | | TITRE DE PROJET | | TITRE DE PROJET | |
|------|-------------|-----------------------------|----------|-----------------------|--------------|
| | | Helical Coil Heat Exchanger | | 405 | |
| | | Bottom plug | | | |
| | | No. Dessin | | | |
| | | DESIGNATEUR | | DATE | |
| | | Feron, Satorfjo 5070 | | 2019-07-01 | |
| | | VERIFICATION | | ECHELLE | |
| | | — | | 2:1 | |
| | | RESUME | | RESPONSABLE TECHNIQUE | |
| | | — | | Fujiki Wurethi | |
| | | FINI DE SURFACE | | | |
| | | 125 µm | | | |
| | | MATERIAU | | | |
| | | PLA Plastic | | | |
| | | TOLERANCES GENERALES | | | |
| | | XXX ±0.007 | | | |
| | | FRACTION ±1/16" | | | |
| | | ANGLE ±0.5° | | | |
| | | REVISIONS | | | |
| | | | FAIT PAR | DATE | VERIFICATION |
| 2 | | | | | |
| 1 | | | | | |
| No. | DESCRIPTION | | | | |

